

**BEHAVIOURAL MODELING OF CONCURRENT
DUAL-BAND POWER AMPLIFIERS**

BY

MOHAMMED ABDALLA ABDELRAHIM ALI

A Thesis Presented to the
DEANSHIP OF GRADUATE STUDIES

KING FAHD UNIVERSITY OF PETROLEUM & MINERALS

DHAHRAN, SAUDI ARABIA

1963 ١٣٨٣

In Partial Fulfillment of the
Requirements for the Degree of

MASTER OF SCIENCE

In

ELECTRICAL ENGINEERING

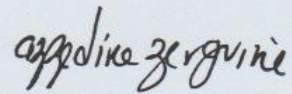
NOVEMBER 2016

KING FAHD UNIVERSITY OF PETROLEUM & MINERALS

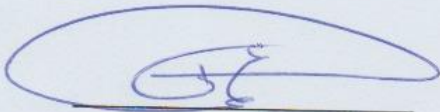
DHAHRAN- 31261, SAUDI ARABIA

DEANSHIP OF GRADUATE STUDIES

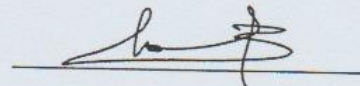
This thesis, written by **MOHAMMED ABDALLA ABDELRAHIM ALI** under the direction his thesis advisor and approved by his thesis committee, has been presented and accepted by the Dean of Graduate Studies, in partial fulfillment of the requirements for the degree of **MASTER OF SCIENCE IN ELECTRICAL ENGINEERING**.



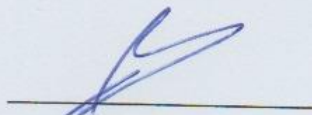
Prof. Azzedine Zerguine
(Advisor)



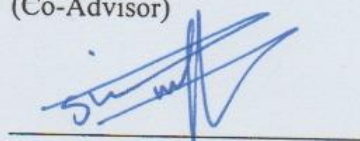
Dr. Ali A. Al-Shaikhi
Department Chairman



Dr. Oualid Hammi
(Co-Advisor)



Prof. Salam A. Zummo
Dean of Graduate Studies



Prof. Mohammad S. Sharawi
(Member)

29/12/16
Date

© Mohammed Abdalla Abdelrahim Ali

2016

To my father, who did not only raise and nurture me but also taxed himself dearly over the years for my education and intellectual development. To my mother whose kind heart has been a source of kindness, care, support and motivation during moments of despair and discouragement.

Last but not least, my deepest gratitude goes to my beloved sisters and brothers, for their prayers and encouragement. To those who indirectly contributed to this research. |

ACKNOWLEDGMENTS

In the name of Allah, the Most Gracious and the Most Merciful Alhamdulillah, all praises to Allah for the strengths and His blessing in completing this thesis,

Special appreciation goes to my supervisor, Prof. Azzedine Zerguine for his supervision, constant support. Also a big thank to Dr. Oualid Hammi for his priceless guidance, his comments and suggestions throughout the duration of this work. I would also like to thanks my committee member Prof. Mohammad S. Sharawi for his helpful comments. Special regards and blessings to all of those who supported me in any aspect during the completion of the project.

TABLE OF CONTENTS

ACKNOWLEDGMENTS	IV
TABLE OF CONTENTS	V
LIST OF TABLES	VIII
LIST OF FIGURES	IX
LIST OF ABBREVIATIONS	XII
ABSTRACT.....	XV
ABSTRACT (ARABIC)	XVI
CHAPTER 1 INTRODUCTION.....	1
1.1 Why Linear Amplifiers?	1
1.2 Distortion in RF Transmitters.....	2
1.3 Carrier Aggregation Configurations	5
1.4 Transmitter Architectures.....	7
1.4.1 Single-Branch Transmitters.....	7
1.4.2 Multi-Branch Transmitters.....	8
1.5 Linearization of Nonlinear Amplifiers	10
1.6 Understanding Distortion Effects in Multi-Band Transmitters	11
1.7 Motivation and Contributions.....	12
CHAPTER 2 DISTORTION IN LTE-A TRANSMITTERS.....	14
2.1 LTE-A Basics	14
2.2 Inter-Modulation Distortions in Nonlinear Power Amplifiers	18
2.3 Summary	24
CHAPTER 3 LITERATURE REVIEW.....	25
3.1 Broadband transmitters.....	25

3.2	Multi-Band Transmitters.....	27
3.3	Behavioural Modeling of Power Amplifiers.....	30
3.4	Memory Effects.....	33
3.4.1	Characterization of Memory Effects	33
3.4.2	Modeling Power Amplifiers with Memory.....	34
3.5	Related Work for Models with Memory Effects.....	35
3.6	Summary	40
 CHAPTER 4 ANALYSIS OF DUAL-BAND MEMORY POLYNOMIAL		
MODELS		
		41
4.1	The Memory-Polynomial Model	41
4.2	Dual-Band General Model.....	43
4.3	Proposed Dual-Band Model.....	45
4.4	Metrics Used for Benchmarking	51
4.5	Summary	54
 CHAPTER 5 PERFORMANCE EVALUATION OF THE PROPOSED MODEL 55		
5.1	Experimental Setup and Test Conditions.....	55
5.2	Simulation Results	57
5.2.1	NMSE Performance for Test Scenario (1).....	57
5.2.2	NMSE Performance for Test Scenario (2)	59
5.2.3	Performance Assessment in Frequency Domain.....	62
5.2.4	Condition Number Performance for Test Scenario (1).....	66
5.2.5	Condition Number Performance for Test Scenario (2).....	67
5.3	Summary	71
 CHAPTER 6 CONCLUSIONS AND FUTURE WORK		
		73
6.1	Conclusion.....	73
6.2	Future Work	75
 APPENDIX A		
		76

APPENDIX B	80
REFERENCES.....	83
VITAE.....	94

LIST OF TABLES

Table 2.1 Two-carrier distortion products up to fifth degree (expansion of equation (2.3)).....	20
Table 3.1 Wideband and dual-band architectures advantages and disadvantages.....	30
Table 3.2 Comparison between behavioral models	36
Table 5.1 Comparison between the proposed model and the conventional models.....	71
Table A.1 2nd, 3rd and the 5th harmonics, 2nd, 3rd and 5th IMD ranges for release 12 inter-bands.....	76

LIST OF FIGURES

Figure 1.1 Block diagram of direct conversion transceiver.....	2
Figure 1.2 Spectral regrowth in a single-carrier LTE-A.....	3
Figure 1.3 Carrier aggregation scenarios.....	6
Figure 1.4 Transmitter architectures: (a) single RF branch transmitter, (b) multi-branch RF transmitter including multi band final stage, (c) multi-band RF transmitter architecture	8
Figure 1.5 The multi-band transmitter power spectrum output.....	11
Figure 2.1 LTE evolution, 3GPP release status for carrier aggregation.....	16
Figure 2.2 Graphical definition of the third order intercept point [14].....	21
Figure 2.3 Two-carrier in-band inter-modulation spectrum	23
Figure 2.4 Inter-modulation spectrum for a typical band-limited digitally modulated signal.....	24
Figure 3.1 Single-band transmitter	25
Figure 3.2 Multi-band transmitter block diagram (single PA).	28
Figure 3.3 Dual-band transmitters (a) Multiple (baseband + IFFT + DAC), single (stage-1IF mixer + combiner at IF + stage-2 RF mixer + PA), (b) Multiple (baseband + IFFT + DAC + mixer), low-power combiner at RF, and single PA, (c) Multiple (baseband + IFFT + DAC + mixer + PA), high-power combiner at RF.	29
Figure 3.4 Behavioural model extraction procedure: Key steps from measurement to model validation.....	32
Figure 3.5 Flow chart of the model’s identification in [15].....	37

Figure 3.6 Block diagram of the CR-BLMP model in [79].....	38
Figure 3.7 Previous work classification based on the LTE-A signal transmission type...	39
Figure 4.1 Memory polynomial model.....	42
Figure 4.2 The flow chart of the model in [85].....	48
Figure 4.3 The flow chart of the model in [16].....	49
Figure 4.4 The flow chart of the proposed model.....	50
Figure 4.5 Behavioural modeling block diagram	54
Figure 5.1 Measurement setup test scenarios.....	56
Figure 5.2 $NMSE_{dB}$ vs memory depth for scenario (1) with nonlinearity order =5	58
Figure 5.3 $NMSE_{dB}$ vs nonlinearity order for scenario (1) with memory depth =3	58
Figure 5.4 $NMSE_{dB}$ vs memory depth for scenario (2) with nonlinearity order =5 for low-band	60
Figure 5.5 $NMSE_{dB}$ vs memory depth for scenario (2) with nonlinearity order =5 for high-band	60
Figure 5.6 $NMSE_{dB}$ vs nonlinearity order for scenario (2) with memory depth =3 for low-band	61
Figure 5.7 $NMSE_{dB}$ vs nonlinearity order for scenario (2) with memory depth =3 for high-band	61
Figure 5.8 The spectrum of low-band with $M=3$ and $N = 5$	62
Figure 5.9 The spectrum of high-band with $M=3$ and $N =5$	63
Figure 5.10 The spectrum of the broadband with $M=3$ and $N= 5$	63
Figure 5.11 The spectrum of dual-band for low-band with $M=3$ and $N = 5$	64
Figure 5.12 A zoom section of figure 5.12	65

Figure 5.13 The spectrum of dual-band for high-band with $M=3$ and $N = 5$	65
Figure 5.14 A zoom section of figure 5.14	66
Figure 5.15 Condition number _{dB} vs non-linearity for scenario (1) with memory depth =3	67
Figure 5.16 Condition number _{dB} vs non-linearity for scenario (2) with memory depth =3 for low-band.....	68
Figure 5.17 Condition number _{dB} vs non-linearity for scenario (2) with memory depth =3 for high-band	68
Figure 5.18 A realistic condition number vs non-linearity for scenario (2) with memory depth =3 for low-band.....	69
Figure 5.19 A realistic condition number vs non-linearity for scenario (2) with memory depth =3 for high -band	70

LIST OF ABBREVIATIONS

3GPP	:	Third Generation Partnership Project
4G	:	Fourth Generation
ADC	:	Analog to Digital Converter
AM/AM	:	Amplitude Modulation to Amplitude Modulation
AM/PM	:	Amplitude Modulation to Phase Modulation
BPF	:	Band Pass Filter
CA	:	Carrier Aggregation
CC	:	Component Carrier
CoMP	:	Cooperative Multi-Point system
CPE	:	Client Premises Equipment
CR-BLMP	:	Complexity-Reduced Band Limited Memory Polynomial
DAC	:	Digital to Analog Converter
DC	:	Direct Current
DL	:	Down Link
DSP	:	Digital Signal Processing
DUT	:	Device Under Test

EVR	:	Error Variation Ranking
FDD	:	Frequency Division Duplex
GaN	:	Gallium Nitride
I	:	In-Phase
ICIC	:	Inter Cell Interference
IF	:	Intermediate Frequency
IM	:	Inter Modulation
IMD	:	Inter Modulation Distortion
IMT-ADV	:	International Mobile Telecommunication Advanced
ITU	:	International Telecommunication Union
LAA	:	Licensed Assisted Access
LNA	:	Low Noise Amplifier
LO	:	Local Oscillator
LPF	:	Low Pass Filter
LTE-A	:	Long-Term Evolution Advanced
LUT	:	Look-Up Table
MP	:	Memory Polynomial

MTC	:	Machine-Type Communications
NMSE	:	Normalized Mean Squared Error
PA	:	Power Amplifier
PAPR	:	Peak-to-Average Power Ratio
PD	:	Predistorter
Q	:	Quadrature
RAN4	:	Radio Access Network Working Group 4
RF	:	Radio Frequency
RFC	:	Radio Frequency Carrier
TCP	:	Transmission Control Protocol
TDD	:	Time Division Duplex
UE	:	User Equipment
UL	:	Up Link

ABSTRACT

Full Name : MOHAMMED ABDALLA ABDELRAHIM ALI
Thesis Title : Behavioural Modeling of Concurrent Dual-Band Power Amplifiers
Major Field : Master of science in electrical engineering department
Date of Degree : November 2016

Because of the expanding need for high capacity communication networks and high performance wireless transmitters, multi-band/multi-standard transmitter architectures become a primary part in present day communication systems. Thus, advances in the design techniques of radio frequency (RF) power amplifiers (PAs) have promoted the wireless transmitter to use single multi-band PA and RF components in order to concurrently process multiple input signals located in different frequency bands. |

In this thesis, a comprehensive analysis and different digital signal processing (DSP) solutions are studied for distortion mitigation of RF PAs in single-band, wideband and dual-band transmitters. Furthermore, the problem of amplifiers' distortions are more highlighted in dual-band transmitters, where two reference models are investigated against the proposed model. These different RF behavioral models are investigated based on memory polynomial. From the results, it has been found that the new dual-band model improves the complexity and the robustness by 33.5% and 18.4%, respectively against the previously reported memory polynomial based models in addition to highlighting the advantage of using dual-band models over the wideband transmitter.

ملخص الرسالة

الاسم الكامل: محمد عبدالله عبدالرحيم علي

عنوان الرسالة: تصميم نموذج متزامن لمضخم الإشارة اللاخطي مزدوج النطاق

التخصص: الهندسة الكهربائية

تاريخ الدرجة العلمية: نوفمبر ٢٠١٦

بسبب الحاجة لشبكات إتصالات ذات عرض نطاق ترددي واسع وأجهزة إرسال لاسلكية عالية لأداء، بنية الإرسال مزدوج النطاق والمعايير أصبحت جزء أساسي في نظم الإتصالات في وقتنا الحالي. ولذلك، فإن التقدم في تصميم تقنيات تردد الراديو ومضخم قدرة لا خطية قد روج لإستخدام نظام الإرسال مزدوج النطاق من أجل معالجة الإشارات المتزامنة والتي تقع في نطاقات ترددية مختلفة.

في هذا البحث، يتم التحقق والتحليل وتحصيل حلول مختلفة لمعالجة الإشارة الرقمية في عيوب تقنية تردد الراديو وتصميم نظام اتصالات لاسلكية أحادية النطاق، عريضة النطاق أو مزدوج النطاق من أجل تقييم ودراسة الإنبعثات والمخرجات خارج النطاق المحدد للإشارة وكيفية الوصول إلى نتيجة بإشارة مضخمة من الإشارة المدخلة مروراً بمضخم إشارة القدرة اللاخطية بأقل تأثير للضجيج والتشويه في الإشارة. فضلاً عن ذلك، يتم التركيز في عيوب اجهزة الارسال مزدوج النطاق حيث يجرى التحقيق في نماذج مرجعية ضد النموذج المقترح. تم التحقيق في مختلف نماذج الإرسال لتردد الراديو باستخدام نموذج الذاكرة متعدد الحدود باستخدام ثلاث عوامل مختلفة (تطبيع متوسط مربع الخطأ، مقياس العدد الشرطي وطيف طاقة الإشارة المخرجة). وفقاً لنتائج المحاكاة التي تم إجراؤها، قد ثبت ان نموذج مزدوجة النطاق الجديد يحسن التعقيد وقوته بنسبة ٣٣,٥% و ١٨,٤% على التوالي ضد نماذج النطاق المزدوج ذو الذاكرة المتعدد الحدود الأخرى بالإضافة الى إبراز مزايا استخدام نماذج إرسال الموجة المزدوجة النطاق على النطاق العريض.

CHAPTER 1

INTRODUCTION

The growth of the wireless industry has been tremendous since the beginning of the last decade, while the thirst for higher data rates has been unquenchable. The proliferation of service providers as a result of this extensive growth, along with the integration of voice and data services, has made the radio frequency (RF) spectrum a rare and valuable commodity. The important question for all commercial communication system manufacturers is “*How do we squeeze as much data as possible in a given portion of the RF spectrum?*” The answer to this question has led researchers to digital modulation schemes that are more bandwidth-efficient, i.e., carry more bits per hertz when compared with a narrowband modulation. This enhancement, however, comes at a cost. The rapidly time-varying envelope of the resultant modulation is unsuitable for a nonlinear RF transmitter, or in particular, a power amplifier (PA).

1.1 Why Linear Amplifiers?

The linearity requirement in a PA is based on the following simple rule: a linear modulation should be processed by linear blocks to limit distortion. With a nonlinear transmitter, the fluctuating envelopes of linear modulation schemes receive non-uniform amplification within the compression region, generating inter-modulation (IM) products.

These products cause out-of-band emissions and in-band distortion, and are known as Inter-Modulation Distortion (IMD). Out-of-band emissions, or spectral regrowth, result in an

increased transmission bandwidth, and act as interference in adjacent channels, thus degrading the system level performance. In-band distortion causes self-interference, which appears as a distortion in the signal constellation.

1.2 Distortion in RF Transmitters

There is a different source of distortion coming from the direct conversion of the transmitter architecture as shown in Figure 1.1[1], the most prominent imperfections are static and dynamic distortion due to mixer and PA nonlinearities [2], image-frequency interference due to in-phase/quadrature (I/Q) imbalance in modulators and non-constant group delay variations in band-pass filters. This thesis is focused on the distortion sources created by the PA as the primary sources of distortion in wireless transmitters [3], [4].

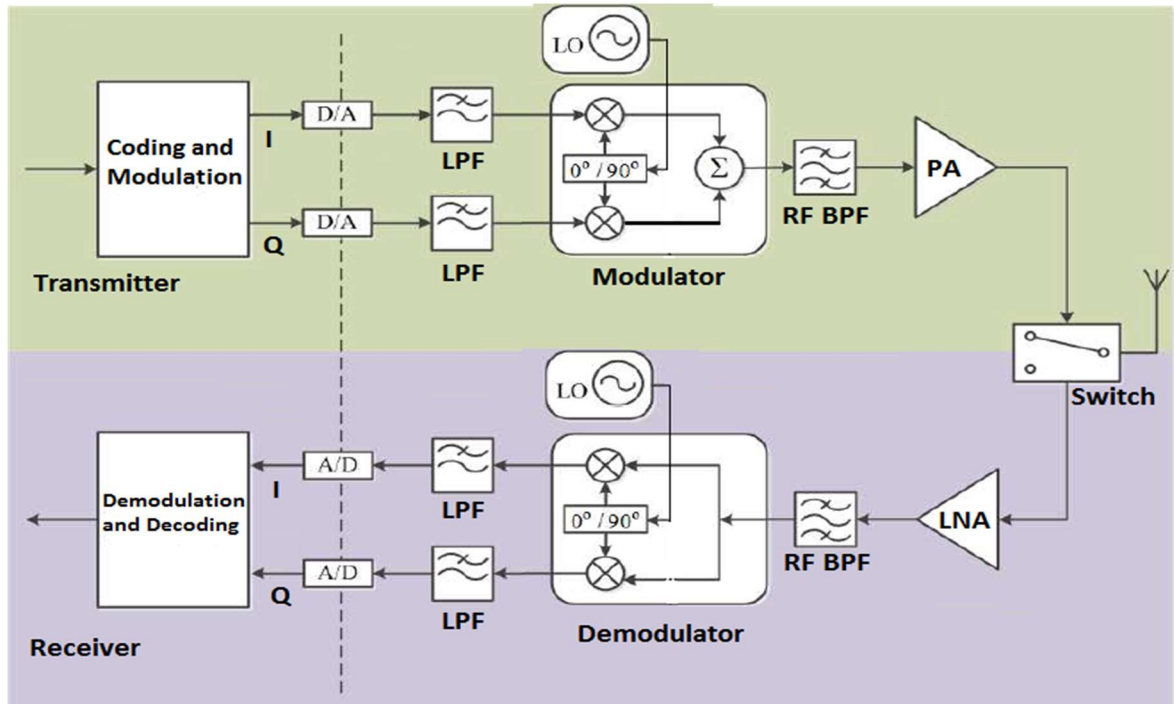


Figure 1.1 Block diagram of direct conversion transceiver

1.2.1 Power Amplifiers Nonlinearity

Wherever there is wireless communication, there are transmitters, and wherever there are transmitters, there are RF PAs [2]. Ideally, a PA is required to amplify signals before they are sent out on the airwaves in a way that results in a constant gain over the entire dynamic range, and frequency spectrum, of the input. Unfortunately, this is not possible for input signal levels approaching the rated value of a PA since it starts to saturate, resulting in gain compression or reduction in available gain. In addition, the input signal experiences phase variations near the compression region, causing synchronization error for analog modulations, or additional skewing of the signal constellation in the case of a digital modulation. A common artifact of amplifier distortion is spectral regrowth in the output spectrum. Figure 1.2 demonstrates a spectrum regrowth in a Long –Term Evolution (LTE) signal following nonlinear amplification.

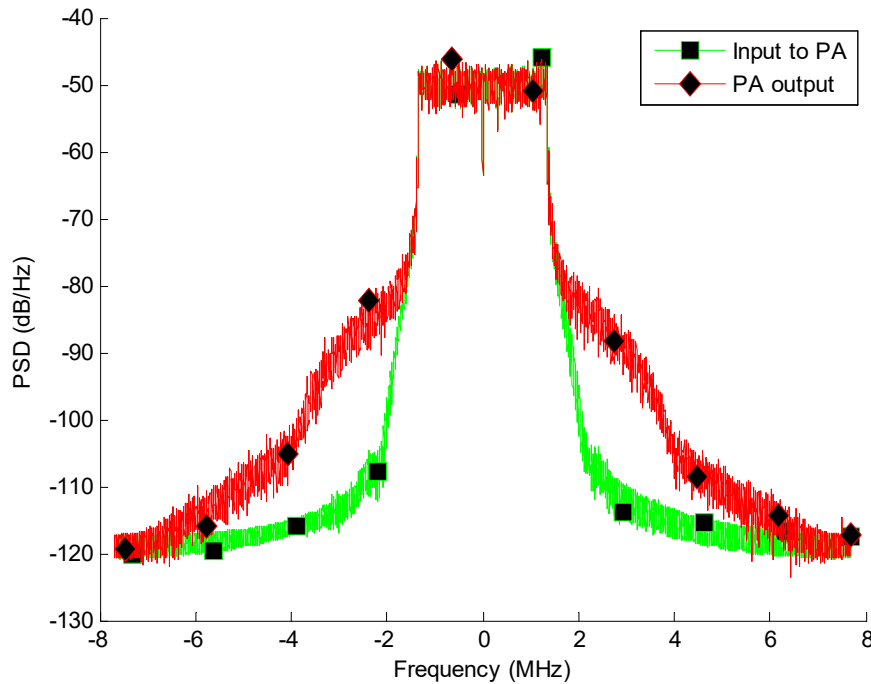


Figure 1.2 Spectral regrowth in a single-carrier LTE-A

One of the key components of the front-ends of wireless transceivers is the RF PA, which is also the main device that generates unwanted nonlinear distortions [2], [5]. The main purpose of this component is to amplify the radio signal to necessary power level at the transmitter to reach the destination. PAs have various classes of operation (e.g. A, AB, B, C, D and F etc.), with respect to their linearity and power efficiency.

The main motivation for linear systems is that the power transmitted by the base station is limited to an allocated channel of a confined bandwidth. However, for the PAs to operate efficiently, they have to be operated as close as possible to the saturation region to maximize its power efficiency. Thus, the PAs exhibit undesired nonlinear behavior that generates distortions over a bandwidth three to five times the allocated channel bandwidth. As today's wireless communication systems have developed to become more spectral efficient, where signals utilize high peak-to-average power ratio (PAPR). The high PAPR signals are caused by complex modulation and generate rapid change in the magnitude of signals. These varying envelope signals cause amplitude modulation to amplitude modulation (AM-AM) and amplitude modulation to phase modulation (AM-PM) distortions as well as spectral regrowth in the adjacent channels when amplified by nonlinear PAs. Therefore, the use of high PAPR signals results in PA operating at a large enough back-off to satisfy the stringent linearity requirement at the expense of degraded efficiency [6]. Therefore, linearization and efficiency enhancement techniques must be employed [5], [7], [8], [9].

1.3 Carrier Aggregation Configurations

Today's development applies at flexible and forward-looking technologies. For example, carrier aggregation (CA) will enable operators, vendors, content providers and the rest of the mobile ecosystem to meet this growing demand. CA is a major feature to meet the international mobile telecommunication advanced (IMT-ADV) requirements for fourth-generation [4G] wireless network deployments [10]-[12], where multiple component carriers of smaller bandwidth are aggregate. CA is an attractive alternative to increasing the data rate. Additional advantages are offered by CA in terms of spectrum efficiency, deployment flexibility, backward compatibility, and more. Having wideband modulated signals with a high PAPR could bring numerous challenges to the design aspects of transmitter linearity, output power gain, and overall efficiency. The efficiency of the CA mechanism comes with an extra focus on the transmitter architecture design and achievable efficiency. With regards to the acknowledgment of CA techniques, the architecture of the transmitter is of high priority [13].

CA combinations are separated to the contiguous intra-band, the non-contiguous intra-band and inter-band. Figure 1.3 demonstrates the three potential scenarios of the CA. The contiguous intra-band CA configuration refers to CA on the same operating band. The non-contiguous intra-band CA configuration indicates to CA in the same operating band but separated by off-carriers. The last configuration (inter-band) indicates to aggregation of component carriers in various operating bands, where in each band it can be non-contiguous or contiguous. The space between two contiguous CCs center frequencies is $N \times 300$ kHz (where N is integer), in the non-contiguous situation, the CCs are isolated by one, or more of the frequency gap(s).

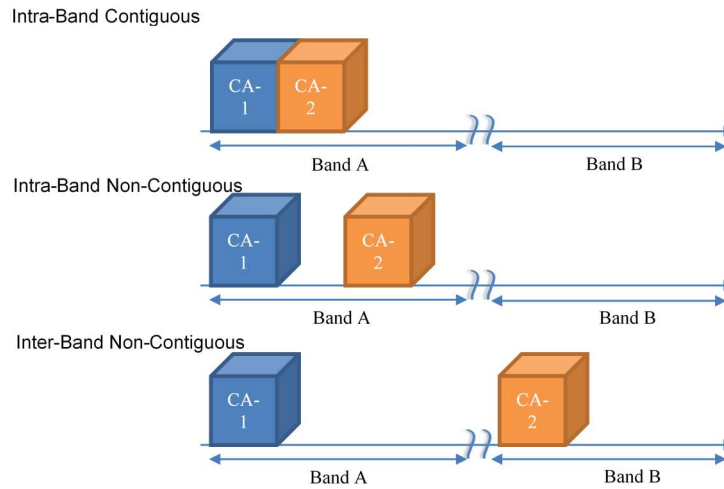


Figure 1.3 Carrier aggregation scenarios

If carriers are at different frequency bands, they have different propagation losses and different interfering systems, all of which affect achievable data rates, transmit power and usage of resources. As for instance, a user equipment (UE) on the edge of the cell site may get better served by a carrier of a low-frequency, while a high-frequency carrier is a better fit for a UE close to the site, the inter-band CA gives extra flexibility to use allocations fragmented spectrum[14].

From RF perspective, contiguous intra-band CA have similar properties as a corresponding wider carrier being transmitted. The inter-band architecture represents a major challenge for UE design as various simultaneous chains have to co-exist.

CA will assume a key part in evolving the IMT-Advanced and the use of emerging allocations spectrum. There additionally will be various and varying deployments of CA to operators' particular requirements.

This seemingly basic idea will stretch the realm of network in addition to device implementation. Strong cooperation over the industry for more evolutions and optimization will make CA as standard technology.

1.4 Transmitter Architectures

Either to use single or multiple PAs, the output power dynamics are correlated to the UE architecture chosen. Figure 1.4 layout different implementation options for PA architectures considered by 3GPP (Third Generation Partnership Project) that can support different types of CA.

Taking a different architectural design, when it comes to CA, the fundamental design choices are essentially either a wideband or multi-band approach. Different transmitter topologies are given in [15]-[21]. Figure 1.4 gives the different transmitter architectures choices according to where component carriers (CCs) are combined, either at the digital baseband, before the RF mixer, after the mixer also before or after the PA and end with a matching network (or circulator network) which duplexes two signals into one channel (e.g. transmit into an antenna).

1.4.1 Single-Branch Transmitters

Figure 1.4 (a) presents a conventional architecture of single band transmitter that consists of a digital baseband processing unit, a single-band RF PA, filters, and other transmitter sub-systems. The RF front-end can be one of the traditional architectures; direct conversion [22], super-heterodyne, or low-IF (Intermediate Frequency) [23]. This single-branch architecture is suitable for contiguous intra-band CA.

1.4.2 Multi-Branch Transmitters

The recent technologies nowadays are evolving towards the concurrent transmission of multicarrier signals at different frequency bands in order to accommodate different standards simultaneously. Indeed, novel transmitter designs allow for different communication signals to be transmitted on different frequency bands, concurrently. Therefore, for multi-band transmission, the conventional single-band transmitter in Figure 1.4 (a) is modified using different topologies as shown in Figure 1.4 (b) and Figure 1.4 (c).

The power amplification unit is the main building block of the transmitter RF front-end in these different topologies. The transmitter architecture in Figure 1.4 (b) is considered as multi-branch transmitter (separate RF PAs), while the transmitter architecture in Figure 1.4(c) is considered as a multi-band transmitter architecture (single PA).

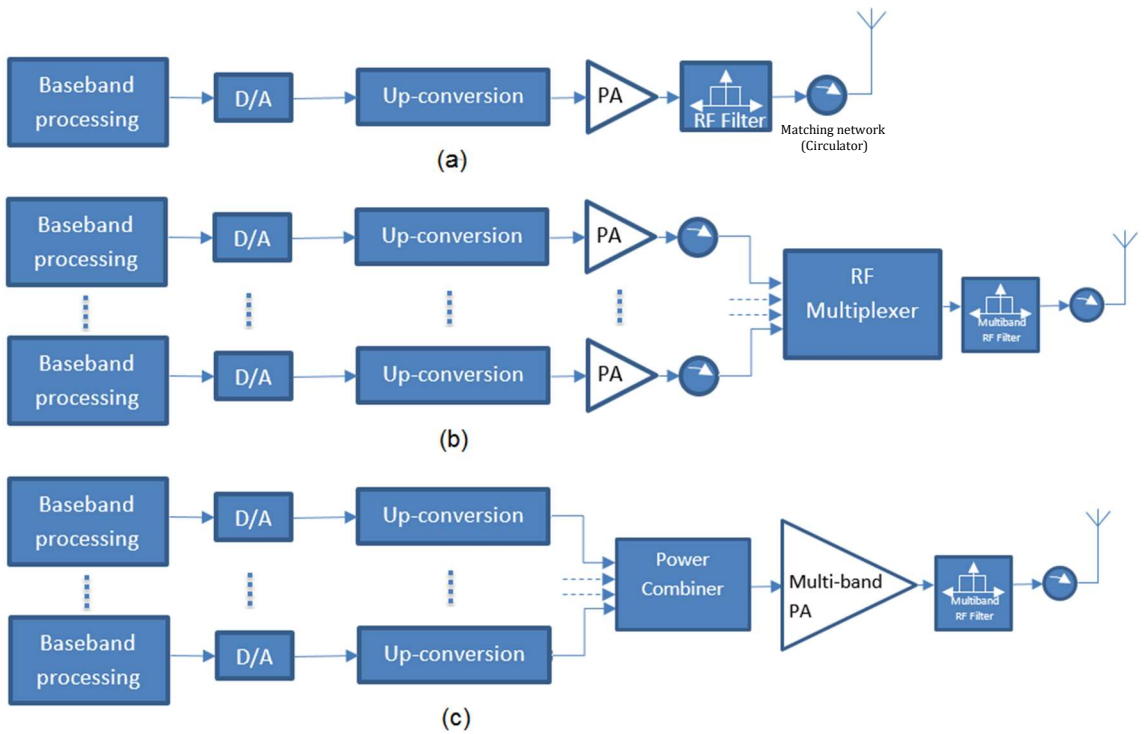


Figure 1.4 Transmitter architectures: (a) single RF branch transmitter, (b) multi-branch RF transmitter including multi band final stage, (c) multi-band RF transmitter architecture.

In Figure 1.4 (b), every RF chain gets its own power amplification stage. At the output of the power amplification stages, the RF signals are combined by using a multiplexer which selects one of several input signals and forwards it into a single line which work as a band selector and after then go through a multi-band RF filter. In this architecture, a linearization unit is required for the compensation of the PA nonlinear distortion in each branch, separately. In order to design more compact and efficient transmitter topologies, a single PA with the multi-band operation is designed in order to replace the different single-band PAs each of which is working at a single operating frequency.

Figure 1.4 (c) presents the multi-band architecture with one PA that could operate at different frequency bands. In this architecture, the RF signals are generated using different modulators and then combined by using a low power combiner instead of the high power combiner of Figure 1.4 (b). The signal at the output of multi-band PA is filtered with the use of a multi-band RF filter.

The quantity of PAs and the position of power combination module before or after the PA affect the overall efficiency of the two transmitters shown in Figure 1.4 (b) and (c). The loss and distortion at the output of the two transmitters are also affected by the two different topologies. The multi-band transmitter architectures are designed to have a flat frequency response among the desired frequency bands. However, a high efficiency and output PA design is difficult when the upper and lower limits of the required frequency bands are further apart. Finally, the multi-band amplifier shown in Figure 1.4 (c) consists of a single amplification device and variable matching networks that can be changed. The multi-band architecture can be designed for different frequency bands as the multi-branch architectures in Figure 1.4 (c).

1.5 Linearization of Nonlinear Amplifiers

The efforts to limit the amount of distortions introduced by an amplifier has been continuing since the advent of power amplification theory itself. The simplest scheme for limiting distortions is to operate a PA in its linear region using “power back-off”, or downscaling of the input signal power. However, the linear region of the PA has a very poor power conversion efficiency [5]. As a result, amplifiers operating at large output power back-off have to be used, which results in increased maintenance cost as the number of base stations per square mile continues to increase. The battery life for handsets is also reduced with such a power back-off scheme, which is unacceptable for the wireless industry as it works on introducing more features in smaller portable units requiring longer battery lives. Thus, power back-off is not a solution for most transmitters today.

Linearization schemes process the signal in a transmitter chain so that the signal at the output of the transmitter is a linearly amplified version of its input. All linearizers use amplitude and phase of the input as a reference for comparison with the output, and use the difference in some form to cancel the IMD. This can be achieved by the complexity of the system, the bandwidth of operation, the performance, and the implementation issues. A common linearization techniques can be used such as feedback schemes, feedforward amplifiers, and predistortion [19].

Not all linearization schemes are suitable for a digital implementation, which is convenient with the growth of digital signal processing technology and software-defined radio architectures. This research effort is focused on digital predistortion. This form has distinct advantages with current digital reconfigurable architectures.

1.6 Understanding Distortion Effects in Multi-band Transmitters

Figure 1.5 shows the output spectrum components of a dual-band nonlinear transmitter when driven with a signal of two-tone in every band. Thus, the nonlinear behavior of transmitter is much more noticeable in dual-band system, in which two modulated signals that are separated in carrier frequencies by $\Delta\omega$ are transmitted simultaneously. The operation of dual-band PA systems result in inherent in-band and cross-band distortions, which are more critical than the spectral regrowth and inter-modulation products distortions observed at the output of single-band transmitters [24],[25].

As shown in Figure 1.5, the output distortion of dual-band transmitters can be categorized into different groups. These groups are the in-band inter-modulation products, the cross-modulation products, and the out-of-band inter-modulation products. The important group consists of the inter-modulation products over every frequency in the carrier band that are caused by the nonlinearity of the PA, similar to what it is in single-band transmitters [26]-[30].

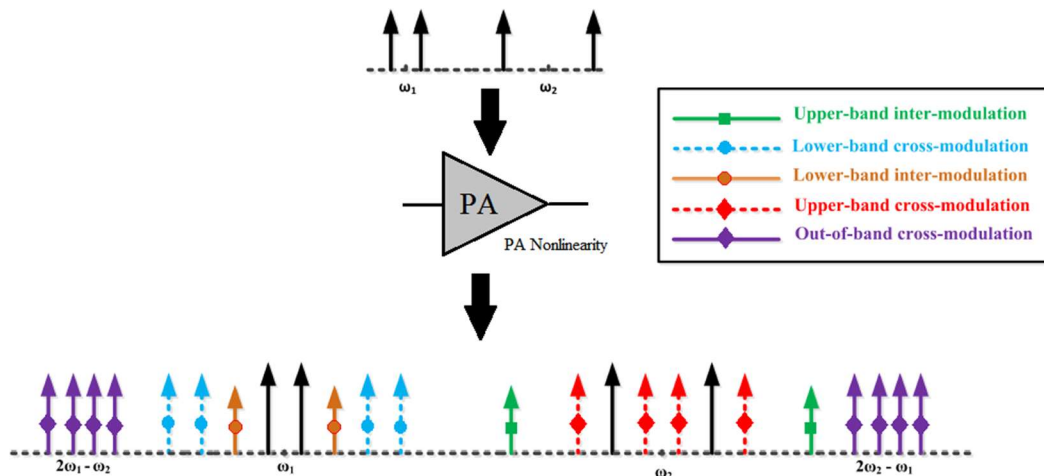


Figure 1.5 The dual-band transmitter power spectrum output

1.7 Motivation and Contributions

PAs have nonlinear characteristics in the most efficient region of operation. Any signal whose envelope is fluctuating inside this region is severely distorted depending on the variance of those fluctuations. The critical trade-off to be made is between linearity and efficiency of a PA and, not surprisingly, the trade-off becomes increasingly complex as the modulation bandwidth increases.

The evolution of the wireless communication market towards higher data rate and more users drives communication systems toward increased capacity. However, the benefit of increased spectrum efficiency is offset by the required fidelity of the digital modulated signal through the transmitter, particularly through the RF PA. The behavioural modeling for the concurrent dual-band PA is a critical problem in practical applications. The nonlinear distortion is quite different from that in the conventional single-band PA, but with careful modeling, the dual-band transmission can give a promising result with better performance than the single-band case and can be comparable with the broadband transmission.

Dual-band transmitter architectures are a straightforward approach to increase the data rates with diversity of the wireless system, and can allow the transmission of various wireless communication signals. Therefore, they are an attractive solutions due to their strong application potential for CA LTE-Advanced systems, especially in concurrent modes of operation. The scope of this thesis is to analyze the nonlinearities in the concurrent dual-band PA by benchmarking different memory polynomial models, and to introduce an enhanced model where the memory and the distortions are the main effects.

The key contributions of this thesis can be summarized as follows:

- Study the different distortions to compensate for in a dual-band transmitter. This includes the inter-modulation and cross-modulation products in PAs.
- To develop a new variant of a memory polynomial behavioural model for the dual-band RF PAs and analyze its performance and benchmark it against the previously reported models for the dual-band PAs.

CHAPTER 2

DISTORTION IN LTE-A TRANSMITTERS

Any system, mechanical, electrical, or electro-mechanical, has two basic regions of operation: a desired region and an undesired region. In order to optimally use a system, careful understanding of its behavior during optimal and suboptimal operation is critical. Likewise, proper understanding of the working of a PA, along with the distortion introduced during its operation, is necessary for maximizing efficiency while keeping distortion at a minimum.

This chapter begins with a discussion of the basis of the signal that has been used recently in wireless mobile communication (LTE-A signal) and the evolution of the CA, then a discussion on the analysis of distortions in a PA follows.

2.1 LTE-A Basics

The LTE-A have been introduced by 3GPP [31], [32] as a requirement for IMT-ADV systems set by the International Telecommunication Union (ITU) [33], [34]. This includes modifying new capabilities to have a wide range of telecommunication services and applications, and surely improved the worldwide development and the quality of services. It is not only about faster data rates, but additionally incorporates new protocols for the transmission that enable easy handoffs among cells, increment throughput at cell ends, and put more bits per second into each Hertz of the spectrum. This will end with a higher network capacity, extra consistent connections, and inexpensive data. LTE-Advanced

gives high data rates over the premier releases of LTE. In the meantime, the spectrum usage efficiency has been enhanced. This only can't give the required data rates (1 Gbps) that are being featured for 4G LTE Advanced. To accomplish these high data rates, it will be important to increment the transmission data transfer bandwidths above those that can be supported by a single carrier or single channel. With work beginning on LTE-Advanced, various key requirements and key features are becoming visible. Until release 10 of LTE-A requirement [35], it allows the aggregation of a maximum of five component carriers in addition to a bandwidth up to 20 MHz each to achieve a bandwidth aggregate transmission up to 100 MHz [36],[37]. Yet, 3GPP's RAN4 (RAN Working Group 4), which is in charge for setting performance requirements, as of now limits aggregation to two element carriers [38]. To guarantee backward compatibility, every carrier is designed to be compliant with the 3GPP most recent Release (Rel-12) [39]. Each of the CAs can also use different bandwidth. In fact, it can give one of these six supported bandwidths inside LTE (1.4, 3, 5, 10, 15 or 20 MHz). This obviously relies on the availability of spectrum to every individual system operator. There are a lot of development goals for LTE Advanced. Their real figures and the real implementation of them should be worked out during the specification phase of the system. LTE is deployed on a wide scale, giving mobile broadband services to a huge number of people. The premier LTE deployments depend on the basic set of LTE specifications, releases 8 and 9 [40], [41]. However, after some time, more advanced features from later releases of the LTE specifications have been deployed. Release 10 expanded and improved LTE radio-access technology in a various dimensions. The most public feature was the introduction of CA to enhance the possibility of using fragmented spectrum allocations and support wider bandwidth – and higher data rates – than the initial

LTE releases. LTE keeps evolving [35], [39]-[42], and 3GPP is now working on release 13. This release will enhance and upgrade LTE in various portions, and support its capacity to serve as a stage for the networked society by giving information/data access and sharing at anyplace and anytime for anybody and anything. Figure 2.1 presents the 3GPP Release status for carrier aggregation.

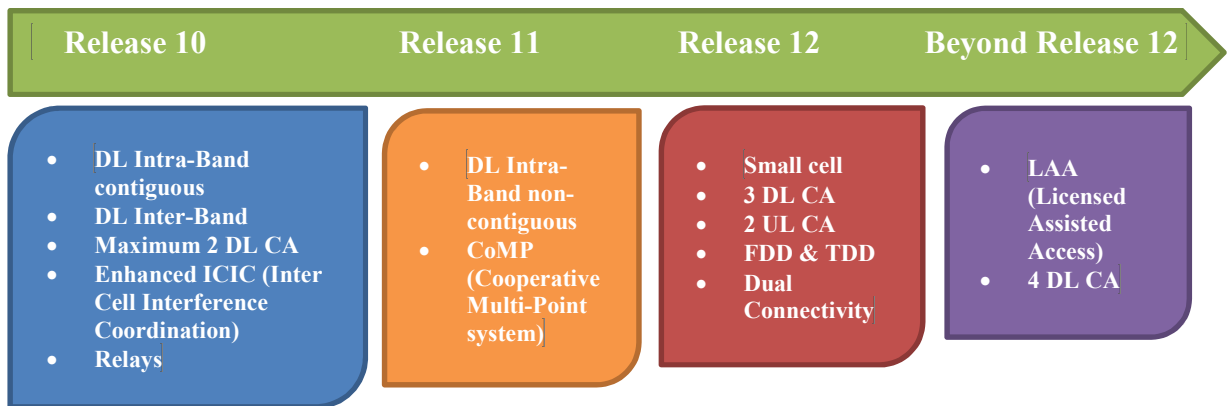


Figure 2.1 LTE evolution, 3GPP release status for carrier aggregation

2.1.1 Evolution of Carrier Aggregation as a Part of LTE-A Feature

3GPP Rel-10 is the first release to support CA. It defines a limited variety of CA configurations, including: contiguous intra-band CA for band 1 as frequency division duplex (FDD) and band 40 as time division duplex (TDD) named CA_1C and CA_40C, respectively, and an inter-band CA between bands 1 and 5, named CA_1A-5A, where (A) and (C) are two of a different supported bandwidth classes [35].

3GPP Rel-11 offers many more CA configurations, including non-contiguous intra-band CA and Band 29 for inter-band CA, which is also referred as supplemental downlink (DL).

Band 29 is a special FDD band in Rel-11 that has only a DL component and no uplink (UL) component [42].

Release 12 included CA of FDD and TDD frequency bands, as well as support for aggregating two UL CCs and three DL CCs. Note that even though certain CA combinations are specified in later releases, these are release independent and can be supported from previous releases' equipment due to backward-compatible signaling. 3GPP Rel-12 offers aggregation of three DL CCs, support for CA configurations for UL inter-band and intra-band non-contiguous CA and band 32 support (1.5GHz L Band), which has a DL component only and further enhanced capabilities that are still under study. In FDD, the number of aggregated carriers can be different in DL and UL, which is also referred to as asymmetric configuration. However, the number of UL component carriers is always equal to or lower than the number of DL component carriers. In the general case, the individual component carriers of DL and UL can also be of different bandwidths. However, in Rel-10, Rel-11 and Rel-12, there are limitations requiring the UL CC bandwidth to be the same as the DL CC bandwidth. The same requirements apply for TDD. [39].

The vision of the networked society, where anything that advantages from being connected will be united, puts new requirements on connectivity. LTE development is a key component in this vision. The next step in this development is LTE release 13. Improvements in this release include licensed assisted access (LAA) [43], which utilizes the CA framework to exploit unlicensed spectrum as a complement. These enhancements will improve total capacity as well as client data rates. Latency reductions in release 13 will also help exploit these very high data rates, in combination with higher-layer protocols such as transmission control protocol (TCP). In the meantime, LTE will extend into new

usage scenarios by giving improved extent for low cost and energy-productive massive machine-type communications (MTC) devices through reduced RF bandwidth. Enhancements in direct device-to-device communication will give progressed support for public safety and also different commercial use cases. Obviously, LTE is an exceptional platform that is constantly evolving to address new requirements and more scenarios.

2.2 Inter-Modulation Distortions in Nonlinear Power Amplifiers

The two-carrier analysis represents the traditional way to analyzing nonlinear effects of RF PAs. Fortunately, when making a two-tone test, the signal distortion is relatively easy to spot than the one tone test. Two-tone testing consists of applying two non-harmonically related signals of approximately equal amplitude to the transmitter. The result, in a linear transmitter, is an RF output that varies from zero to maximum at a rate determined by the difference in frequency between the two inputs. As an initial step, considering a weakly nonlinear amplifier in which input and output voltages can be related utilizing the standard power series formulation:

$$y(t) = a_1x(t) + a_2x^2(t) + a_3x^3(t) + a_4x^4(t) + a_5x^5(t) \quad (2.1)$$

where x and y represent time varying RF input and output signals, respectively. For the sake of simplicity, the a_n coefficients are taken to be scalar amounts which describe the amplifier and are determined experimentally. As a rule, one set of coefficients will apply for a fixed set of biasing and operating conditions.

Now, for an input signal consisting of two, equal amplitude, in-band RF Carrier (RFC) signals, whose spacing is much smaller than either RF frequency:

$$x(t) = A\cos(\omega_1t) + A\cos(\omega_2t) \quad (2.2)$$

where $\omega_1 > \omega_2$.

The output voltage will be:

$$\begin{aligned}
 y(t) &= a_1 A [\cos(\omega_1 t) + \cos(\omega_2 t)] \\
 &+ a_2 A^2 [\cos(\omega_1 t) + \cos(\omega_2 t)]^2 \\
 &+ a_3 A^3 [\cos(\omega_1 t) + \cos(\omega_2 t)]^3 \\
 &+ a_4 A^4 [\cos(\omega_1 t) + \cos(\omega_2 t)]^4 \\
 &+ a_5 A^5 [\cos(\omega_1 t) + \cos(\omega_2 t)]^5
 \end{aligned} \tag{2.3}$$

And taking the expansion of the second degree in equation (2.3) as an example will be:

$$a_2 A^2 [\cos(\omega_1 t) + \cos(\omega_2 t)]^2 = a_2 A^2 \left\{ \begin{array}{l} 1 + \frac{1}{2} \cos(2\omega_1 t) \\ + \frac{1}{2} \cos(2\omega_2 t) \\ + \cos[(\omega_1 + \omega_2)t] \\ + \cos[(\omega_1 - \omega_2)t] \end{array} \right\} \tag{2.4}$$

Each line of equation (2.3) represents a degree of signal distortion. Every level of distortions creates a various number of distortion products, which have either the same or lower orders. For instance, the second degree term creates second order products at frequencies $2\omega_1, 2\omega_2, \omega_1 \pm \omega_2$; the fourth degree term yields fourth order products at $4\omega_1, 4\omega_2, 2\omega_1 \pm 2\omega_2, 3\omega_1 \pm \omega_2, 3\omega_2 \pm \omega_1$, additionally yields second order products at $2\omega_1, 2\omega_2, \omega_1 \pm \omega_2$. As a rule, the even order distortion terms will be well out of band and are of less concern than the odd order distortion terms. Table 2.1 demonstrates the expanded form of equation (2.3) that contains all of the distortion products up to and including the fifth order [17].

The products of most interest are the inter-modulation of the 3rd order, at frequencies ($2\omega_1 - \omega_2$ and $2\omega_2 - \omega_1$), which come basically from the third degree term and have amplitudes

$(3/4.a_3.A^3)$. It likewise has parts which come from higher odd degree terms in the power series expansion. In this manner, the fifth degree terms, not just contribute near-to-carrier fifth order inter-modulation items (at frequencies $3\omega_2- 2\omega_1$, $3\omega_1- 2\omega_2$ and amplitudes $(5/8.a_5.A^5)$) but additionally add a contribution to the third order inter-modulation products (amplitude $(5/8.a_5.A^5)$).

Table 2.1 Two-carrier distortion products up to fifth degree (expansion of equation (2.3))

	$a_1.A$	$a_2.A^2$	$a_3.A^3$	$a_4.A^4$	$a_5.A^5$
(DC)		1		9/4	
ω_1	1		9/4		25/4
ω_2	1		9/4		25/4
$2\omega_1$		1/2		2	
$2\omega_2$		1/2		2	
$\omega_1 \pm \omega_2$		1		3	
$2\omega_1 \pm \omega_2$			3/4		25/8
$2\omega_2 \pm \omega_1$			3/4		25/8
$3\omega_1$			1/4		25/16
$3\omega_2$			1/4		25/16
$2\omega_1 \pm 2\omega_2$				3/4	
$3\omega_2 \pm \omega_1$				1/2	
$3\omega_1 \pm \omega_2$				1/2	
$4\omega_1$				1/8	
$4\omega_2$				1/8	
$3\omega_1 \pm 2\omega_2$					5/8
$3\omega_2 \pm 2\omega_1$					5/8
$4\omega_1 \pm \omega_2$					5/16
$4\omega_2 \pm \omega_1$					5/16
$5\omega_1$					1/16
$5\omega_2$					1/16

Figure 2.2 brings graphical derivation of second and third order intercept points. The third order intercept point (IP3) is a widely used metric in PAs, which gives information about the linearity of an amplifier. A higher IP3 means better linearity and lower distortion generation. It is the theoretical point at which the desired output signal and undesired third-order IM signal are equal in levels considering an ideal linear gain for the PA. The theoretical input point is the input IP3 (IIP3) and the output point is the output IP3 (OIP3). For solid state PAs, the third order output intercept point is typically 10dB higher than output power at the 1dB compression point.

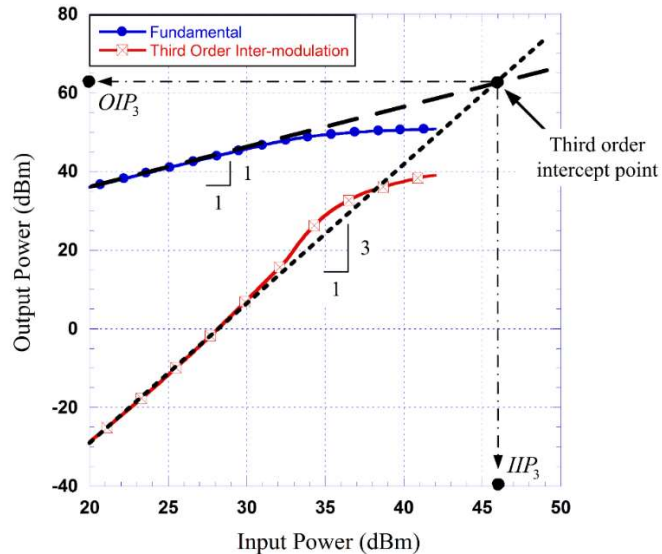


Figure 2.2 Graphical definition of the third order intercept point [14]

The fifth order intercept point is defined in the same way by considering the extrapolated linear portions of the output power at the fundamental frequency and the output power at the frequency corresponding to the fifth order inter-modulation products (for example,

$P_{out,3f_1-2f_2}$). In this case, the $P_{out,3f_1-2f_2}$ vs. P_{in} characteristic will have a 5:1 slope.

These higher degree orders can be disregarded when operating well below the compression level. However, it can turn into the dominant contributors in the compression and saturation regimes.

Figure 2.3 depicts the frequency content at the output of a PA driven by a two-tone signal. The inter-modulation sidebands appear at either side of every carrier, at a frequency spacing equivalent to that of the two input carriers. Some work has been done on modeling the harmonics at the output of PA in time domain as well as frequency domain. The carrier to inter-modulation distortion ratio (C/IMD) is a metric that quantifies the amount of distortion at the output of a PA driven by a two-tone, or in a more general case, a multi-tone test signal. It represents the ratio (in a linear scale) or equivalently the difference (in a logarithmic scale) between the power at the fundamental frequency (carrier) and the power generated at an inter-modulation frequency. The C/IMD is expressed in decibels relative to the carrier (dBc).

For an amplifier driven by a two-tone test signal at frequencies f_1 and f_2 (with $f_1 < f_2$), inter-modulation frequencies of interest commonly are the lower and upper third order inter-modulations ($2f_1 - f_2$ and $2f_2 - f_1$, respectively) and fifth order inter-modulations ($3f_1 - 2f_2$ and $3f_2 - 2f_1$, respectively).

Figure 2.3 presents the power spectrum (in dBm) at the output of a memoryless PA having a fifth order nonlinearity and driven by a two-tone test signal at frequencies f_1 and f_2 (with $f_1 < f_2$). This figure graphically defines the lower and upper carrier to third order

inter-modulation distortion ratios (C/IMD_{3L} and C/IMD_{3U} , respectively) and those of the fifth order [18].

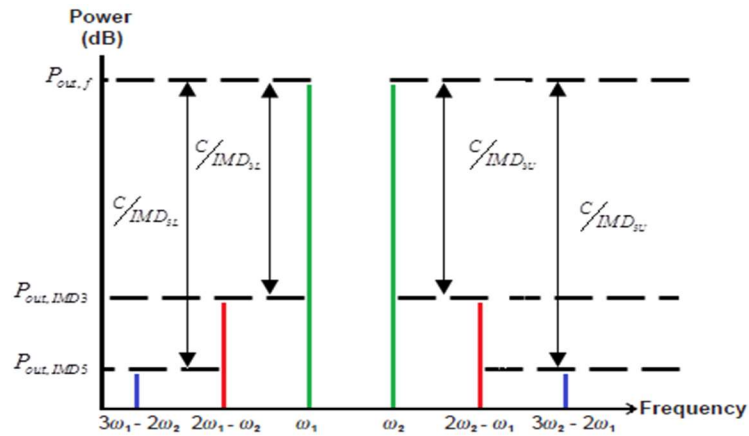


Figure 2.3 Two-carrier in-band inter-modulation spectrum

This analysis assumes two separate carriers with fixed spacing. Practically speaking, such a signal will usually be the result of the amplitude modulation of a single carrier, the two-carrier signal would be the spectrum from a double sideband suppressed carrier AM system, with a single, fixed frequency modulating tone. Practically speaking, even a basic AM transmitter of this kind would have a modulation band that would randomly fill a prescribed bandwidth either side of the carrier frequency. The key point to note is that the in-band inter-modulation products stretch out three times of the original modulation band limits, in the case of the third-order distortion products, and five times these limits for fifth-order, as appeared in Figure 2.4. Likewise, the spectrum resulting from nonlinear amplification has a stepped appearance, with every step corresponding to a higher order of distortion. These steps have more recently become known as spectral regrowth sidebands, although there is nothing at all recent about the nature of the phenomenon. This is not an issue as far as measurement is concerned, because the distortion levels can be measured

where they emerge from the main spectral zone. Spectral regrowth, or inter-modulation distortion, is often looked to be strongly an issue of adjacent channel interference, because of the way that PA linearity is also given in terms of demodulation error rates. In appendix A, table A-1 gives the 2nd, 3rd and the 5th harmonics, 2nd, 3rd and 5th IMD ranges under Rel-12.

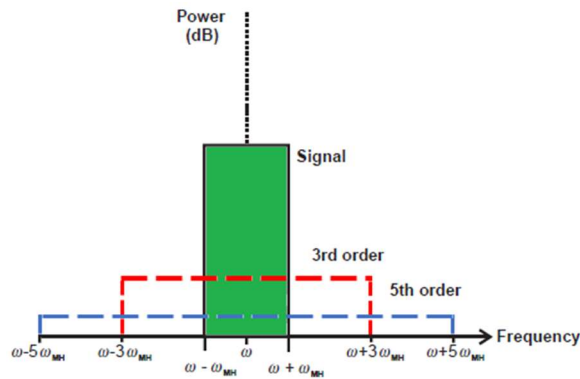


Figure 2.4 Inter-modulation spectrum for a typical band-limited digitally modulated signal

2.3 Summary

The larger bandwidth provided by LTE-Advanced CA obviously results in improved user data rates. But equally important, CA is a powerful feature that enables more flexible and optimal utilization of frequency assets. Especially, non-contiguous CA offers new opportunities to use more and more frequency resources for LTE in different bands.

To fully realize the need for the linearization of an amplifier, a discussion of distortion effects in a PA is necessary. This chapter presented a brief, but useful numerical analysis of IMD using a simple nonlinearity with two-tone signal. Generation of IMD is the fundamental issue with nonlinear PAs. Third-order products are most critical in determining the end-to-end performance. Another distortion phenomenon is the appearance of frequency-dependent memory effects in a PA as the bandwidth of modulation grows, which will be discussed in the next chapter.

CHAPTER 3

LITERATURE REVIEW

After the discussions in the previous two chapters, the advantages and disadvantages of traditional linearization schemes, and in particular predistortion, can be appreciated. This chapter focuses on comparing the advantages and the disadvantages of using the wideband/broadband system over the dual-band system. Moreover, behavioural models suitable for different transmission architectures will be discussed as a related work.

3.1 Broadband transmitters

For the broadband modulation as shown in Figure 3.1, the PA output typically shows a signs of memory effects. These effects are also known as “frequency-dependent effects” since they have a pronounced dependency on the instantaneous frequency of the signal as the bandwidth of modulation increases. In order to minimize the overall distortions introduced by a PA operating on LTE signals, a detailed study of memory effects, along with the more common non-linearity issue, is a must.

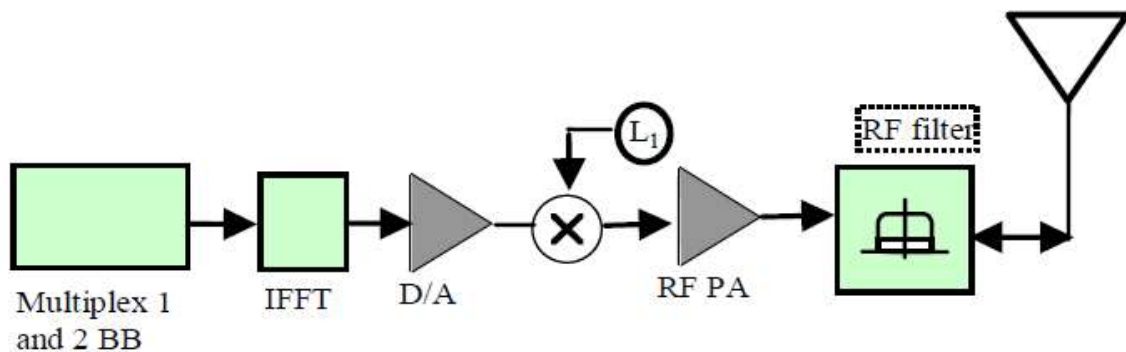


Figure 3.1 Single-band transmitter

Broadband communication uses - as the name states - a wider portion of the spectrum. This has some advantages and disadvantages:

- Broadband communication allows for a higher bandwidth and therefore for a faster communication.
- Broadband communication allows for spreading the signal to encrypt it.
- Broadband communication allows for notching out narrow noise sources in the spectrum.
- Broadband communication puts high demands on the linearity of filters.
- It's harder to send and detect broadband signals as the energy of the signal is distributed across the width of the spectrum which makes the signal weaker the wider it gets (transmitting on a given power level)
- Broadband communication is almost exclusively done at higher frequencies, as it is easier to design integrated circuits which have wider filters.
- A high sampling-rate is required.
- High dynamic range in order to mitigate the impact of strong adjacent disturbing signals, which are within the wide input RF bandwidth but outside of one of the useful frequency bands.
- Broadband transceivers provide lower complexity and cost [44].

The layout of broadband transceivers is affected by several factors [44], for example:

- Sampling frequency: getting the whole spectrum sampled from the lowest to highest frequency requires high sampling frequency.

- Output data rate and D/A dynamic range: This likewise translates into high power consumption which couldn't be employed in UE.

These components, beside others, will decide the design requirements for the RF components, and signal processing that can be done in LTE-A devices.

As indicated in [44], the current technologies can't address every one of the limitations and requirements already recorded for the design of a broadband transceiver.

3.2 Multi-Band Transmitters

With the rapid development of modern high speed wireless communications, more devices are required to have multi-standard/multi-mode operation in order to support compatibility across different systems. As a result, multi-band PAs will be very desirable components in future wireless communication systems, especially for LTE-A networks. Some recent studies have been reported on the design and operation of concurrent multi-band PAs [45], [46]. Multi-band PAs, however, have different forms of distortions [47] including inter-modulation and cross-modulation products, which are more severe than the distortion products of PAs operating in single-band mode [48], [49]. In Figure 3.2, the UE has one PA. The UE has two inverse fast Fourier transforms (IFFTs), after which the UE combines analog waveforms from the CCs (e.g., via a mixer operating at an intermediate frequency of roughly the bandwidth of the other component carrier). Then the resulting signal going through the RF filter.

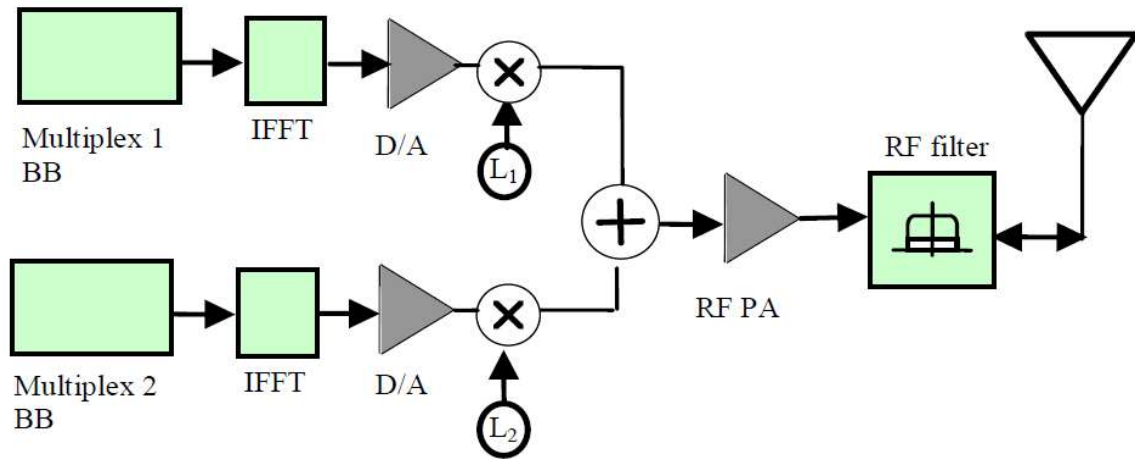


Figure 3.2 Multi-band transmitter block diagram (single PA).

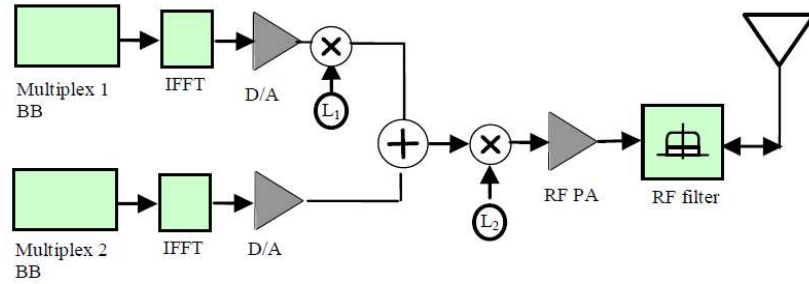
Advantages and disadvantages of the multi-band transmitters can be summarized as:

- The multi-band signal is directly synthesized at the final transmission band frequencies.
- Removing the modulation stage allows the system designer to lower the system noise figure by taking advantage of the D/A's low noise floor and the high gain of the RF amplifier [50].
- This transmitter is complex. The different RF chains may require filters, amplifiers, mixers and local oscillators for each different bands.
- Potentially, amplifiers, mixers and local oscillators can be re-used for different part-bands by changing RF-filters and local oscillator frequencies.

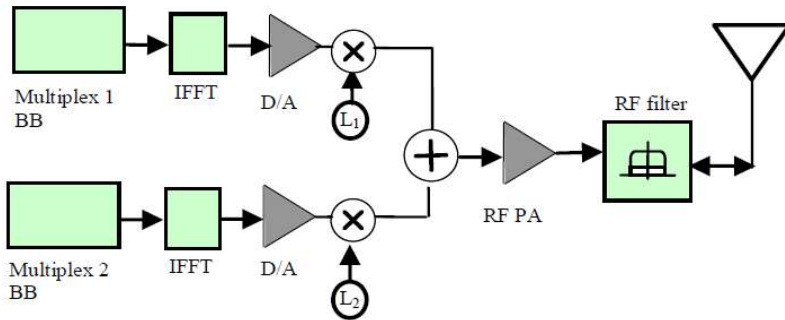
Nonetheless, this translates into increment of the cost and size of cell phone.

The design of multi-band ultra linear RF transmitters becomes increasingly complex when combined with the requirement for high power efficiency. Cascade of different hardware optimized for every standard as show in Figure 3.3 can be deployed in order to enable

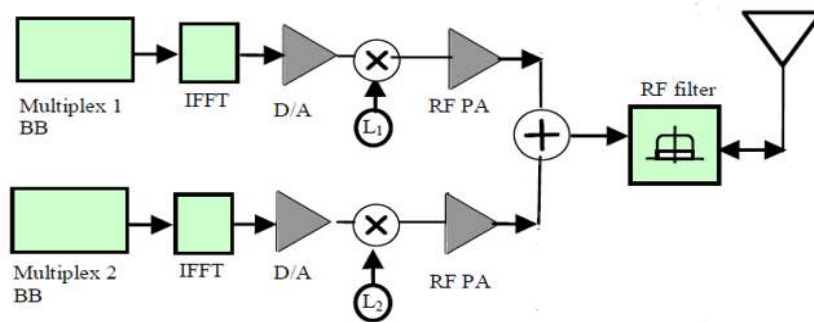
multi-band standards. In any case, this solution suffers from two drawbacks. First, the cost of the network increases due to the deployment of different hardware. Second, the size of the resulting cascaded RF systems becomes large. This is contradictory to wireless evolution toward remote radio heads [51], where the size and the cost of the RF system should be small enough to be mobile and easily installed.



(a)



(b)



(c)

Figure 3.3 Dual-band transmitters (a) Multiple (baseband + IFFT + DAC), single (stage-1 IF mixer + combiner at IF + stage-2 RF mixer + PA), (b) Multiple (baseband + IFFT + DAC + mixer), low-power combiner at RF, and single PA, (c) Multiple (baseband + IFFT + DAC + mixer + PA), high-power combiner at RF.

As it has been described, the power consumption and complexity level of the transmitters are high. In this way, enabling high end CA modes might be unfeasible for cell phones. However, LTE-Advanced is focusing on cell phones, as well as laptops and different sorts of CPE (client-premises equipment). These devices don't have the same limitations as cellular phones which makes them more suitable for the high-end CA modes, as described in [52]. Table 3.1 gives a brief summary of the advantage and disadvantage wideband and dual-band architectures.

Table 3.1 Wideband and dual-band architectures advantages and disadvantages

	Advantage	Disadvantage
Wideband	<ul style="list-style-type: none"> • Notching out narrow noise sources in the spectrum. • lower complexity and cost. 	<ul style="list-style-type: none"> • Makes the signal weaker the wider it gets. • Requires wide-band RF components. • High sampling-rate. • The RF components must be highly linear also to handle signals with high amplitude.
Multi-band	<ul style="list-style-type: none"> • Amplifiers can be re-used for different part-bands. • Supports high bandwidth requirements. • Not suffering from high sampling rate. 	<ul style="list-style-type: none"> • Complex with the need for high power efficiency. • Increase the size and the cost of the RF system.

3.3 Behavioural Modeling of Power Amplifiers

A behavioral model of a device is defined as numerical mapping between its input and output, depicting a specific characteristic or behavior of the device. Modeling of devices is very important for computer-aided design of systems. Such models are necessary for conducting numerical simulations on systems.

In general, distortions refer to the alternation of the signal due to the imperfections of the transmitter's hardware. Distortions observed in wireless transmitters have various origins such as frequency response distortions, in addition to modulator impairments, and so on. Among these distortions, the predominant ones are those due to the nonlinearity present in the transmitter's RF front-end and mainly the RF PA. In reality, wireless transmitters are built of a cascade of different stages. Along these subsystems, PA is identified as main source of the non-linear distortions. Accordingly, compensating and modeling for transmitter non-linear distortions is often trimmed down to compensating and modeling of the non-linearity PA.

3.3.1 DUT Model Extraction

Predistortion applies an integral PA non-linearity upstream so that the cascade of predistortion and PA acts as a linear system [53]. Behavioural modelling is essential to predict the PA nonlinearity basically. The synthesis of the predistortion function can be considered equal to behavioural modelling of PA's inverse transfer function got by substitution of input/output signals of the PA with proper small-signal gain normalization [53].

Behavioural modelling of device under test (DUT) is very important in order to accurately quantify PA nonlinearities and memory effects [53]-[59]. Figure 3.4 shows the procedure of DUT behavioural modeling. The propagation delay over the DUT will present a mismatch between the use of data samples to calculate the instantaneous AM/AM and AM/PM characteristics of the DUT.

Therefore, captured PA output signal have to be time aligned with the captured input signal [53]. The time aligned input/output waveforms are then used to identify a behavioural model of the DUT.

To sum up, one can say that the behavioural modelling procedure can be divided into two major parts: the observation and formulation.

1. The perception / observation relates to the accurate acquisition of the input/output signals of the PA. This part includes experimental capturing of the signals [53].
2. The formulation corresponds to the choice of a proper mathematical relation that characterizes all significant interaction between input/output signals of the PA, its identification and validation [53].

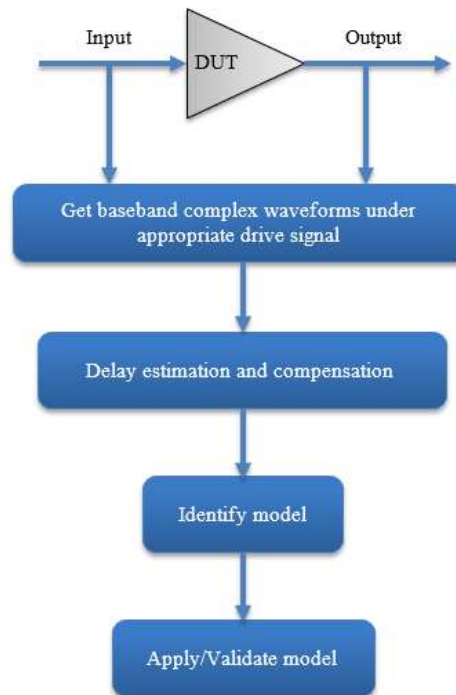


Figure 3.4 Behavioural model extraction procedure: Key steps from measurement to model validation.

3.4 Memory Effects

In reality, the output of the PA depends on previous inputs as well as the current input of the amplifier. This phenomenon is called memory effects. These memory effects are due to thermal effects, and longtime constants in DC bias circuits. It can be observed as asymmetries in lower and upper sidebands, and bandwidth dependent variations in the magnitude of inter-modulation products. For higher bandwidth applications, e.g. LTE, the memory effects become severe, and cannot be ignored. A system can be nonlinear, have memory, or be nonlinear with memory. A nonlinear system generates new frequency components as seen in the previous section, while a system with memory shapes existing frequency components. When an input signal does not justify the narrowband assumption, the envelope characteristics at the output of a PA do not remain static over the bandwidth of operation.

3.4.1 Characterization of Memory Effects

There is growing interest in the characterization of memory effects, and research efforts at various levels are continually taking place. A two tones, although being a good test for memory effects, is not capable of the detailed characterization that is needed to better understand its causes. Thus, schemes using real modulated signals are being developed.

The direct impact of PA distortions on these modulations can be monitored and analyzed. This leads to recommendations for amplifier design and compensation techniques that are customized for the specific signal format.

A two-tone test signal can be used to appreciate the presence of memory as outlined in [63], [64]. The two-tone test cannot measure the memory effects due to the IM components and thus [64] has modified the basic two-tone test to include an IM distortion signal with

two tones to measure the optimal input signal for canceling IM memory effects. A more accurate method of characterizing memory effects is to drive a PA with real modulated test signals, and analyze the resultant distortion. This customized analysis can result in better strategies to counter PA distortion for the tested signal environment.

3.4.2 Modeling Power Amplifiers with Memory

The Volterra series can be used to describe any nonlinear stable system with fading memory. PA memory effect is reflected as a distortion associated with the signal bandwidth and power [60]. However, Volterra series main disadvantages are the dramatic increase in the number of parameters with respect to nonlinear order and memory length, which causes drastic increase of complexity in the identification of parameters. As the input signal bandwidth becomes wider, the time span of the PA memory becomes comparable to the time variations of the input signal envelope. A Volterra series is a combination of linear convolution and a nonlinear power series so that it can be used to describe the input/output relationship of a general nonlinear, causal, and time-invariant system with fading memory [61]. The Volterra series in discrete-domain can be represented by equation (3.1).

$$y(n) = \sum_{p=1}^K \sum_{i_1=0}^M \dots \sum_{i_p=0}^M h_p(i_1, i_2, \dots, i_p) \prod_{j=1}^p x_{in}(n - i_j) \quad (3.1)$$

where $x(n)$ and $y(n)$ represent the input and the output of the model, $h_p(i_1, i_2, \dots, i_p)$ are the parameters (kernels) of the Volterra model, K is the nonlinearity order of the model, and M is the memory depth. It can be observed that the number of coefficients of the Volterra series increases exponentially as the memory length and the nonlinear order increase making it unpractical for modeling PAs in real time applications [62].

3.5 Related Work for Models with Memory Effects

Dynamic systems, or systems having memory, are the most common members of the nonlinear class of systems. Almost all systems have delay associated with them and that delay appears as phase shifts between input and output. Systems which show an instantaneous phase variation, apart from a nonlinear gain pattern, are called quasi-memoryless systems. A nonlinear system with memory, such as a PA operating on broadband signals, is most comprehensively modeled using a Volterra series.

Various mathematical representations of the model (formulations) have been introduced for behavioural modelling of transmitters and RF PAs. PA behavioral modeling is not a trivial problem, and different PA model schemes have been suggested. These models can be classified in two types: memoryless models [65] and memory capable models [63]-[70] such as the look-up-table model [66], the Volterra Models [67]-[69], the Memory Polynomial Models [70], [71], Wiener Model, Hammerstein Model [72], [73].

However, as the bandwidth increases nowadays in the different wireless communication systems, the memory effects can no longer be neglected. Hence, the memory effects emulated by the PA are dependent on the operating conditions of the DUT and also signal dependent, such as signal statistics, bandwidth and PAPR. Therefore, in order to achieve a relevant good performance of the behavioural models, memory effects should be taken into consideration. Some of these models have the great advantage of simplicity and are easier to implement in real-time systems, for example, the conventional Wiener and Hammerstein models. However, they can predict only the linear memory effects.

On the other hand, the Volterra series is only limited for modeling mildly nonlinear systems. To overcome the computational complexity of the Volterra series. The memory polynomial (MP) model is the most widely used pruned Volterra series. Even though, MP models are reduced Volterra models, but they still could result in over-sized models, due to the use of nonlinear polynomials in all branches, which will also translate into large number of coefficients. A brief comparison between these models are listed in Table 3.2 taking 1 as the best model and 5 as the worse model in case of complexity and overall performance.

Table 3.2 Comparison between behavioral models

	Complexity	Performance
look-up-table	1	5
Wiener	4	3
Hammerstein	2	2
Volterra	5	3
Memory Polynomial	3	1

Starting with the simple MP model, in [59], the dynamic nonlinearity reduction concept was introduced and applied to reduce the number of coefficients required in the MP function using the conventional twin-nonlinear two-box (TNTB) model, where the MP function of the proposed dynamic nonlinearity reduction (DNR) based TNTB model is re-written as:

$$y(n) = \sum_{j=0}^M \sum_{i=1}^{N_j} a_{ij} \cdot x(n-j) \cdot |x(n-j)|^{i-1} \quad (3.2)$$

All parameters of (3.2) are similar to the standard MP model except for the nonlinearity order (N_j) which is made dependant on the memory index (j).

Based on the fact that the nonlinearity order of the high order memory effects are decaying, the following dynamic nonlinearity reduction constraint has been introduced in the proposed model:

$$\text{for } j_1 < j_2 \Rightarrow N_{j_1} \geq N_{j_2} \quad (3.3)$$

The DNR based reverse TNTB (RTNTB) model is identified according to the flow chart presented in Figure 3.5. First, the RTNTB model is constructed. Then, the nonlinearity orders of the memory branches are successively reduced in an iterative fashion while satisfying the constraint of (3.3). To prevent degradation of the model accuracy, the nonlinearity order reduction at one iteration is conditional to the performances of the model obtained from the previous iteration. The effectiveness of the proposed model reduces the number of coefficients by 60% while degrading the normalized mean square error (NMSE) by only 0.1dB.

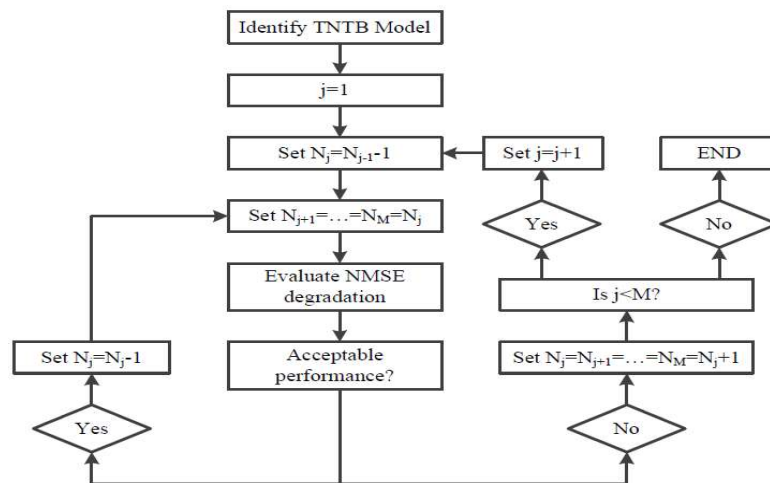


Figure 3.5 Flow chart of the model's identification in [15]

Many references has introduced the standard MP model for single band PAs [18], [68], [72], [74]-[78].

In [79], a complexity-reduced band-limited memory polynomial (CR-BLMP) model was proposed for behavioral modeling of RF PAs in the presence of a band-limited feedback loop. Considering the complexity and the hardware resource of the system, the band-limiting filter used in BLMP model cannot be set too high. The block diagram of the proposed CR-BLMP model is depicted in Figure 3.6. The first branch of it is the band-limited part with a baseband low pass filter (LPF), selecting the conventional bandlimited basis function; and the second branch is the residual part detained by subtracting the band-limited region from the "full-band" basis function. Even though the conventional BLMP model has bad performance and low accuracy with the low order filter, the error between the output of the BLMP mode and the output of real PA is modeled accurately by the basis function of the error residual region. In theory, it has better performance than both the conventional MP and band-limited models. More related works can found in [76], [80]-[83].

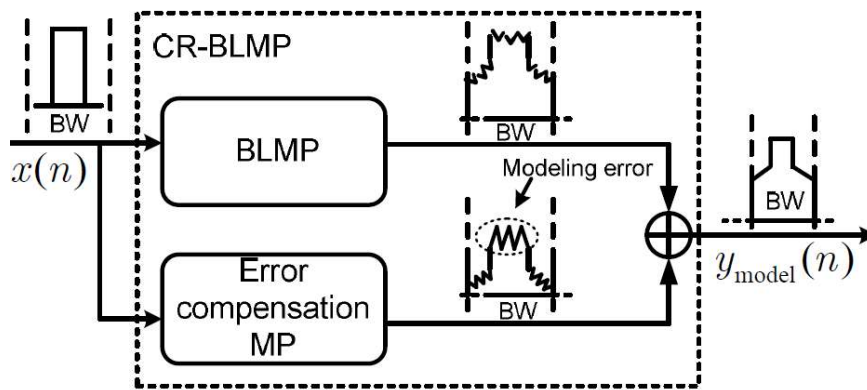


Figure 3.6 Block diagram of the CR-BLMP model in [79]

The CR-BLMP model has been widely applied for the behavioral modeling of RF PAs and transmitters exhibiting memory effects. However, its computational cost linearly increases with the memory depth. Since such identification is required on a regular basis as the characteristics of the PA and the test signal change, it is essential to develop computationally efficient models that will ease this step.

For the dual-band models, there are different behavioural modeling techniques developed for the concurrent dual-band systems in the earlier literature. [84] reported a 2-D digital predistortion (DPD) model using memory polynomials (MPs). This 2-D DPD model is rearranged in [85] to use 1-D LUTs instead of 2-D LUTs, but the performance is still limited by the 2-D-DPD model. This will be discuss in the next chapter.

As a layout from the literature review,

Figure 3.7 gives the different distribution of previous works for the three different LTE-A signals (single, Broadband and multi-band signals). This illustrates that most of the previous works was done for the single and broadband signals. On the other hand, fewer research works produced for the multi-band modeling. As high data rates and less complexity are required, more work and research in the multi-band modeling is required.

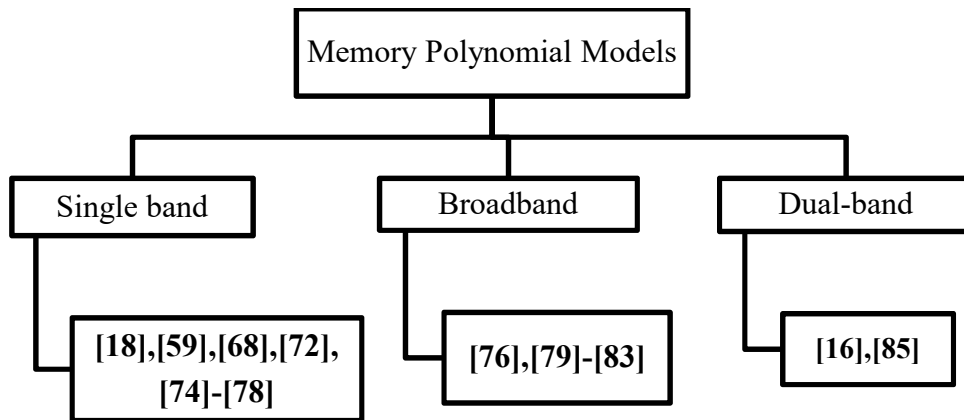


Figure 3.7 Previous work classification based on the LTE-A signal transmission type.

3.6 Summary

A brief section, covering the causes for memory effects was presented, followed by a discussion of behavioral modeling methods for a nonlinear amplifier. Traditionally, a polynomial function has been sufficient to model gain and phase nonlinearities, assuming that the envelope bandwidth is very small compared with the carrier frequency, so that the PA offers a flat gain to the entire input spectrum (known as the narrowband assumption). However, the polynomial model becomes inaccurate for solid-state amplifiers operating on broadband-envelope signals and showing memory.

CHAPTER 4

ANALYSIS OF DUAL-BAND MEMORY POLYNOMIAL

MODELS

As the PAs are inherently non-linear, they exhibit a memory effect as well, which means the actual output of an amplifier is stimulated by not only the present input but also previous inputs. A Full Volterra series (which do not include any simplifying assumptions) is one way to model the memory effect, but it is typically difficult to manipulate and results in unrealistically large models that are not suitable in practice [86]. This led to the development of new models such as memory polynomial model that are derived from the original Volterra model.

4.1 The Memory-Polynomial Model

The memory-polynomial model [56] consists of several delay taps and nonlinear static functions. This model is a truncation of the general Volterra series, which consists of only the diagonal terms of the Volterra kernels. Thus, the number of parameters is significantly reduced compared to general Volterra series in addition to keep reasonable modeling accuracy and performance. Consequently, MP models are along most generally used structures for modeling of PAs with memory effect. The block diagram of MP model is shown in Figure 4.1.

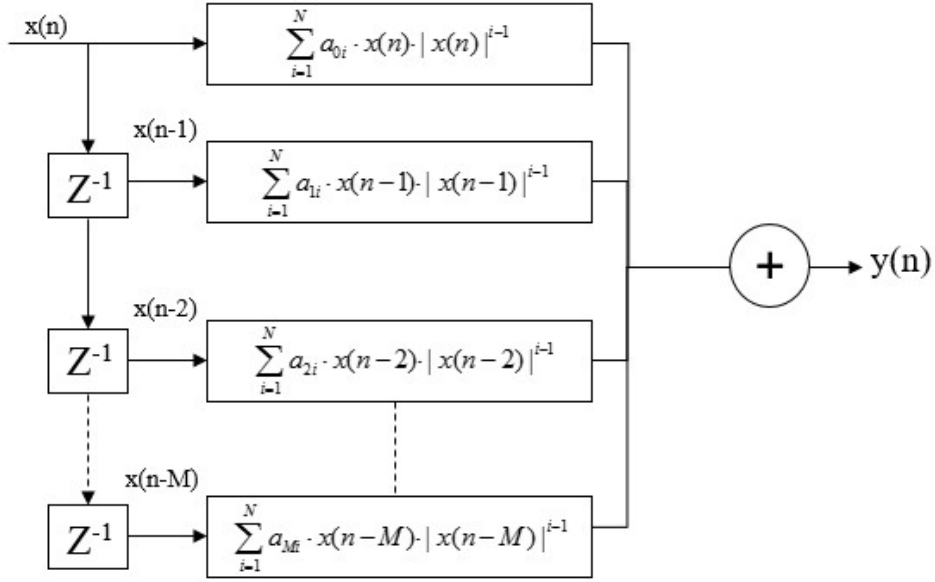


Figure 4.1 Memory polynomial model

MP models are characterized with two dimensions: the memory depth (M) and the nonlinearity order (N). It is essential to accurately identify the dimensions of the model to avoid over or under modeling of the system. The output waveform $y_{\text{modeled}}(n)$ of the MP model is expressed in a terms of the $x(n)$ (input signal) and the a_{ij} (model coefficients) according to:

$$y(n) = \sum_{j=0}^M \sum_{i=1}^N a_{ji} \cdot x(n-j) \cdot |x(n-j)|^{i-1} \quad (4.1)$$

The model's coefficients can be computed using the measured output and input signals of the device under test.

The MP model dimension estimation can efficiently give the RF designer an essential data about non-linear behavior of the system, also the complexity of the model require. This data can be used to enhance its performance in terms of linearizability.

4.2 Dual-Band General Model

To start with some related work, the model proposed in [84] is a 2D-DPD model that applied to linearize a widely spaced dual-band PA transmitter taking into account the in-band intermodulation and the cross-modulation. The model is in form of:

$$y_1(n) = \sum_{m=0}^{M-1} \sum_{k=0}^N \sum_{j=0}^k a_{k,j,m}^{(1)} x_1(n-m) |x_1(n-m)|^{k-j} |x_2(n-m)|^j \quad (4.2)$$

$$y_2(n) = \sum_{m=0}^{M-1} \sum_{k=0}^N \sum_{j=0}^k a_{k,j,m}^{(2)} x_2(n-m) |x_1(n-m)|^{k-j} |x_2(n-m)|^j \quad (4.3)$$

Where $a_{k,j,m}^{(1)}$, $a_{k,j,m}^{(2)}$ are the model coefficients, N is the nonlinearity order and M is the memory depth. $y_1(n), y_2(n)$ are the output signal corresponding to the dual-band inputs $x_1(n), x_2(n)$, respectively.

The 2-D MP output is dependent only on the compound amplitude effect of the two input signals, and does not have phase information of the second input. Also, as the 2-D MP model is depending on the memory polynomial basis function, which has a fixed polynomial order for each branch that results in an over-sized model.

In [85], the joint predistortion of modulator imperfections and dual-band PA nonlinearity was proposed. The structure of model is extended in order to model the cross-modulation effects and modulator imperfections in the dual-band transmitter, which also results in an inherently complex model. The main issue of this model is taking into consideration the odd and the even orders which results in having more parameters and leads to more complexity in the model.

In [16], a technique for the joint mitigation of dual-band PA distortion in a complexity-reduced structure was proposed. A dual-input two-box structure was developed to accurately characterize and mitigate the in-band and cross-band distortion of the dual-band PA operating in concurrent mode. As given in [16], the non-linear behavior of concurrent dual-band PAs is more complex than that of single model, because of cross-modulation products between dual-bands and inter-modulation terms. This can be seen by exciting a multi-band PA including two inputs and capturing the resulting distortion at the output of the PA.

The model proposed in [16] relates the input and output waveforms [$x_1(n)$ and $x_2(n)$ and $y_1(n)$ and $y_2(n)$, respectively] of a non-linear PA through the dual-band memory polynomial model according to:

$$y_1(n) = \sum_{m=0}^M \sum_{k=1}^N \sum_{r=0}^k \sum_{k_1=0}^{k-r} \sum_{k_2=0}^r A_{kr}^{(1)} x_1(n-m) |x_1(n-m)|^{2k_1} |x_2(n-m)|^{2k_2} \quad (4.4)$$

$$y_2(n) = \sum_{m=0}^M \sum_{k=1}^N \sum_{r=0}^k \sum_{k_1=0}^{k-r} \sum_{k_2=0}^r A_{kr}^{(2)} x_2(n-m) |x_1(n-m)|^{2k_1} |x_2(n-m)|^{2k_2} \quad (4.5)$$

Where A_{kr} are the model coefficients, and M, N are the memory depth and the nonlinearity order, respectively. The model coefficients A_{kr} are given by:

$$A_{kr} = \frac{1}{2^{k-1}} a_{kr} C_r^k C_{k_1}^{k-r} C_{k_2}^r \quad (4.6)$$

where

$$C_b^a = \frac{a!}{b!(a-b)!}$$

This model has the advantage of using only the even order to reduce the number of the parameters but it suffers from resulting in more complex model than in [85] which may

affect the overall performance. These two models (in [16] and [85]) were carefully studied to come up with a new model that has the advantages of both. The proposed new model is introduced in the next section.

The dimensionality of the model in [16] is, however, greater than that of the MP model [85]. This increase is unavoidable, due to the addition of the cross effects of both inputs at the output of each band, which significantly increases the number of coefficients.

4.3 Proposed Dual-Band Model

For a dual-band model, each communication band composed of two cells that are fed with the dual inputs. This can be described by taking the general memoryless nonlinear model:

$$y(n) = \sum_{k=1}^N a_k x^k(n) \quad (4.7)$$

where N is the nonlinear polynomial order, a_k is the set of model coefficients, $y(n)$ is the model output and $x(n)$ is the input.

Generally, in concurrent dual-band mode, the discrete time baseband equivalent input signal with the angular frequency separation $\Delta\omega = |\omega_2 - \omega_1|$ can be given by:

$$x(n) = x_1(n)e^{j\omega_1 n T_s} + x_2(n)e^{j\omega_2 n T_s} \quad (4.8)$$

where ω_1 and ω_2 are the carrier frequencies, $x_1(n)$ and $x_2(n)$ are the complex envelopes of each band, and T_s is the sampling time intervals $T_s = 1/f_s$.

The nonlinear behavior of concurrent dual-band PA can be modeled by seventh-order MP model:

$$y(n) = A_1 x(n) + A_3 x(n) |x(n)|^2 + A_5 x(n) |x(n)|^4 + A_7 x(n) |x(n)|^6 \quad (4.9)$$

where $x(n)$ and $y(n)$ are the input and output baseband signal, and A_i ($i = 1, 3, 5, 7$) are the model coefficients. Substituting (4.8) into (4.9), the complex baseband output signals around each carrier frequency can be represented as (4.9):

$$y_i = x_i(A_1 + A_3|x_i|^2 + A_5|x_i|^4 + A_7|x_i|^6) + x_i(2A_3|x_j|^2 + 3A_5|x_j|^4 + 4A_7|x_j|^6) + x_i(6A_5|x_i|^2|x_j|^2 + 18A_7|x_i|^2|x_j|^4 + 12A_7|x_i|^4|x_j|^2) \quad (4.10)$$

where $x_i(n)$ and $x_j(n)$ ($i \neq j$) are replaced by x_i and x_j for simplification. The expression illustrates that output signal in each band is related to both input signals. Based on (4.10), as the general proposed model for the dual-band transmitter output y is derived in the Appendix B, the model can be derived by consider the terms around the two center frequencies (including in-band inter-modulation and cross-band inter-modulation products) proposed in the form of:

$$y_1(n) = \sum_{m=0}^M \sum_{k=1}^N \sum_{r_1=0}^{k-1} \sum_{r_2=0}^{k-r_1-1} A_{k,r_1,r_2}^{(1)} x_1(n-m) |x_1(n-m)|^{2r_1} |x_2(n-m)|^{2r_2} \quad (4.11)$$

$$y_2(n) = \sum_{m=0}^M \sum_{k=1}^N \sum_{r_1=0}^{k-1} \sum_{r_2=0}^{k-r_1-1} A_{k,r_1,r_2}^{(2)} x_2(n-m) |x_1(n-m)|^{2r_1} |x_2(n-m)|^{2r_2} \quad (4.12)$$

where

$y_1(n), y_2(n)$: The modeled output of the dual-band inputs.

$x_1(n), x_2(n)$: The input signals.

$A_{k,r_1,r_2}^{(1)}, A_{k,r_1,r_2}^{(2)}$: Model coefficients.

M, N : the memory depth and the nonlinearity order, respectively.

The new model can be further enhanced to include the memory effects exhibited by a dual-band PA, for better characterization of the static and dynamic nonlinearities exhibited by the PA (see Appendix B). The proposed model can lead to a similar model in [85] except

for taking only the even order of the parameters. One benefit of taking the even-order nonlinear terms is increased modeling accuracy and reduces the modeling error. Moreover, it allows the use of lower-order polynomials, which have better numerical properties.

The computational complexity of the proposed model is much reduced compared to that of other models, since only the mildly nonlinear dynamic function is multiplied twice by the signal and its conjugate image. Therefore, the number of complex-valued multiplications is significantly decreased. In the parallel-MP model, each input signal and its conjugate image are applied to both the static and dynamic functions of the model's compound structure, which significantly increases the computational complexity of the model. In the proposed model, the mildly nonlinear dynamic function is applied to the output for the lower and upper bands, without the need to duplicate this function again for each signal and its conjugate image. Since both the proposed and the reported models are linear in terms of their coefficients, a least squares algorithm is used for estimating the model coefficients. Furthermore, the model in [85] has added identification complexity than the proposed model. The identification of the model in [85] is done in two steps: the first step is the identification of the parallel dual-input Volterra filters. The second step is the de-embedding of the output signals for the identification of the memoryless nonlinear behavior of the 2-D LUT. On the other hand, the identification of the proposed model is done in only one step. This identification step reduced the identification complexity to the proposed model, which leads to improve the performance of the proposed model and the significant reduction in computational complexity over that of the model in [85]. The proposed model will be investigated against the one in [16] and [85]. Figure 4.2, 4.3 and 4.4 describe the model identification and its use to compute the output signal for the models in [16], [85] and the

proposed model. These models will be compared to the single and broadband model in term of NMSE and condition number metrics in addition to the assessment of their performance in the frequency domain.

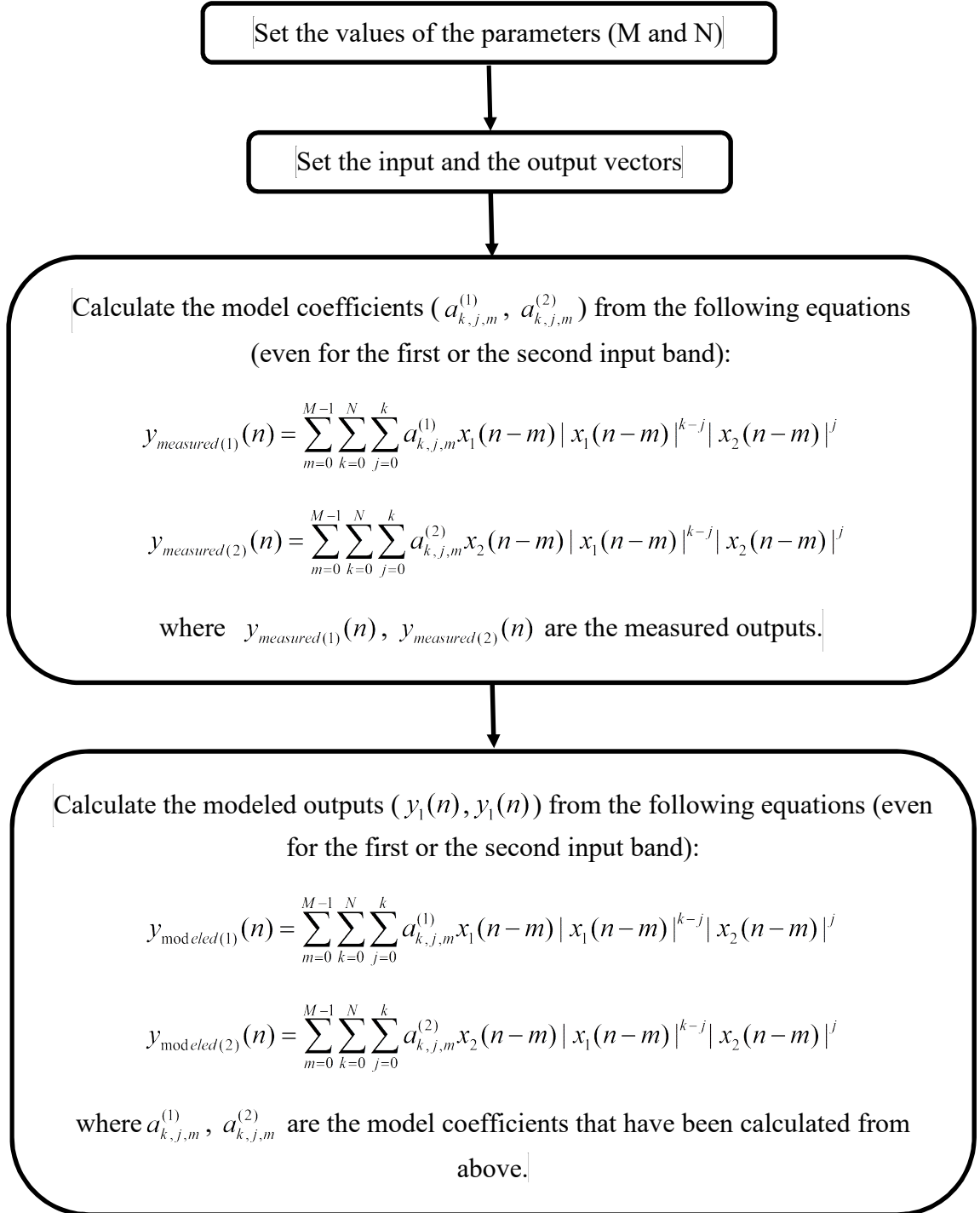


Figure 4.2 The flow chart of the model in [85]

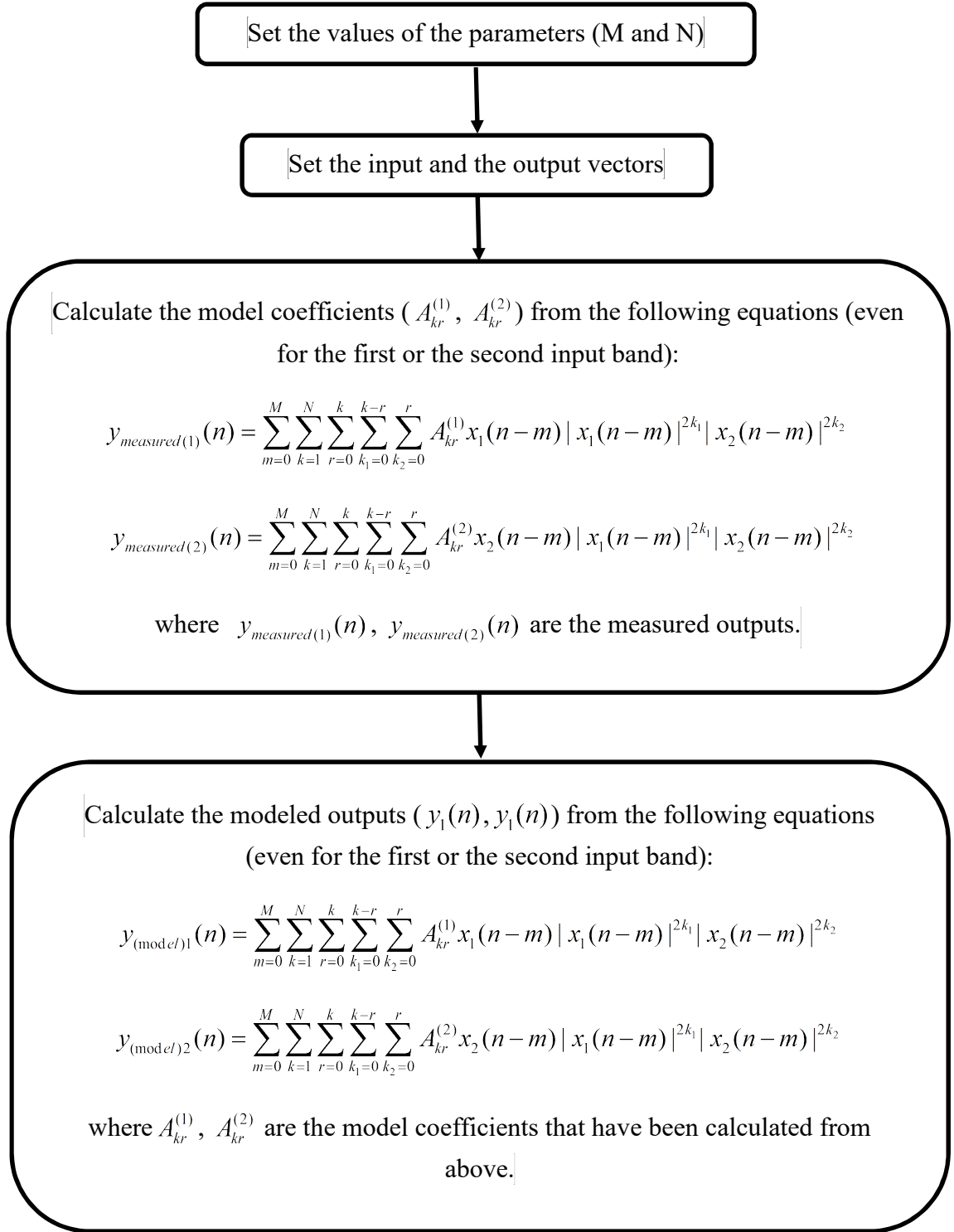


Figure 4.3 The flow chart of the model in [16]

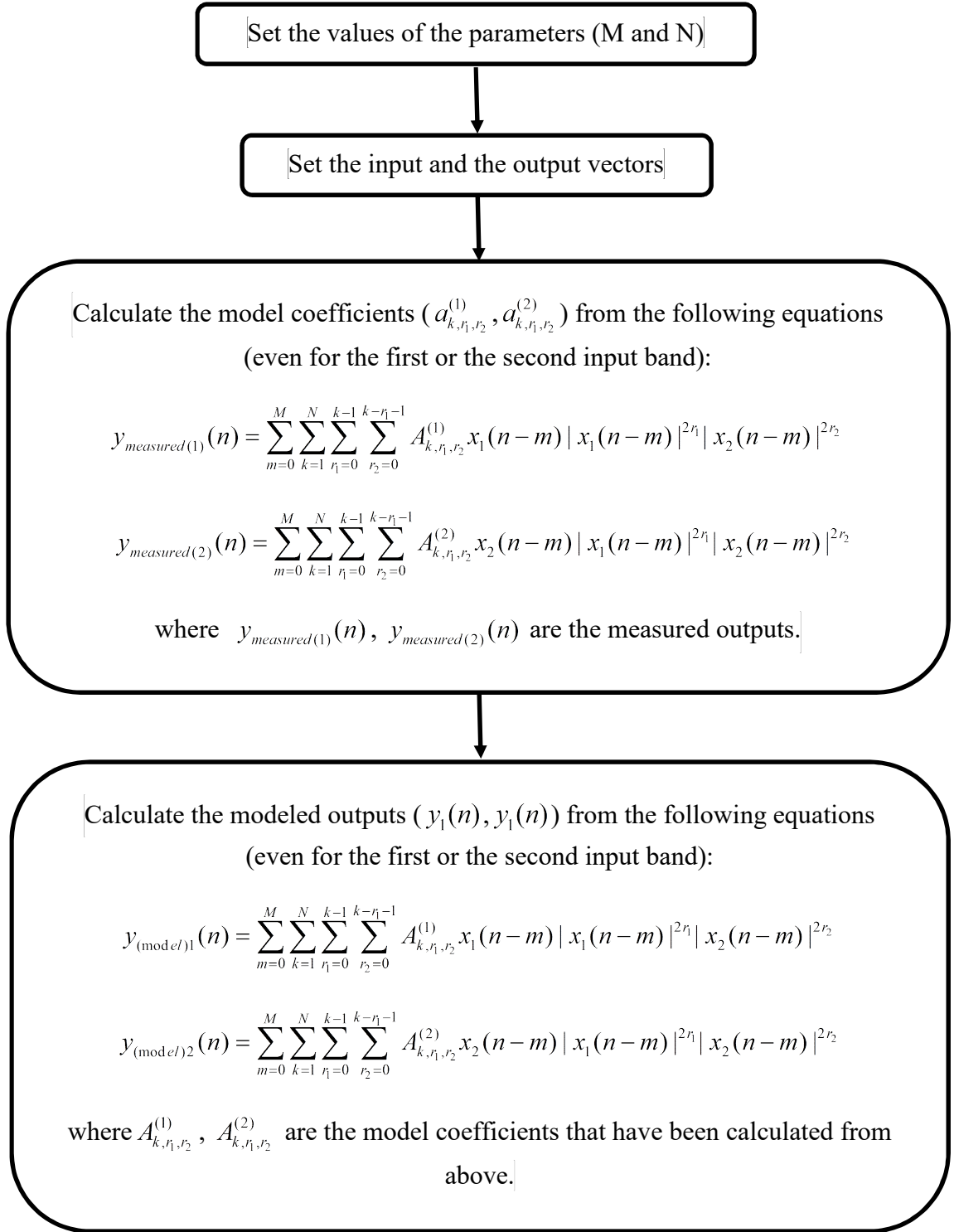


Figure 4.4 The flow chart of the proposed model

4.4 Metrics Used for Benchmarking

To benchmark the performances of the proposed technique, two metrics were considered: the normalized mean square error (NMSE), and the condition number.

(1) The NMSE: In this case, the error was taken between the PA measured output and the estimated output. The performances were evaluated in terms of NMSE. Every iteration consists of incrementing the non-linearity order (N) by 1 and estimating the corresponding NMSE [$NMSE_{dB}(N)$], additionally by increment the memory depth (M) by 1, estimating every one of the coefficients of the model, also calculating the corresponding NMSE [$NMSE_{dB}(M)$]. This defined by:

$$NMSE_{dB}(N, M) = 10 \log_{10} \left[\frac{\sum_{n=1}^K |y_{measured}(n) - y_{modeled}(n)|^2}{\sum_{n=1}^K |y_{measured}(n)|^2} \right] \quad (4.13)$$

where N , M , $y_{modeled}(n)$, $y_{measured}(n)$ are the nonlinearity order, the memory depth, the modeled output and the measured output waveform respectively, and K is the number of data samples of the output waveforms.

(2) The condition number of the models' data matrices: This is the condition number of the model matrix, given in dB units as described in [87]. A lower condition number indicates that a matrix can be solved more robustly.

Generally as the MP model is presented in a memoryless form by:

$$y(n) = \sum_{i=1}^N a_i x(n) |x(n)|^{i-1} \quad (4.14)$$

where $x(n)$ and $y(n)$ are the input and the output complex envelopes and N is the polynomial order. a_i are complex valued coefficients enabling the model to characterize the PA. The matrix of equation (4.14) is:

$$Y = \Phi.A \quad (4.15)$$

where

$$\Phi_i(x) = x |x|^{i-1} \quad (4.16)$$

$$Y = [y(n_1), y(n_2), \dots, y(n_N)]^T \quad (4.17)$$

$$\phi(x) = [\phi(x_1), \phi(x_2), \dots, \phi(x_k)] \quad (4.18)$$

$$A = [a_1, a_2, \dots, a_k]^T \quad (4.19)$$

Then

$$\phi_k(x) = [x(n_1) |x(n_1)|^{k-1}, x(n_2) |x(n_2)|^{k-1}, \dots, x(n_N) |x(n_N)|^{k-1}]^T \quad (4.18)$$

hence equation 4.14 becomes:

$$y(n) = \sum_{i=1}^N a_i \Phi_i(x(n)) \quad (4.19)$$

To extract the model coefficients a_i , it is necessary to provide the complex baseband samples at the input and output of the PA after time alignment. The use of least square algorithm, leads to the vector of coefficients A_{LS} such that:

$$A_{LS} = (\Phi^H \Phi)^{-1} \Phi^H y \quad (4.20)$$

where Φ^H is the Hermitian transpose of Φ .

The conventional polynomial model represented by equations 4.14 and 4.19 was described such a memoryless PA behaviour model. However, most of the RF PAs exhibit memory

effects under wideband excitations. Therefore, to characterize nonlinear PA with memory effects, it is possible to extend the previously described model such that:

$$y(n) = \sum_{i=1}^N \sum_{q=0}^M a_{iq} x(n-q) \cdot |x(n-q)|^{i-1} \quad (4.21)$$

where N and M are the polynomial order and the memory depth respectively. As it can be seen from the discrete model described by equation 4.21, the current value of y depends on the current value of x(n) as well as its previous values x(n-m). Equation 4.21 can be rewritten in the form:

$$y(n) = \sum_{i=1}^N \sum_{q=0}^M a_{iq} \Phi_{iq}(x(n-m)) \quad (4.22)$$

Using the same matrix expression format as in (4.15) with the update of the input matrix Φ , one can get the model parameters with the linear least square method. The accuracy of the solution (A_{LS}) is affected by the numerical condition of the matrix ($\Phi^H \Phi$), characterized by its condition number defined as the ratio between the maximum and the minimum eigenvalues of the matrix [87].

$$\zeta(\omega^H \omega) = \frac{\lambda_{\max}}{\lambda_{\min}} \quad (4.23)$$

To sum up, Figure 4.5 gives a block diagram of the behavioural modeling system output against the PA output.

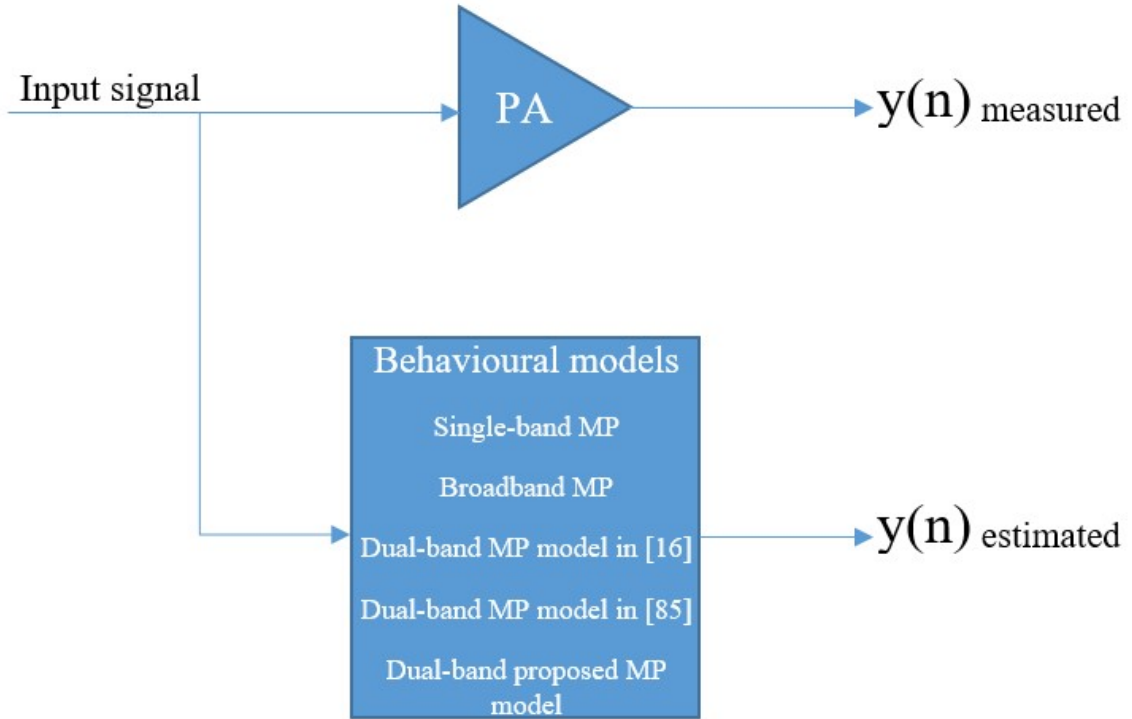


Figure 4.5 Behavioural modeling block diagram

4.5 Summary

A wide assortment of structures based on the memory polynomial has been proposed for the modeling and predistortion of RF PAs and transmitters. Although the functions reported in this chapter are commonly referred to as models, they can be seamlessly used in both behavioral modeling and digital predistortion applications. The behavioural modeling will be investigated in terms of NMSE, condition number metrics and output spectrum. All the single-band, broadband and the dual-band models mentioned earlier were applied and their results are compared in the next chapter.

CHAPTER 5

PERFORMANCE EVALUATION OF THE PROPOSED

MODEL

5.1 Experimental Setup and Test Conditions

A highly nonlinear class AB GaN PA was characterized using LTE signals with different carrier configurations. The output power is approximately 10W. The operating frequency is 2.4 GHz and the sampling frequency was 15.36 MHz for the single carrier signal and 92.16 MHz for the broadband carrier LTE signal. This data has been collected from iRadio laboratory at the University of Calgary, Canada.

The data includes three input carriers and three measured PA output, explained as follow:

Single carrier (low-band): single input carrier, single output.

Single carrier (high-band): single input carrier, single output.

Broadband signal : broadband input, broadband output.

The data acquisition was done first by considering the two carriers individually, then the broadband signal. This can setup as scenario (1). As scenario (2), the characterization was done having two widely spaced carriers to emulate a dual-band.

The simulations for the models identification and performance assessment were performed using MATLAB software. First, a code that can predict the single output and the broadband output from its inputs was built. A second code that can predict the dual-band output from both single band input carriers. Figure 5.1 shows a block diagram of each scenario as a measurement setup.

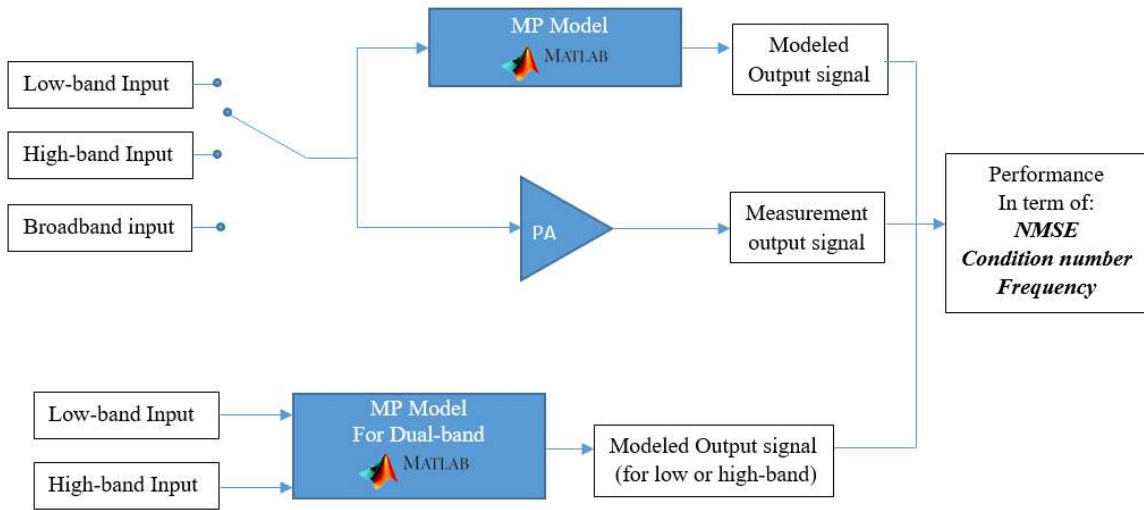


Figure 5.1 Measurement setup test scenarios

For every nonlinearity order and memory depth (N, M) pair and test signal, a behavioral model was extracted, and the condition number metric in addition to the NMSE between the measured and estimated output signals were calculated. For each scenario, the model parameters were verified and the performances in the time domain and frequency domain were evaluated.

5.2 Simulation Results

5.2.1 NMSE Performance for Test Scenario (1)

The given algorithm for model dimension estimation was applied to the DUT when driven by LTE signal. First, a single and broadband signal was applied to the model to emulate memory effects. The nonlinearity order of the DUT was then derived according to the given algorithms.

Figure 5.2 and Figure 5.3 illustrate the value for the NMSE. In Figure 5.2, the nonlinearity order was 5 and the memory depth was varied between 1 and 10. In Figure 5.3, the memory depth was 3 as a constant and the nonlinearity order swept between 3 and 11. For the low-band input, the best nonlinearity order of the DUT was found to be 7 with a small change of the NMSE while the memory depth varies between 4 and 9.

In the other hand, the single high-band input gives almost the same result as observed for the low-band input, with a small improvement in NMSE by 1 dB against the memory effect and 0.7 dB for the nonlinearity order. The model dimensions corresponding to the combination resulting in the lowest number of coefficients that achieves the lowest NMSE are selected as 7 for the nonlinear order and 6 as for the memory depth.

Indeed, the contribution of the static nonlinearity to the DUT behavior is significantly stronger than that of the memory effects. In fact, these results show that either the single band signal that emulates a memory effects behavior of the DUT or the actual test signal can be used to estimate the nonlinearity order. Also in Figure 5.2 and Figure 5.3, it can be clearly seen that the broadband signal either for the nonlinear order or the memory effects

gives a better performance than the single band. At the same rate, it gives an optimal nonlinear order as 7 but with a memory depth of 8.

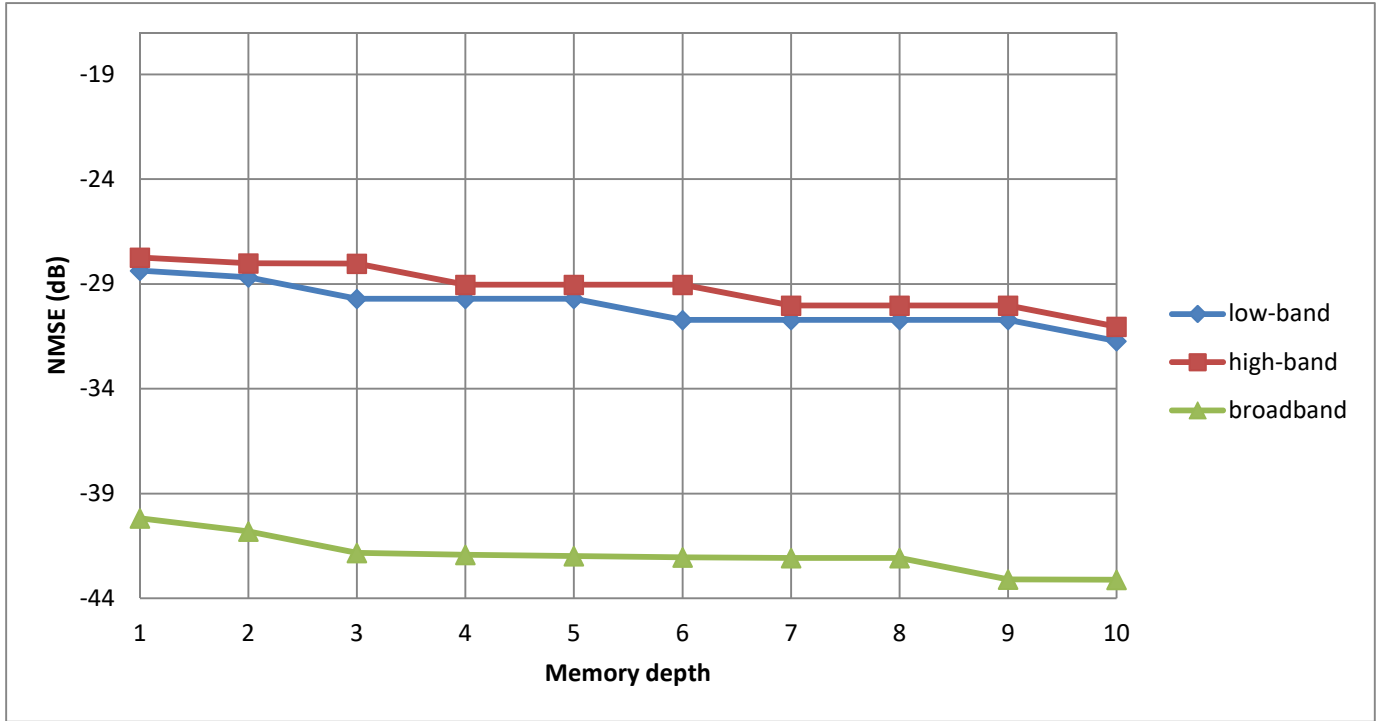


Figure 5.2 $NMSE_{dB}$ vs memory depth for scenario (1) with nonlinearity order =5



Figure 5.3 $NMSE_{dB}$ vs nonlinearity order for scenario (1) with memory depth =3

5.2.2 NMSE Performance for Test Scenario (2)

After getting the model inputs as the two carriers (low-band) and (high-band), the model should be identified twice: once to predict the output at the lowest frequency band corresponding to low-band input using the inputs in the low and high bands, and then to predict the output at the highest frequency band corresponding to high-band input using the inputs in the low and high bands.

Figure 5.4, 5.5, 5.6 and 5.7 illustrate the value for the NMSE for each model. In Figure 5.4 and Figure 5.5, the nonlinearity order was 5 and the memory depth varies between 1 and 10 for the high and low bands. In Figure 5.6 and Figure 5.7, the memory depth was 3 as a constant and the nonlinearity order varies between 3 and 11 for the high and low bands. The model in [16] gives the worse value of NMSE compared to the one in [85] and the proposed model. On the other hand, the proposed model shows a competition against model [85] in terms of having less amount of normalized mean squared error in both the low and the high band of the LTE signals. It can be seen that the performance of the proposed model can be better than the one in [85] for both low and high bands.

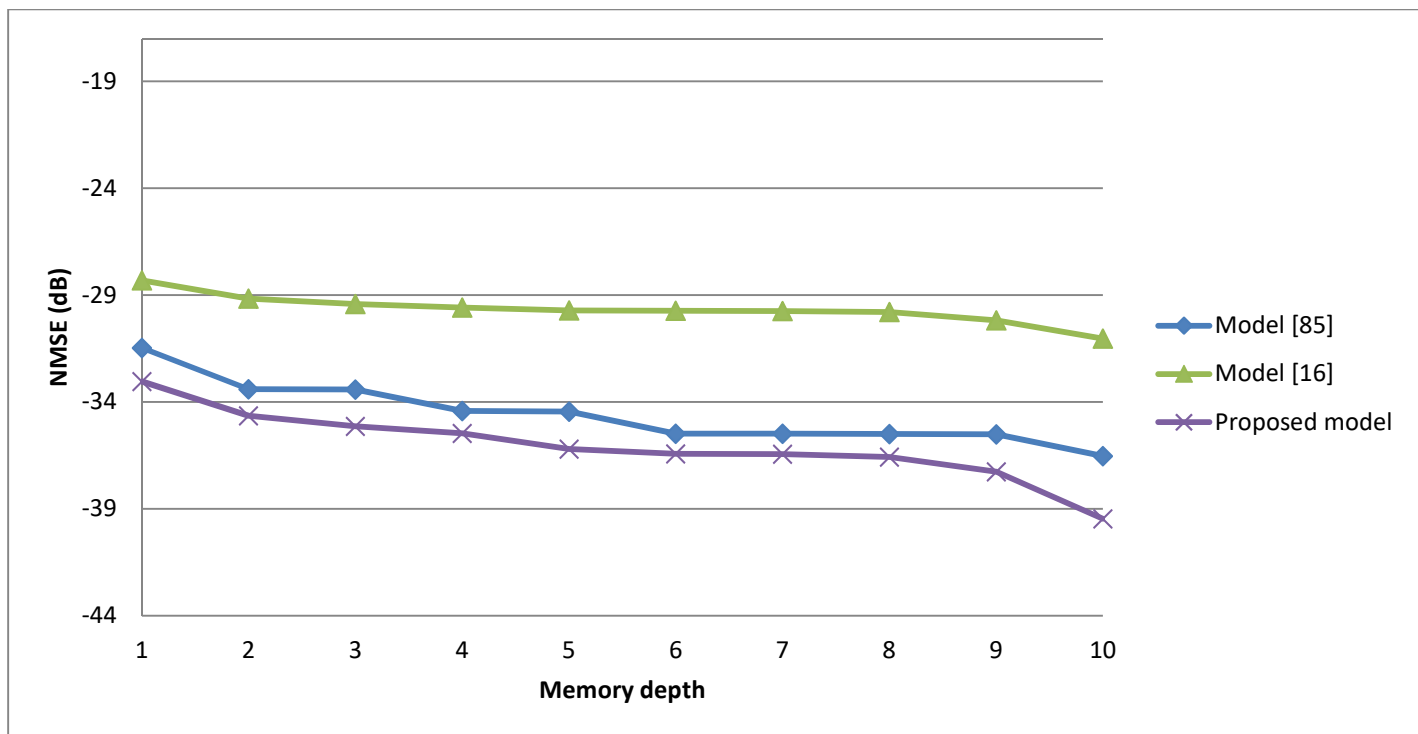


Figure 5.4 $NMSE_{dB}$ vs memory depth for scenario (2) with nonlinearity order =5 for low-band

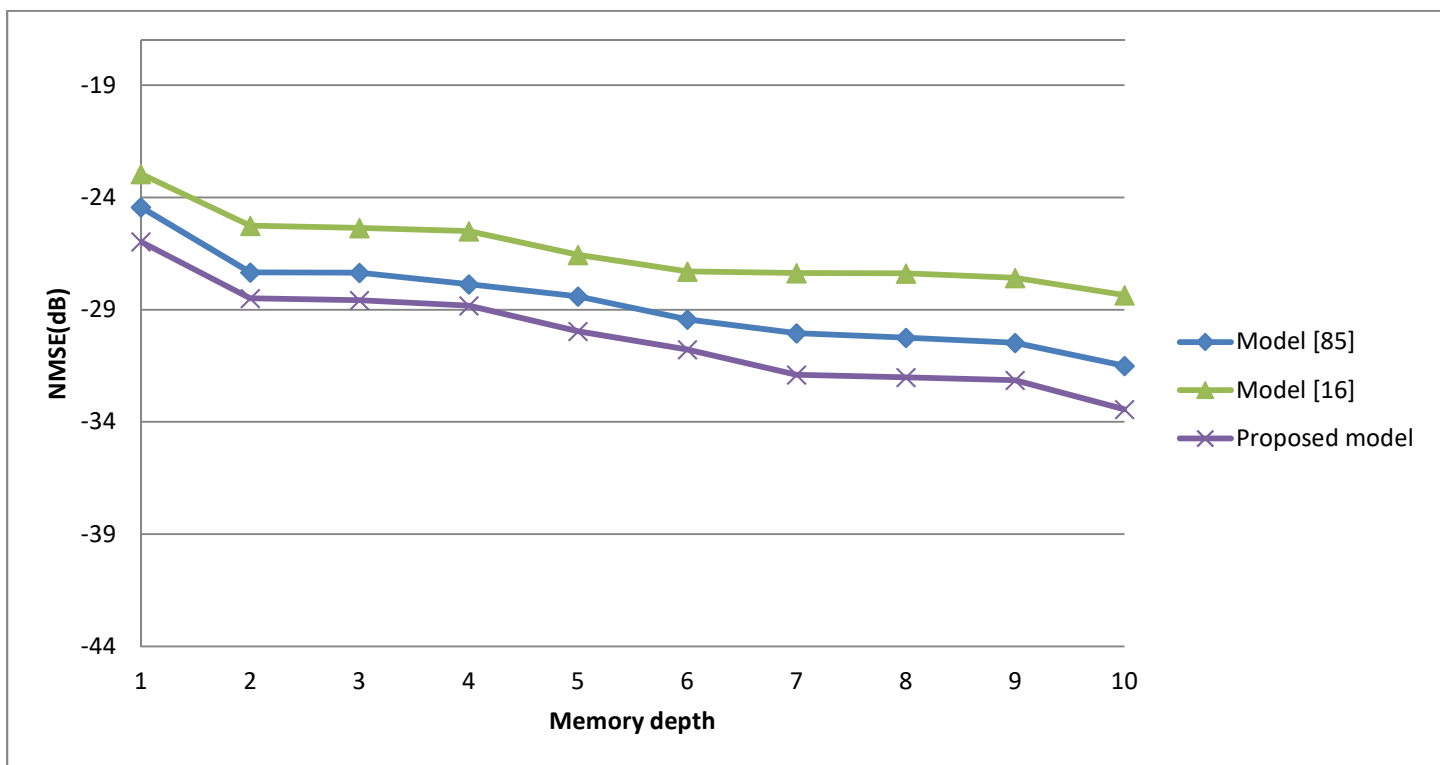


Figure 5.5 $NMSE_{dB}$ vs memory depth for scenario (2) with nonlinearity order =5 for high-band

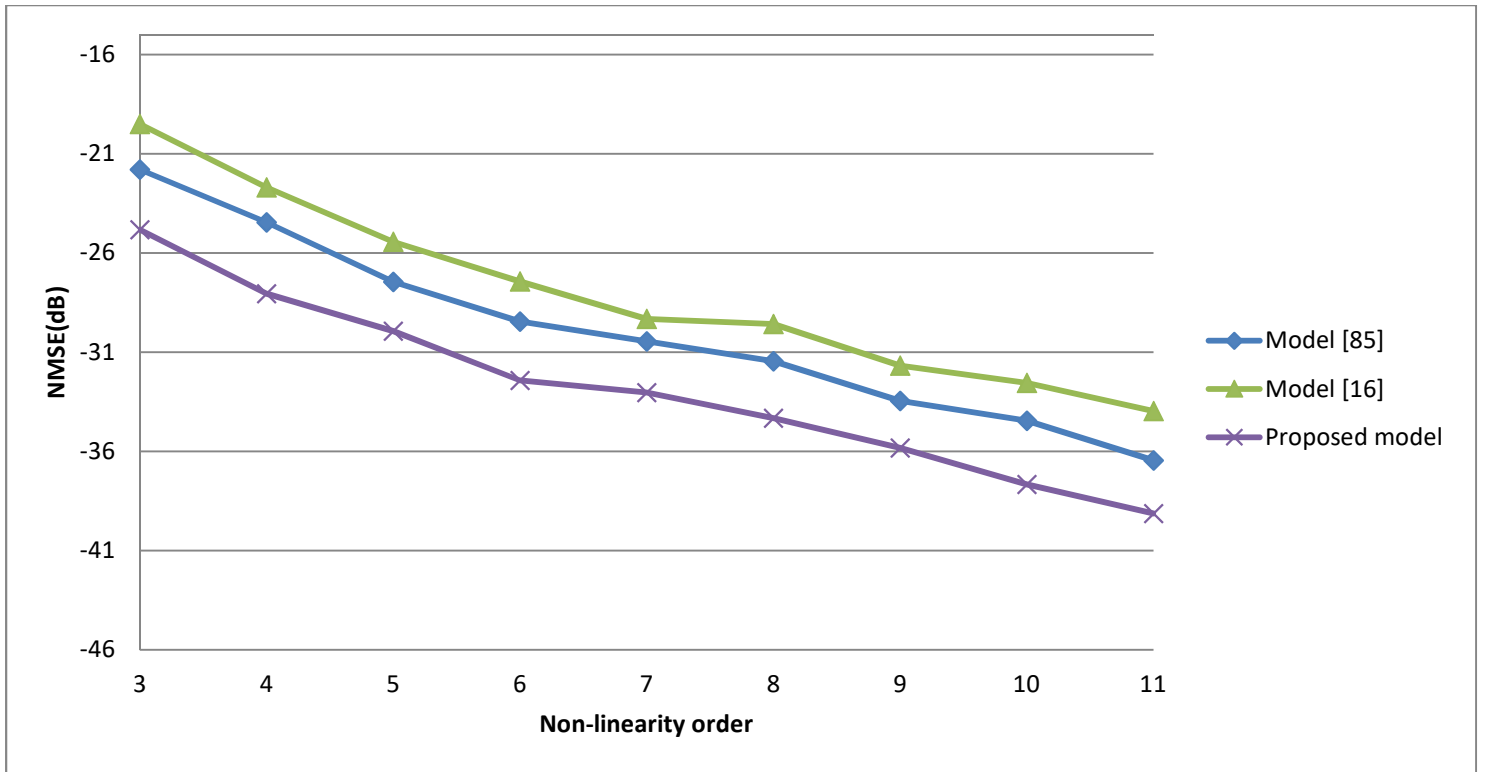


Figure 5.6 NMSE_{dB} vs nonlinearity order for scenario (2) with memory depth =3 for low-band

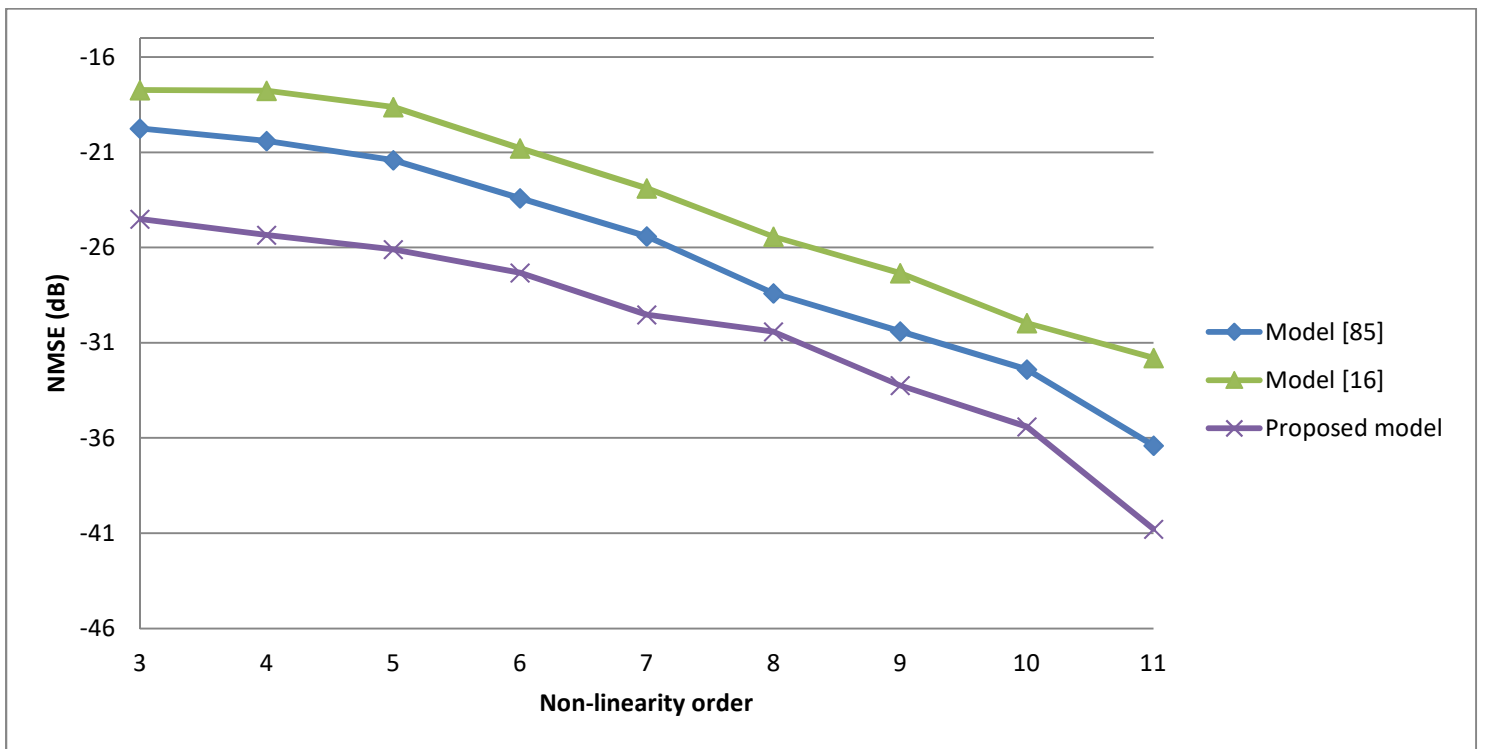


Figure 5.7 NMSE_{dB} vs nonlinearity order for scenario (2) with memory depth =3 for high-band

5.2.3 Performance Assessment in Frequency Domain

- For test scenario (1):

Figures 5.8, 5.9 and 5.10 further confirm the ability of the proposed model to accurately predict the measured PA spectrum, with the addition of the distortions that accounts for the nonlinear memory effects of the DUT. For that, the output of the model which is the summation of the outputs of the two loops, accounts for both nonlinearity and memory effects and will consequently allow for better modeling accuracy and mimicking of the dynamic nonlinear effects of the DUT.

As it can be seen from Figures 5.8, 5.9 and 5.10, the modeled output spectrum of the broadband signal is more efficient than the single ones, and it can predict the out-of-band spectrum and give a better performance against the inter-modulation and cross-modulation.

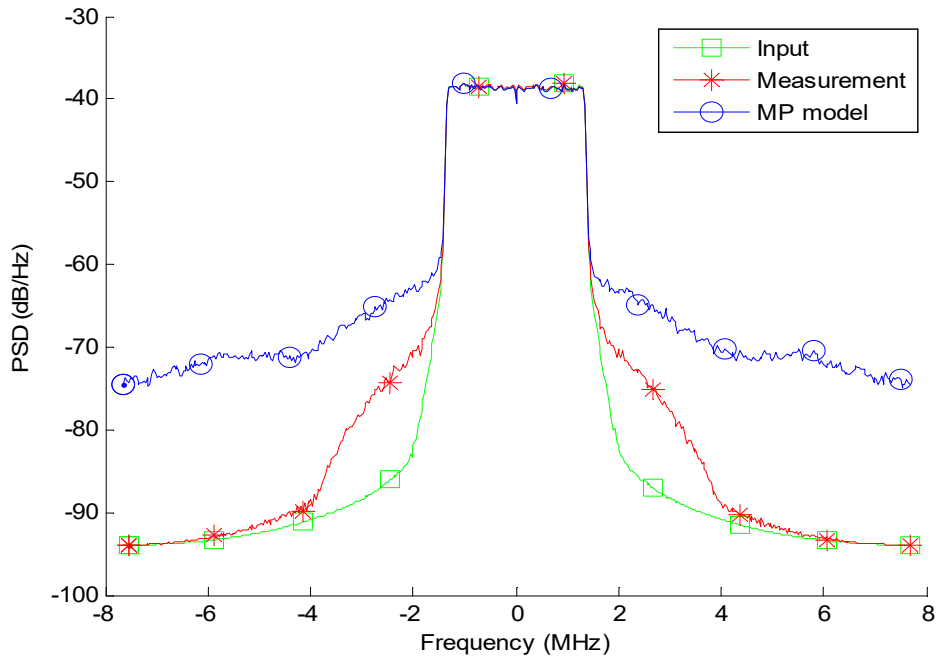


Figure 5.8 The spectrum of low-band with $M=3$ and $N = 5$

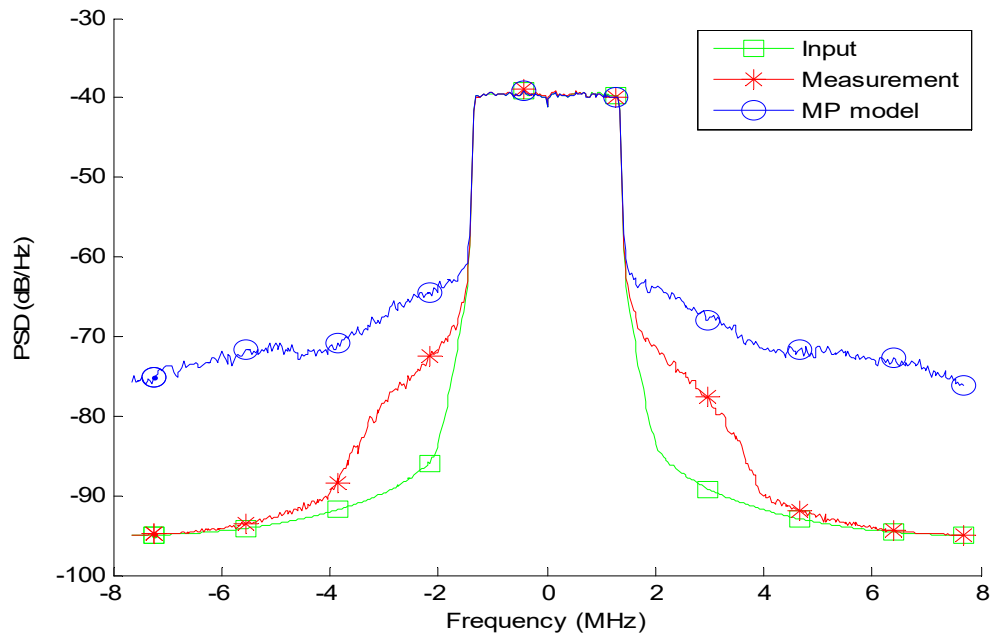


Figure 5.9 The spectrum of high-band with M=3 and N =5

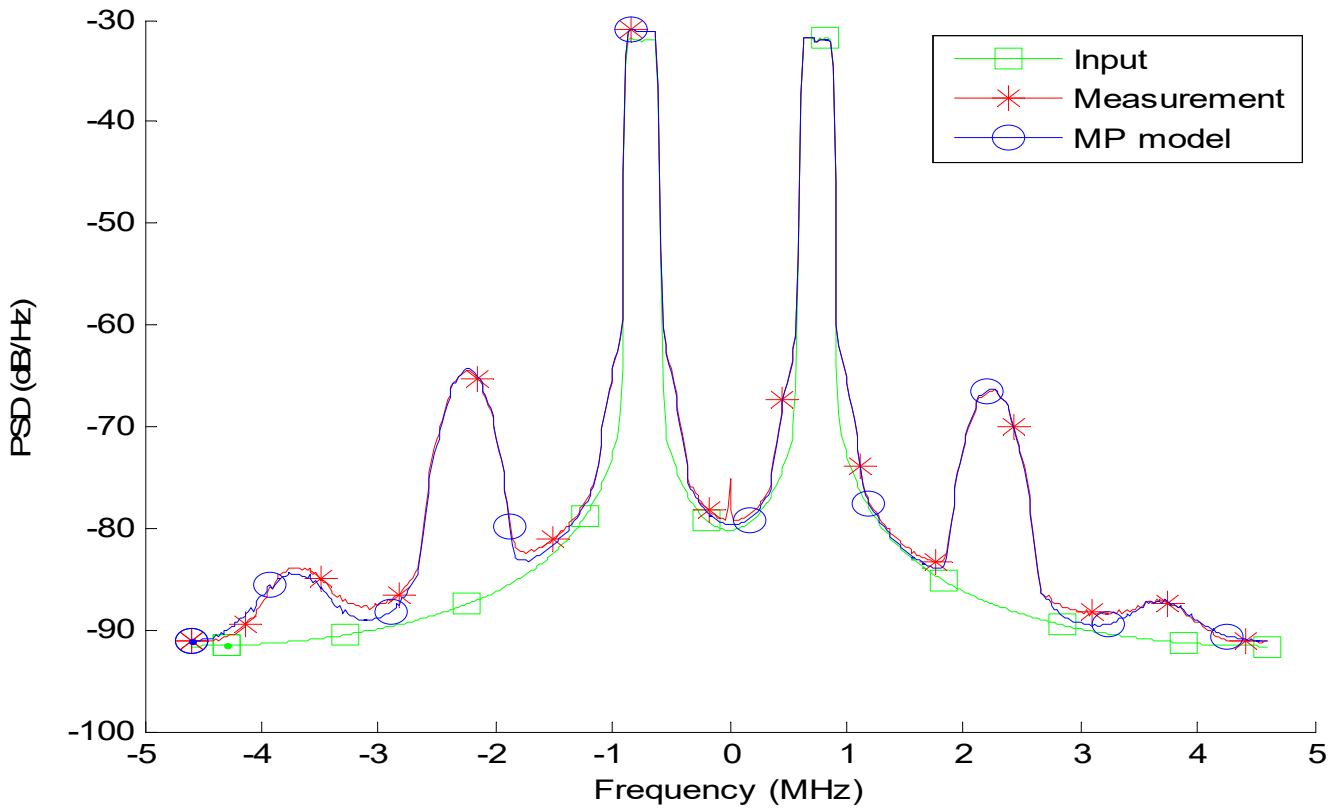


Figure 5.10 The spectrum of the broadband with M=3 and N= 5

- For test scenario (2):

Figure 5.11 and Figure 5.13 give the output spectrum of the comparison between the MP models in terms of which model will give the closer spectrum to the measured output of the PA. In Figure 5.11, it appears that for the low-band the output spectrum for the model in [16] gives the highest nonlinearity while the model in [85] with the proposed model gives a close shape to the measurement output as appear in the zoomed output plot in Figure 5.12. The same goes to the high-band in Figure 5.13, where the proposed model shows more similarity to the measurement output signal with a various change for both models in [85] and [16] which give a linearity worse than the measurement output as appear in Figure 5.13. Figure 5.14 gives a zoomed version of the high-band output power spectrum.

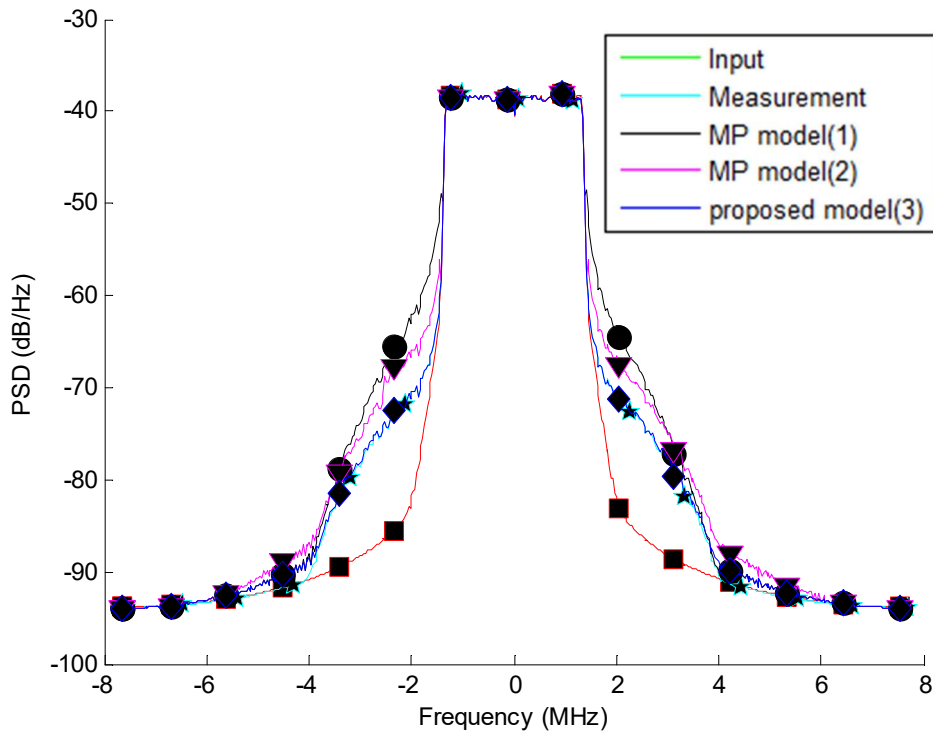


Figure 5.11 The spectrum of dual-band for low-band with $M=3$ and $N=5$

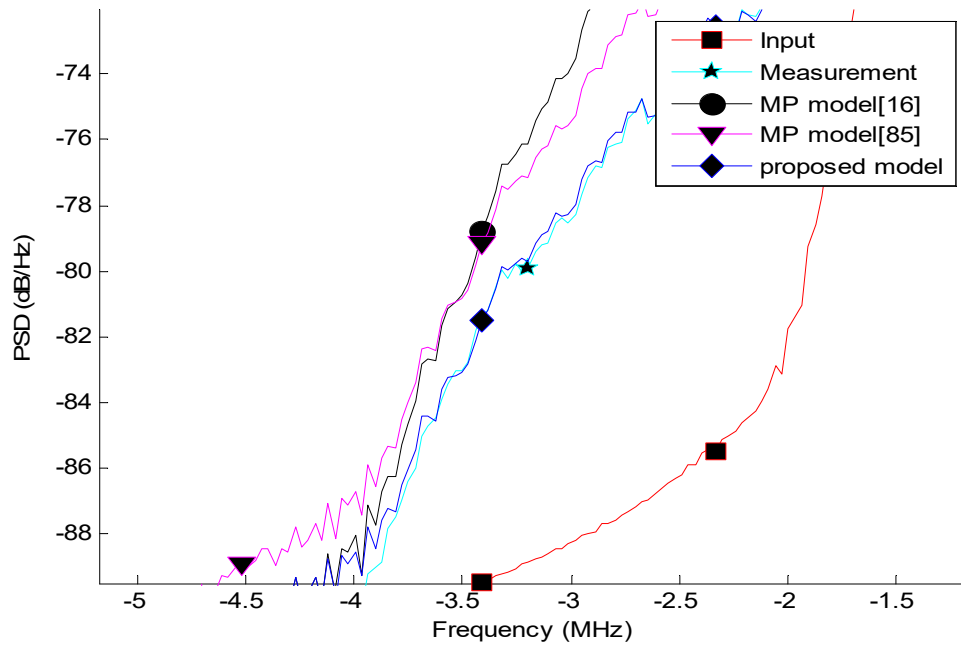


Figure 5.12 A zoom section of figure 5.12

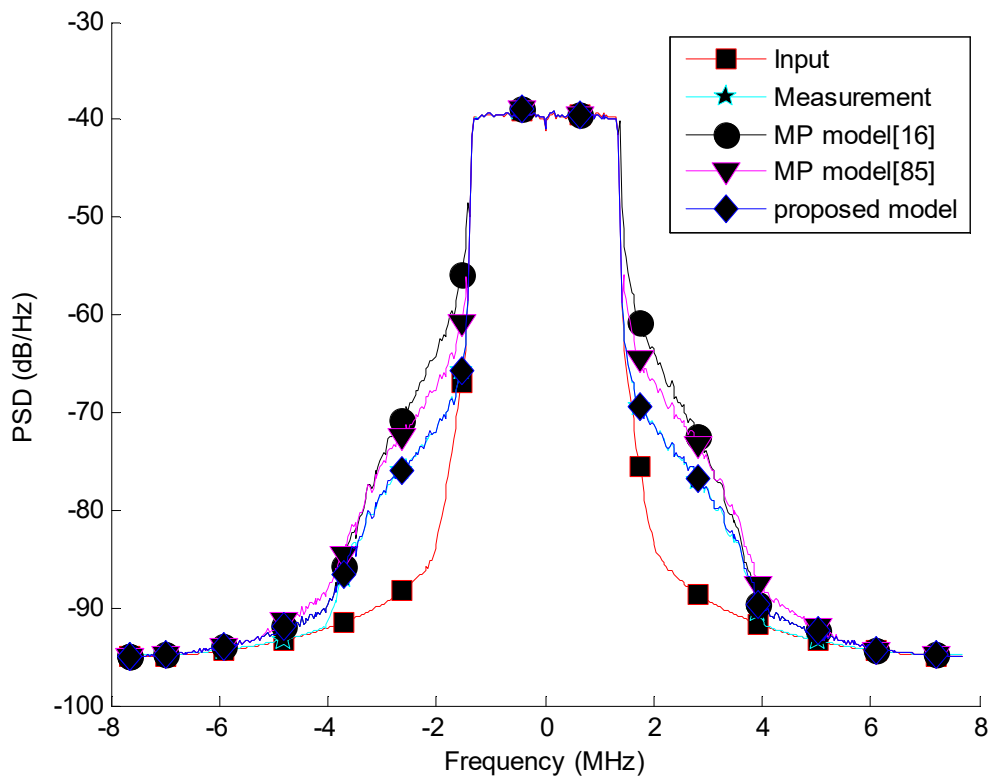


Figure 5.13 The spectrum of dual-band for high-band with $M=3$ and $N=5$

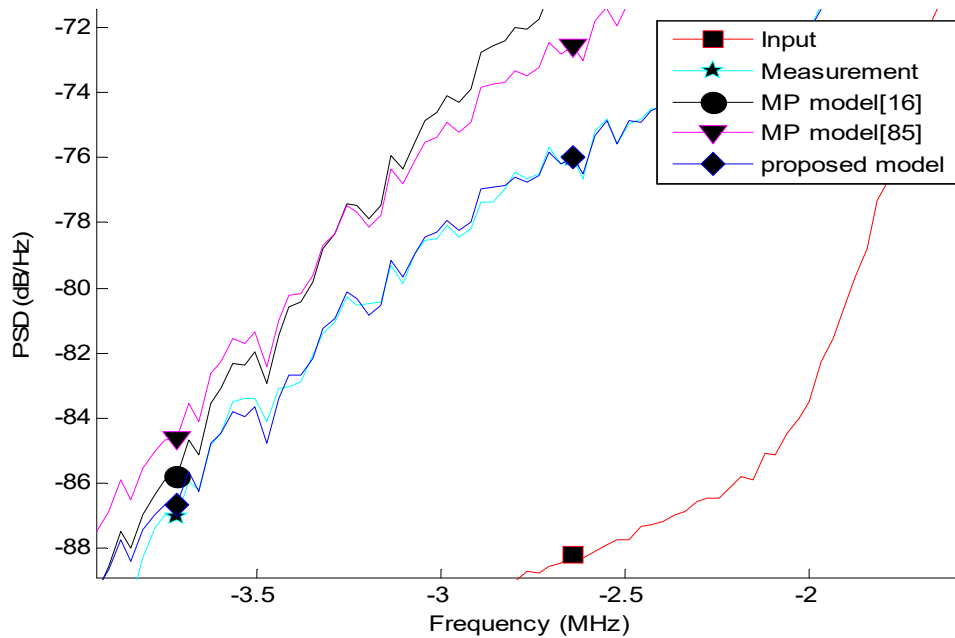


Figure 5.14 A zoom section of figure 5.14

5.2.4 Condition Number Metric Performance for Test Scenario (1)

In this section, the focus is on expressing the output of the models in terms of their condition number as a function of the non-linearity order N used for a fixed memory depth ($M = 3$). The value of N was varied between 3 and 7 based on the modeling results of the previous section. According to Figure 5.15, for the considered nonlinearity orders, the resulting matrix has a large condition number, which leads to higher sensitivity to disturbance. It is difficult to accurately identify the coefficients with very high nonlinear order due to the fact that the condition number increases very quickly with increasing nonlinear order where a large condition number means inaccurate identification results.

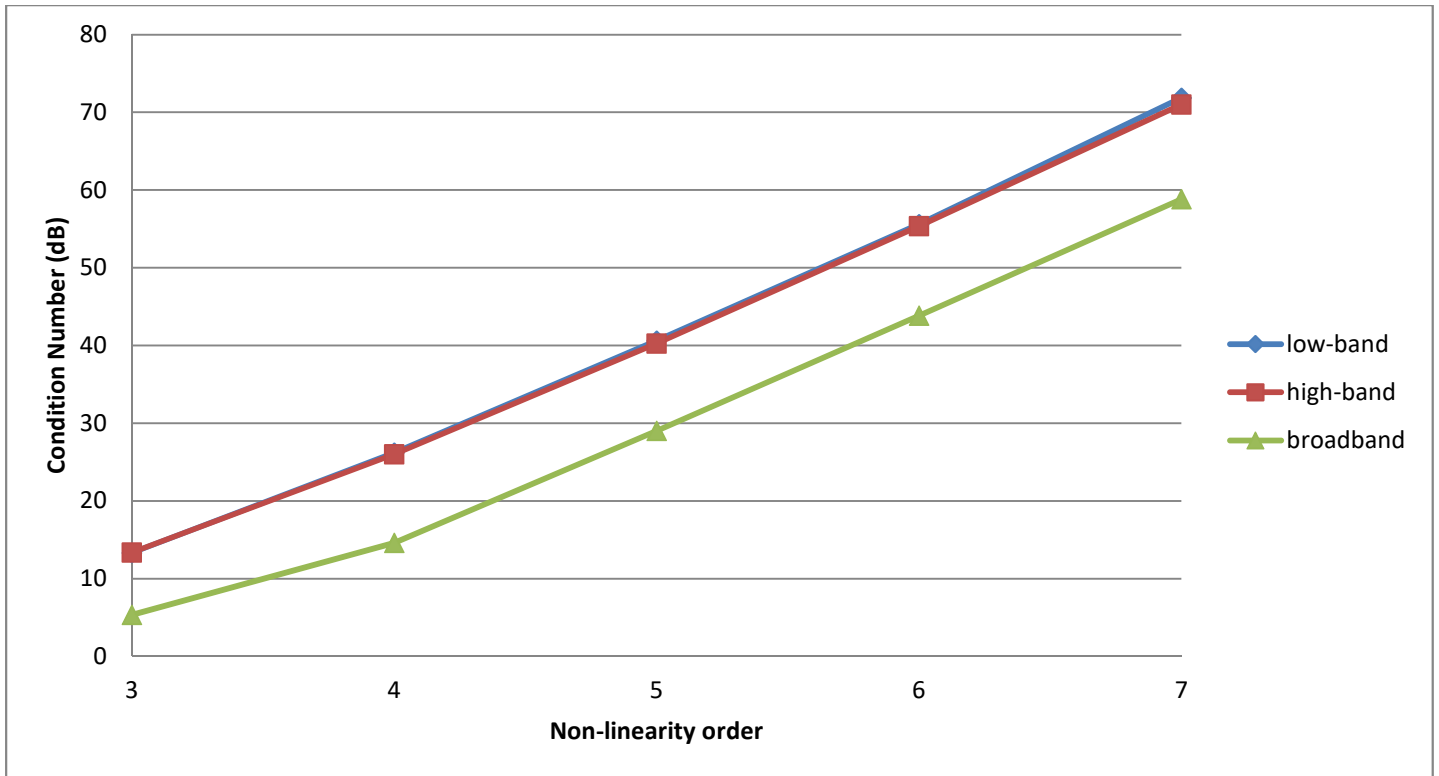


Figure 5.15 Condition number_{dB} vs non-linearity for scenario (1) with memory depth =3

5.2.5 Condition Number Performance for Test Scenario (2)

In Figure 5.16 and Figure 5.17, the proposed model gives the lowest condition number (less than 40 dB) for N=7. The selected value provides satisfactory modelling accuracy for the proposed models against the earlier MP models ([85] and [16]) in both the low and the high bands. Here, it can be seen that the condition number of the proposed model is significant, which result in having better performance with the dual-band MP model for PAs behavioural modeling.

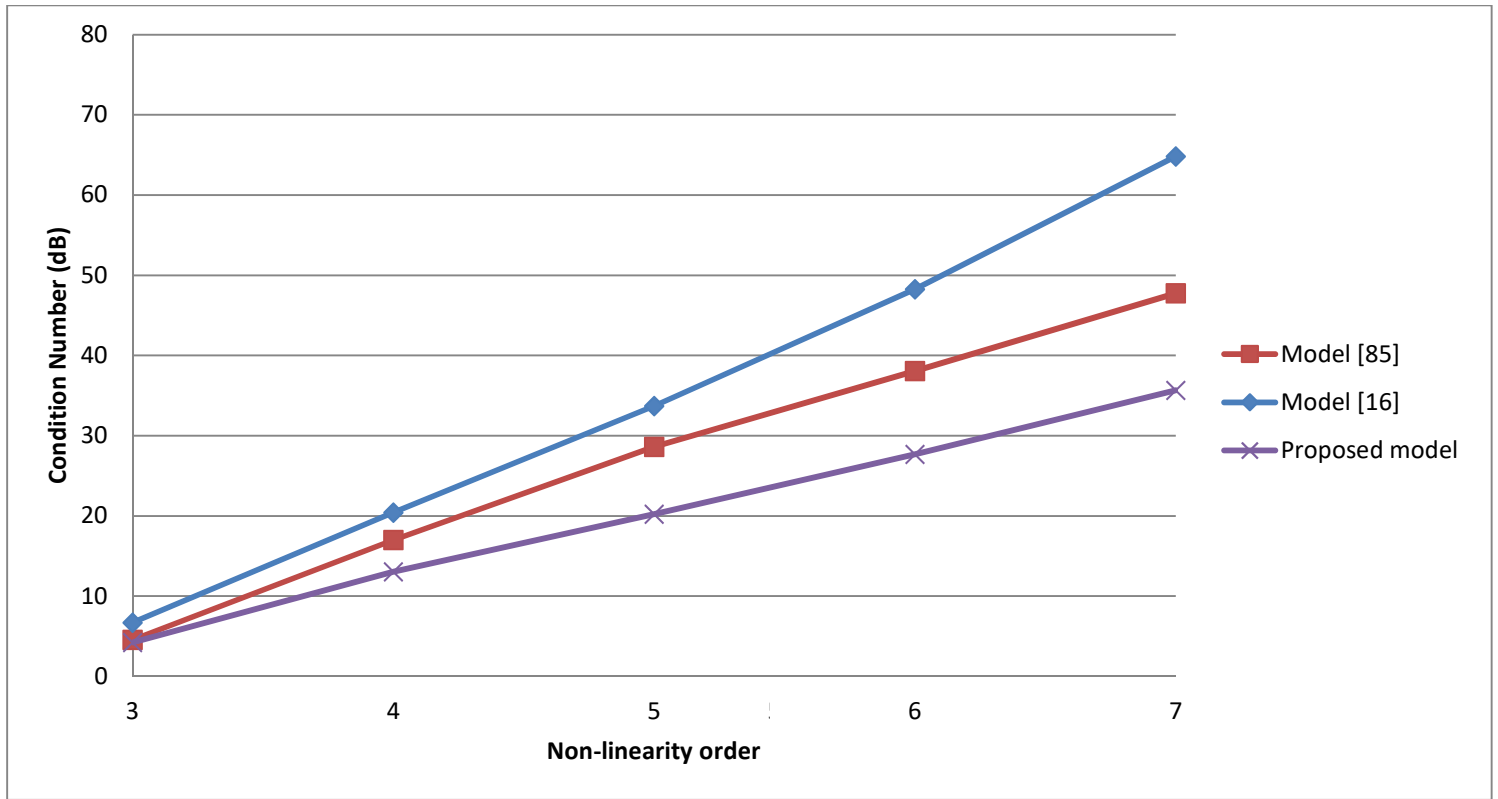


Figure 5.16 Condition number_{dB} vs non-linearity for scenario (2) with memory depth =3 for low-band

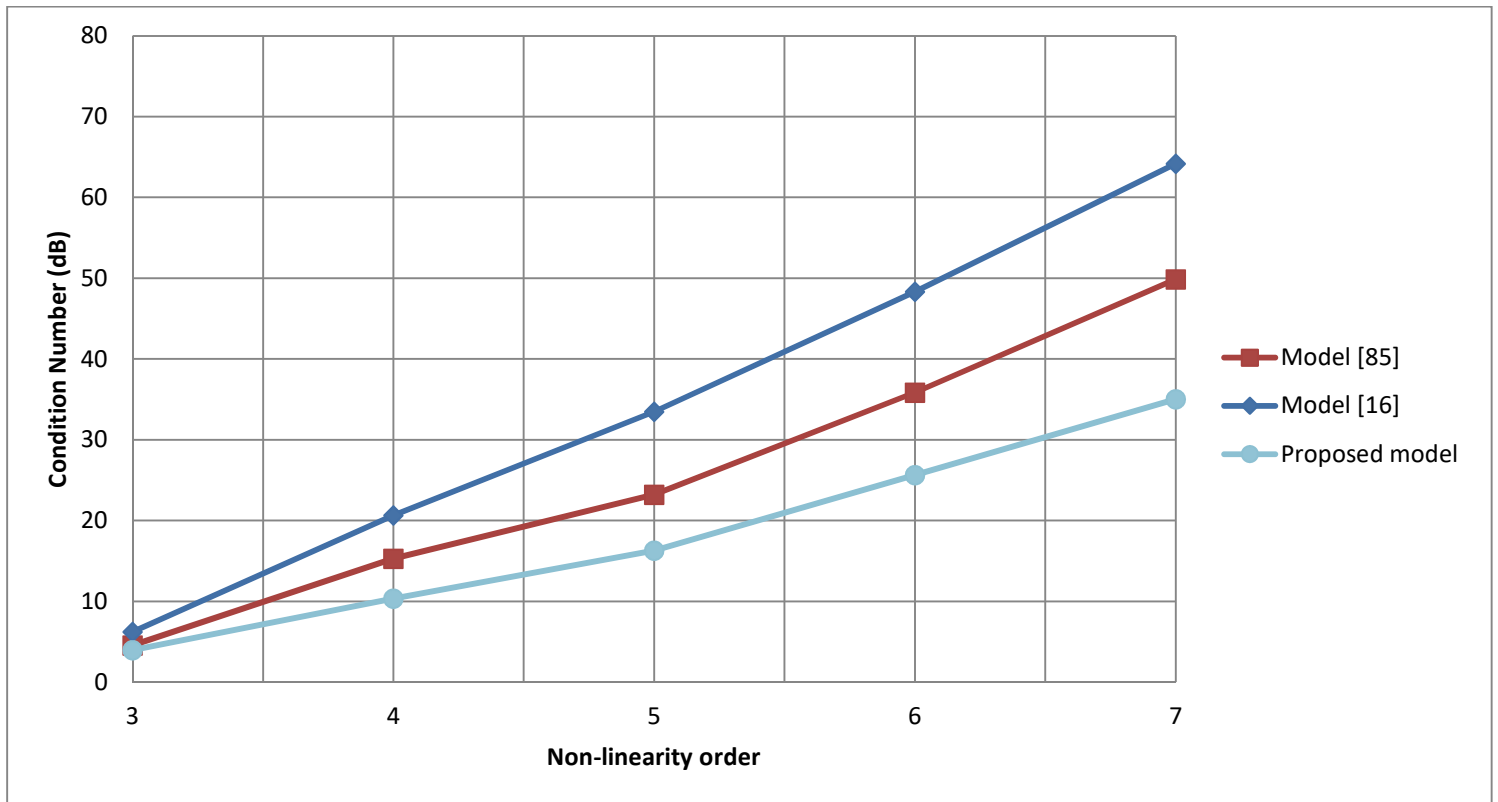


Figure 5.17 Condition number_{dB} vs non-linearity for scenario (2) with memory depth =3 for high-band

As the condition number increases significantly as nonlinearity order increases. The maximum condition number that can be handle by the DSPs for a 64 bits computer in real implementation has a dynamic range no more than 10^{20} . Thus in such case numerical instability may become unavoidable. It can also be shown that the condition number is an indicator of the transfer of error from the matrix to the solutions. As a rule of thumb, if a condition number is 10^n , then one can expect to lose at least n digits of precision in solving the system [88]. Figure 5.18 and 5.19 shows the matrix condition number for three dual band models in real implementation.

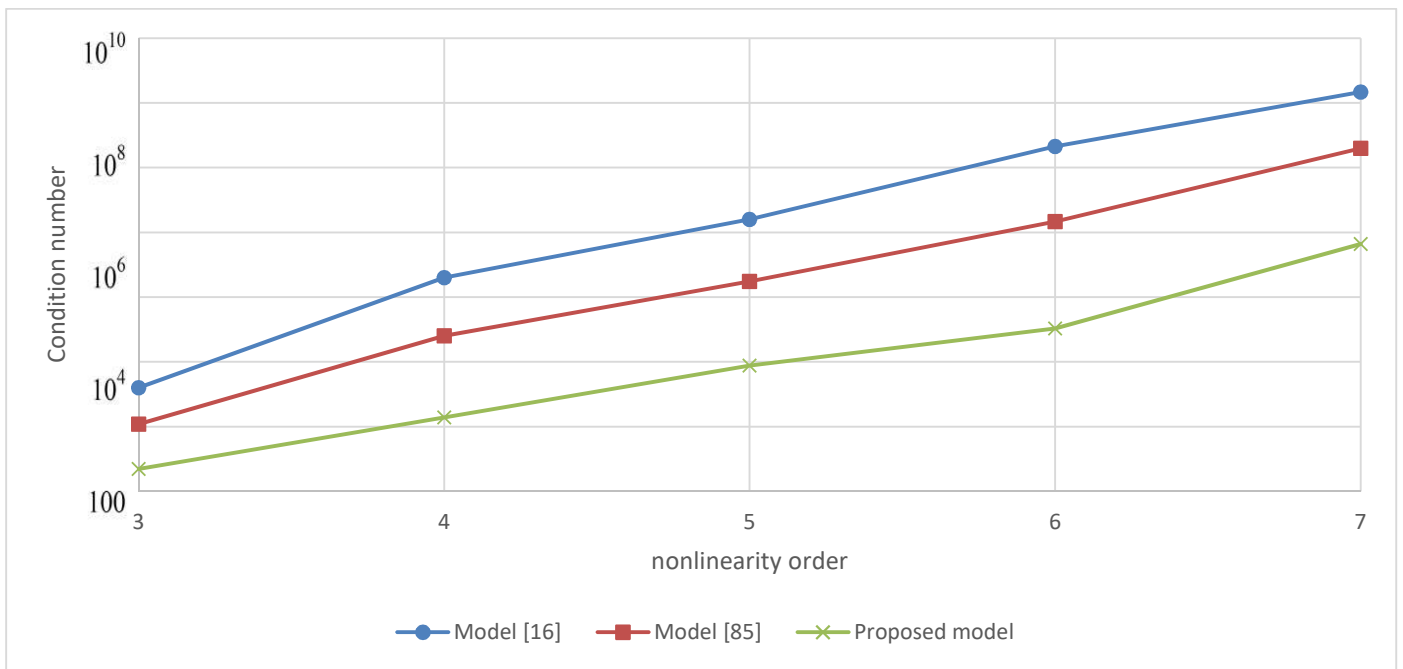


Figure 5.18 A realistic condition number vs non-linearity for scenario (2) with memory depth =3 for low-band

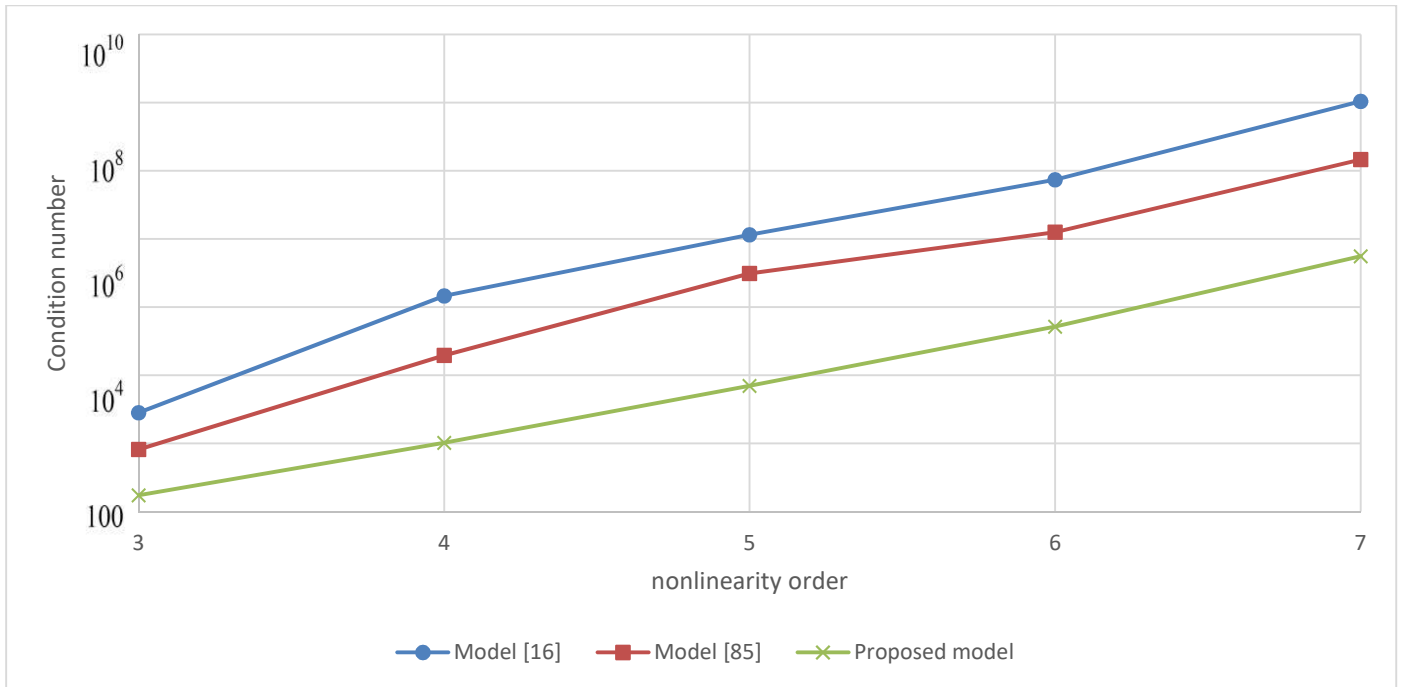


Figure 5.19 A realistic condition number vs non-linearity for scenario (2) with memory depth =3 for high -band

A thorough comparison in the performances of the proposed model and the conventional models of the considered test signals is presented in Table 1 by taking a sample of the output with a memory depth ($M=3$) and nonlinearity order ($N=5$). The table shows the difference in NMSE between the proposed model and the conventional models in [85] and [16] for the low and high band signals. Moreover, the use of the proposed model improves the conditioning number metrics by up to 13 dB (approximately 18.4%) comparing to the best of the conventional models which is due to the drastic decrease in the number of coefficients. Furthermore, the total number of coefficients is decrease by almost 33.5% in the considered cases.

Table 5.1 Comparison between the proposed model and the conventional models

	MP model in [16]	MP model in [85]	Proposed MP model
Number of Coefficients	3476	1084	684
Low band			
(M,N)	(3,5)		
NMSE (dB) vs memory depth	-29.42	-33.41	-35.13
NMSE (dB) vs nonlinear order	-25.43	-27.45	-29.94
Condition number (dB)	33.70	28.58	20.20
High band			
(M,N)	(3,5)		
NMSE (dB) vs memory depth	-26.54	-28.40	-29.96
NMSE (dB) vs nonlinear order	-18.61	-21.40	-26.10
Condition number (dB)	33.47	23.23	16.29

5.3 Summary

For the proposed model, the results show that this model can give more improvement and better performance than the models in [16] and [85] in both the high and the low bands. This new model gives a promising result for mimicking the memory effects and distortion present in the measurement output spectrum with high accuracy.

Based on choosing the accurate model dimensions for a trade-off between the model accuracy (evaluated in terms of NMSE), model robustness (evaluated in terms of conditioning number), and the model complexity (evaluated in terms of total number of coefficients) the proposed model was found to outperform the previously represented ones. The results show that the proposed dual-band memory polynomial model led to good

comparable performance in time domain and frequency domain in addition to have lower computational complexity.

While taking into account that the broadband model can still be the best model and gives better performance in some aspects like the NMSE compared to the dual-band model, it still have a major drawback related to the need to use a high sampling rate. In addition to that, a maximum change in the modeled output compared to the measurement output for the proposed model was 1.09 dB while in case of the broadband model it was 4.51 dB.

CHAPTER 6

CONCLUSIONS AND FUTURE WORK

6.1 Conclusion

CA LTE-A is an efficient approach to increment the signal bandwidth inside the available spectrum. Therefore, multi-band transmitter architectures are expected to work in both simultaneous and single modes of operation in order to support the intra-band and inter-band CAs in LTE-advanced. Thus, a comprehensive analysis of the distortion output of various RF requirements and their effects on direct conversion and multi-band transmitters was presented.

The conventional PA behavioural models schemes have been limited to single- and narrow-band signals. The direct application of these conventional models to multi-band signals creates challenging requirements. These challenges include unrealistic sampling rates in the observation path of PA input/output signals. In addition, the complexity of existent PA behavioural models schemes increases linearly as a function of the PA nonlinearity order and memory effects, which lead to a high number of coefficients. To that end, newer modeling schemes are needed to handle these problems and new approaches are essential to reduce their complexity.

The topic of behavioural modeling of single band RF PA was investigated. Behavioural modeling is an efficient tool in modeling and analyzing the PAs behavior. At this sort of system level modeling, the PA is treated as a black box, where the model provides a computationally efficient means of relating the input/output PA signals without any knowledge of the physical aspects of the system.

As a contribution of the thesis, the nonlinear distortion in dual-band transmitters was analyzed. The proposed behavioural model using memory polynomial model with an enhancement in the conventional methods was thoroughly investigated. Ultimately, the proposed method was found to perform well compared to the other models in terms of NMSE, the number of coefficient and condition number, in addition to the output spectrum. The proposed technique was experimentally assessed by modeling a dual-band Class AB PA with two different scenarios of MP models. In fact, the proposed model improves the complexity and the robustness by 33.5% and 18.4%, respectively. The proposed model demonstrated enhancement in the performance and lower computational complexity than the best in class models.

6.2 Future Work

The results obtained for the proposed MP model suggest some potential further research in the following areas:

1. Implement the scheme in real-time measurements and compare it with the simulation results.
2. Making further generalization and investigation of the power analysis when more complicated signals are used.

Therefore, other architectures capable of representing memory with nonlinearity and other cost functions useful for achieving global optimization for the cancellation schemes for the dual-band should be taken into consideration.

APPENDIX A

Table A.1 2nd, 3rd and the 5th harmonics, 2nd, 3rd and 5th IMD ranges for release 12 inter-bands

CA Inter-band	Carrier Frequency band (MHz)	2 nd Harmonics range (MHz)	3 rd Harmonics range (MHz)	5 th Harmonics rang (MHz)	2 nd IMD ranges (MHz)	3 rd IMD ranges (MHz)		5 th IMD ranges (MHz)		5 th IMD ranges (MHz)	
						$(3\omega_1 \pm 2\omega_2 \text{ \& } 3\omega_2 \pm 2\omega_1)$		$(4\omega_1 \pm \omega_2 \text{ \& } 4\omega_2 \pm \omega_1)$			
CA_1-3	2110-2170 1805-1880	4220-4340 3610-3760	6330-6510 5415-5640	10550-10850 9025-9400	230-365 3915-4050	2340-2535 1440-1650	6025-6220 5720-5930	2570-2900 1075-1420	9940-10270 9635-9980	6560-6875 5050-5410	10245-10560 9330-9690
CA_1-5	2110-2170 869-894	4220-4340 1738-1788*	6330-6510 2607-2682	10550-10850 4345-4470	1216-1301* 2979-3064	3326-3471 322-432	5089-5234 3848-3958	4542-4772 1538-1733*	8068-8298 6827-7022	7546-7811 1306-1466*	9309-9574 5586-5746
CA_1-7	2110-2170 2620-2690	4220-4340 5240-5380	6330-6510 7860-8070	10550-10850 13100-13450	450-580 4730-4860	1530-1720 3070-3270	6840-7030 7350-7550	950-1270 3520-3850	11570-11890 12080-12410	5750-6060 8310-8650	11060-11370 12590-12930
CA_1-8	2110-2170 925-960	4220-4340 1850-1920**	6330-6510 2775-2880	10550-10850 4625-4800	1150-1245** 3035-3130	3260-3415 190-320	5145-5300 3960-4090	4410-4660 1340-1565*	8180-8430 6995-7220	7480-7755 1530-1730*	9365-9640 5810-6010
CA_1-11	2110-2170 1475.9-1495.9	4220-4340 2951.8-2991.8	6330-6510 4427.7-4487.7	10550-10850 7379.5-7479.5	614.1-694.1 3585.9-3665.9	2724.1-2864.1 781.8-881.8	5695.9-5835.9 5061.8-5161.8	3338.2-3558.2 87.7-267.7	9281.8-9501.8 8647.7-8827.7	6944.1-7204.1 3733.6-3873.6	9915.9-10175.9 8013.6-8153.6
CA_1-18	2110-2170 860-875	4220-4340 1720-1750*	6330-6510 2580-2625	10550-10850 4300-4375	1235-1310* 2970-3045	3345-3480 360-450	5080-5215 3830-3920	4580-4790 1595-1760*	8050-8260 6800-6965	7565-7820 1270-1390*	9300-9555 5550-5670
CA_1-19	2110-2170 875-890	4220-4340 1750-1780*	6330-6510 2625-2670	10550-10850 4375-4450	1220-1295* 2985-3060	3330-3465 330-420	5095-5230 3860-3950	4550-4760 1550-1715*	8080-8290 6845-7010	7550-7805 1330-1450*	9315-9570 5610-5730
CA_1-20	2110-2170 791-821	4220-4340 1582-1642*	6330-6510 2373-2463	10550-10850 3955-4105	1289-1379* 2901-2991	3399-3549 468-588	5011-5161 3692-3812	4688-4928 1757-1967**	7912-8152 6593-6803	7619-7889 994-1174**	9231-9501 5274-5454
CA_1-21	2110-2170 1495.9-1510.9	4220-4340 2991.8-3021.8	6330-6510 4487.7-4532.7	10550-10850 7479.5-7554.5	599.1-674.1 3605.9-3680.9	2709.1-2844.1 821.8-911.8	5715.9-5850.9 5101.8-5191.8	3308.2-3518.2 147.7-312.7	9321.8-9531.8 8707.7-8872.7	6929.1-7184.1 3813.6-3933.6	9935.9-10190.9 8093.6-8213.6
CA_1-26	2110-2170 859-894	4220-4340 1718-1788*	6330-6510 2577-2682	10550-10850 4295-4470	1216-1311* 2969-3064	3326-3481 322-452	5079-5234 3828-3958	4542-4792 1538-1763*	8048-8298 6797-7022	7546-7821 1266-1466*	9299-9574 5546-5746
CA_1-28	2110-2170 758-803	4220-4340 1516-1606*	6330-6510 2274-2409	10550-10850 3790-4015	1307-1412* 2868-2973	3417-3582 504-654	4978-5143 3626-3776	4724-4994 1811-2066**	7846-8116 6494-6749	7637-7922 862-1102**	9198-9483 5142-5382
CA_1-41	2110-2170 2496-2690	4220-4340 4992-5380	6330-6510 7488-8070	10550-10850 12480-13450	326-580 4606-4860	1530-1844 2822-3270	6716-7030 7102-7550	950-1518 3148-3850	11322-11890 11708-12410	5750-6184 7814-8650	10936-11370 12094-12930

CA_1-42	2110-2170 3400-3600	4220-4340 6800-7200	6330-6510 10200-10800	10550-10850 17000-18000	1230-1490 5510-5770	620-940 4630-5090	7620-7940 8910-9370	870-290 5860-6580	13130-13710 14420-15140	4840-5280 11430-12290	11840-12280 15710-16570
CA_2-4	1930-1990 2110-2155	3860-3980 4220-4310	5790-5970 6330-6465	9650-9950 10550-10775	120-225 4040-4145	1705-1870 2230-2380	5970-6135 6150-6300	1480-1750 2350-2605	10010-10280 10190-10445	5565-5850 6450-6690	9830-10115 10370-10610
CA_2-5	1930-1990 869-894	3860-3980 1738-1788**	5790-5970 2607-2682	9650-9950 4345-4470	1036-1121** 2799-2884	2966-3111 142-252	4729-4874 3668-3778	4002-4232 1178-1373*	7528-7758 6467-6662	6826-7091 1486-1646*	8589-8854 5406-5566
CA_2-12	1930-1990 729-746	3860-3980 1458-1492*	5790-5970 2187-2238	9650-9950 3645-3730	1184-1261* 2659-2736	3114-3251 438-532	4589-4726 3388-3482	4298-4512 1622-1793*	7248-7462 6047-6218	6974-7231 926-1054**	8449-8706 4846-4974
CA_2-13	1930-1990 746-756	3860-3980 1492-1512*	5790-5970 2238-2268	9650-9950 3730-3780	1174-1244* 2676-2746	3104-3234 418-498	4606-4736 3422-3502	4278-4478 1592-1742*	7282-7482 6098-6248	6964-7214 994-1094*	8466-8716 4914-5014
CA_2-17	1930-1990 734-746	3860-3980 1468-1492*	5790-5970 2202-2238	9650-9950 3670-3730	1184-1256* 2664-2736	3114-3246 438-522	4594-4726 3398-3482	4298-4502 1622-1778*	7258-7462 6062-6218	6974-7226 946-1054*	8454-8706 4866-4974
CA_2-29	1930-1990 717-728	3860-3980 1434-1456*	5790-5970 2151-2184	9650-9950 3585-3640	1202-1273* 2647-2718	3132-3263 474-556	4577-4708 3364-3446	4334-4536 1676-1829**	7224-7426 6011-6164	6992-7243 878-982*	8437-8688 4798-4902
CA_2-30	1930-1990 2350-2360	3860-3980 4700-4720	5790-5970 7050-7080	9650-9950 11750-11800	360-430 4280-4350	1500-1630 2710-2790	6210-6340 6630-6710	1070-1270 3070-3220	10490-10690 10910-11060	5360-5610 7410-7510	10070-10320 11330-11430
CA_3-5	1805-1880 869-894	3610-3760 1738-1788**	5415-5640 2607-2682	9025-9400 4345-4470	911-1011** 2674-2774	2716-2891 17-142	4479-4654 3543-3668	3627-3902 928-1153**	7153-7428 6217-6442	6326-6651 1596-1771**	8089-8414 5281-5456
CA_3-7	1805-1880 2620-2690	3610-3760 5240-5380	5415-5640 7860-8070	9025-9400 13100-13450	740-885 4425-4570	920-1140 3360-3575	6230-6450 7045-7260	35-400 4100-4460	10655-11020 11470-11830	4530-4900 8600-8955	9840-10210 12285-12640
CA_3-8	1805-1880 925-960	3610-3760 1850-1920***	5415-5640 2775-2880	9025-9400 4625-4800	845-955*** 2730-2840	2650-2835 30-115	4535-4720 3655-3800	3495-3790 730-985***	7265-7560 6385-6640	6260-6595 1820-2035***	8145-8480 5505-5720
CA_3-19	1805-1880 875-890	3610-3760 1750-1780**	5415-5640 2625-2670	9025-9400 4375-4450	915-1005** 2680-2770	2720-2885 25-130	4485-4650 3555-3660	3635-3890 940-1135**	7165-7420 6235-6430	6330-6645 1620-1755**	8095-8410 5305-5440
CA_3-20	1805-1880 791-821	3610-3760 1582-1642*	5415-5640 2373-2463	9025-9400 3955-4105	984-1089** 2596-2701	2789-2969 163-298	4401-4581 3387-3522	3773-4058 1387-1147*	6997-7282 5983-6223	6399-6729 1284-1479*	8011-8341 4969-5164
CA_3-26	1805-1880 859-894	3610-3760 1718-1788**	5415-5640 2577-2682	9025-9400 4295-4470	911-1021** 2664-2774	2716-2901 17-162	4469-4654 3523-3668	3627-3922 928-1183**	7133-7428 6187-6442	6326-6661 1556-1771**	8079-8414 5241-5456
CA_3-27	1805-1880 852-869	3610-3760 1704-1738**	5415-5640 2556-2607	9025-9400 4260-4345	936-1028** 2657-2749	2741-2908 67-176	4462-4629 3509-3618	3677-3936 1003-1204*	7119-7378 6166-6367	6351-6668 1528-1671*	8072-8389 5213-5356
CA_3-28	1805-1880 758-803	3610-3760 1516-1606*	5415-5640 2274-2409	9025-9400 3790-4015	1002-1122* 2563-2683	2807-3002 199-364	4368-4563 3321-3486	3809-4124 1201-1486*	6931-7246 5884-6169	6417-6762 1152-1407*	7978-8323 4837-5092
CA_4-5	2110-2155 869-894	4220-4310 1738-1788*	6330-6465 2607-2682	10550-10775 4345-4470	1216-1286* 2979-3049	3326-3441 322-417	5089-5204 3848-3943	4542-4727 1703-1538*	8068-8253 6827-6992	7546-7751 1321-1466*	9309-9514 5586-5731
CA_4-7	2110-2155 2620-2690	4220-4310 5240-5380	6330-6465 7860-8070	10550-10775 13100-13450	465-580 4730-4845	1530-1690 3085-3270	6840-7000 7350-7535	950-1225 3550-3850	11570-11845 12080-12380	5750-6000 8325-8650	11060-11310 12590-12915
CA_4-12	2110-2155 729-746	4220-4310 1458-1492*	6330-6465 2187-2238	10550-10775 3645-3730	1364-1426* 2839-2901	3474-3581 618-697	4949-5056 3568-3647	4838-5007 1982-2123***	7788-7957 6407-6548	7694-7891 761-874**	9169-9366 5026-5139

CA_4-13	2110-2155 746-756	4220-4310 1492-1512*	6330-6465 2238-2268	10550-10775 3730-3780	1354-1409* 2856-2911	3464-3564 598-663	4966-5066 3602-3667	4818-4973 1952-2072**	7822-7977 6458-6578	7684-7874 829-914**	9186-9376 5094-5179
CA_4-17	2110-2155 734-746	4220-4310 1468-1492*	6330-6465 2202-2238	10550-10775 3670-3730	1364-1421* 2844-2901	3474-3576 618-687	4954-5056 3578-3647	4838-4997 1982-2108**	7798-7957 6422-6548	7694-7886 781-874**	9174-9366 5046-5139
CA_4-27	2110-2155 852-869	4220-4310 1704-1738*	6330-6465 2556-2607	10550-10775 4260-4345	1241-1303* 2962-3024	3351-3458 372-451	5072-5179 3814-3893	4592-4761 1613-1754*	8034-8203 6776-6917	7571-7768 1253-1366*	9292-9489 5518-5631
CA_4-29	2110-2155 717-728	4220-4310 1434-1456*	6330-6465 2151-2184***	10550-10775 3585-3640	1382-1438* 2827-2883	3492-3593 654-721***	4937-5038 3544-3611	4874-5031 2036-2159***	7764-7921 6371-6494	7712-7903 713-802***	9157-9348 4978-5067
CA_4-30	2110-2155 2350-2360	4220-4310 4700-4720	6330-6465 7050-7080	10550-10775 11750-11800	195-250 4460-4515	1860-1960 2545-2610	6570-6670 6810-6875	1610-1765 2740-2860	11030-11185 11270-11390	6080-6270 7245-7330	10790-10980 11510-11595
CA_5-7	869-894 2620-2690	1738-1788* 5240-5380	2607-2682*** 7860-8070	4345-4470 13100-13450	1726-1821* 3489-3584	832-952*** 4346-4511	4358-4478 6109-6274	2558-2773*** 6072-6332	7847-8062 9598-9858	786-956*** 9586-9891	6096-6266 11349-11654
CA_5-12	869-894 729-746	1738-1788 1458-1492	2607-2682 2187-2238	4345-4470 3645-3730	123-165 1598-1640	992-1059 564-623	2467-2534 2327-2386	1115-1224 399-500	4065-4174 3925-4026	2730-2847 2022-2115	4205-4322 3785-3878
CA_5-13	869-894 746-756	1738-1788 1492-1512	2607-2682 2238-2268	4345-4470 3730-3780	113-148 1615-1650	982-1042 598-643	2484-2544 2361-2406	1095-1190 450-530	4099-4194 3976-4056	2720-2830 2090-2155	4222-4332 3853-3918
CA_5-17	869-894	1738-1788	2607-2682	4345-4470	123-160	992-1054	2472-2534	1115-1214	4075-4174	2730-2842	4210-4322
CA_5-17	734-746	1468-1492	2202-2238	3670-3730	1603-1640	574-623	2337-2386	414-500	3940-4026	2042-2115	3805-3878
CA_5-25	869-894 1930-1995	1738-1788* 3860-3990	2607-2682 5790-5985	4345-4470 9650-9975	1036-1126* 2799-2889	142-257 2966-3121	3668-3783 4729-4884	1178-1383* 4002-4247	6467-6672 7528-7773	1481-1646* 6826-7111	5406-5571 8589-8874
CA_5-30	869-894 2350-2360	1738-1788* 4700-4720	2607-2682 7050-7080	4345-4470 11750-11800	1456-1491* 3219-3254	562-622 3806-3851	4088-4148 5569-5614	2018-2113* 5262-5342	7307-7402 8788-8868	1116-1226* 8506-8571	5826-5936 10269-10334
CA_7-8	2620-2690 925-960	5240-5380 1850-1920*	7860-8070 2775-2880	13100-13450 4625-4800	1660-1765* 3545-3650	4280-4455 700-840	6165-6340 4470-4610	5940-6220 2360-2605**	9710-9990 8015-8260	9520-9835 1010-1220**	11405-11720 6320-6530
CA_7-12	2620-2690 729-746	5240-5380 1458-1492*	7860-8070 2187-2238*	13100-13450 3645-3730	1874-1961* 3349-3436	4494-4651 1128-1232*	5969-6126 4078-4182	6368-6612 3002-3193	9318-9562 7427-7618	9734-10031 226-364	11209-11506 5536-5674
CA_7-20	2620-2690 791-821	5240-5380 1582-1642*	7860-8070 2373-2463*	13100-13450 3955-4105	1799-1899* 3411-3511	4419-4589 978-1108*	6031-6201 4202-4332	6218-6488 2777-3007	9442-9712 7613-7843	9659-9969 474-664*	11271-11581 5784-5974
CA_7-28	2620-2690 758-803	5240-5380 1516-1606*	7860-8070 2274-2409*	13100-13450 3790-4015	1817-1932* 3378-3493	4437-4622 1014-1174*	5998-6183 4136-4296	6254-6554 2831-3106	9376-9676 7514-7789	9677-10002 342-592	11238-11563 5652-5902
CA_8-11	925-960 1475.9-1495.9	1850-1920 2951.8-2991.8	2775-2880 4427.7-4487.7	4625-4800 7379.5-7479.5	515.9-570.9 2400.9-2455.9	354.1-444.1 1991.8-2066.8	3325.9-3415.9 3876.8-3951.8	216.8-71.8 2507.7-2637.7	5726.8-5871.8 6277.7-6407.7	2204.1-2364.1 4943.6-5058.6	5175.9-5335.9 6828.6-6943.6
CA_8-20	925-960 791-821	1850-1920 1582-1642	2775-2880 2373-2463	4625-4800 3955-4105	104-169 1716-1781	1029-1129 622-717	2641-2741 2507-2602	1133-1298 453-613	4357-4522 4223-4383	2879-3049 2204-2359	4491-4661 4089-4244
CA_8-40	925-960 2300-2400	1850-1920* 4600-4800	2775-2880 6900-7200	4625-4800 11500-12000	1340-1475* 3225-3360	380-550 3640-3875	4150-4320 5525-5760	1720-2025* 4980-5350	7375-7680 8750-9120	1300-1540* 8240-8675	6000-6240 10125-10560
CA_11-18	1475.9-1495.9 860-875	2951.8-2991.8 1720-1750	4427.7-4487.7 2580-2625	7379.5-7479.5 4300-4375	600.9-635.9 2335.9-2370.9	2076.8-2131.8 224.1-274.1	3811.8-3866.8 3195.9-3245.9	2677.7-2767.7 411.8-326.8	6147.7-6237.7 5531.8-5616.8	5028.6-5123.6 1944.1-2024.1	6763.6-6858.6 4915.9-4995.9

CA_12-25	729-746 1930-1995	1458-1492* 3860-3990	2187-2238 5790-5985	3645-3730 9650-9975	1184-1266* 2659-2741	438-537 3114-3261	3388-3487 4589-4736	1622-1803* 4298-4527	6047-6228 7248-7477	921-1054* 6974-7251	4846-4979 8449-8726
CA_12-30	729-746 2350-2360	1458-1492* 4700-4720	2187-2238* 7050-7080	3645-3730 11750-11800	1604-1631* 3079-3106	858-902* 3954-3991	3808-3852 5429-5466	2533-2462 5558-5622	6887-6958 8508-8572	556-634 8654-8711	5266-5344 10129-10186
CA_18-28	860-875 758-803	1720-1750 1516-1606	2580-2625 2274-2409	4300-4375 3790-4015	57-117 1618-1678	917-992 641-746	2478-2553 2376-2481	974-1109 524-689	4096-4231 3994-4159	2637-2742 2157-2352	4198-4303 3892-4087
CA_19-21	875-890 1495.9-1510.9	1750-1780 2991.8-3021.8	2625-2670 4487.7-4532.7	4375-4450 7479.5-7554.5	605.9-635.9 2370.9-2400.9	239.1-284.1 2101.8-2146.8	3245.9-3290.9 3866.8-3911.8	396.8-321.8 2707.7-2782.7	5616.8-5691.8 6237.7-6312.7	1989.1-2064.1 5093.6-5168.6	4995.9-5070.9 6858.6-6933.6
CA_19-42	875-890 3400-3600	1750-1780* 6800-7200	2625-2670* 10200-10800	4375-4450 17000-18000	2510-2725* 4275-4490	1620-1850* 5910-6325	5150-5380 7675-8090	4575-4130 8420-9050	9425-9870 11950-12580	100-160 12710-13525	6900-7160 14475-15290
CA_20-32	791-821 1452-1496	1582-1642 2904-2992	2373-2463 4356-4488	3955-4105 7260-7480	631-705 2243-2317	86-190 2083-2201	3034-3138 3695-3813	619-441 2714-2906	5277-5455 5938-6130	1668-1832 4987-5193	4616-4780 6599-6805
CA_23-29	2180-2200 717-728	4360-4400 1434-1456*	6540-6600 2151-2184***	10900-11000 3585-3640	1452-1483* 2897-2928	3632-3683 724-766***	5077-5128 3614-3656	5084-5166 2176-2249***	7974-8056 6511-6584	7992-8083 668-732***	9437-9528 5048-5112
CA_25-41	1930-1995 2496-2690	3860-3990 4992-5380	5790-5985 7488-8070	9650-9975 12480-13450	501-760 4426-4685	1170-1494 2997-3450	6356-6680 6922-7375	410-993 3498-4210	10782-11365 11348-12060	5030-5484 7989-8830	10216-10670 11914-12755
CA_26-41	859-894 2496-2690	1718-1788* 4992-5380	2577-2682*** 7488-8070	4295-4470 12480-13450	1602-1831* 3355-3584	708-972*** 4098-4521	4214-4478 5851-6274	2803-2310 5700-6352	7569-8062 9206-9858	746-1080*** 9090-9901	5932-6266 10843-11654
CA_29-30	717-728 2350-2360	1434-1456* 4700-4720	2151-2184* 7050-7080	3585-3640 11750-11800	1622-1643* 3067-3088	894-926* 3972-4003	3784-3816 5417-5448	2569-2516 5594-5646	6851-6904 8484-8536	508-562 8672-8723	5218-5272 10117-10168
CA_39-41	1880-1920 2496-2690	3760-3840 4992-5380	5640-5760 7488-8070	9400-9600 12480-13450	576-810 4376-4610	1070-1344 3072-3500	6256-6530 6872-7300	260-768 3648-4310	10632-11140 11248-11910	4830-5184 8064-8880	10016-10370 11864-12680
CA_41-42	2496-2690 3400-3600	4992-5380 6800-7200	7488-8070 10200-10800	12480-13450 17000-18000	710-1104 5896-6290	1392-1980 4110-4704	8392-8980 9296-9890	288-1270 4820-5808	14288-15270 15192-16180	6384-7360 10910-11904	13384-14360 16096-17090

Note:

- ~~XXXXXX~~ : bands that can be filter easily (out of the two carrier bands).
- * : Bands that between the two carrier bands but away from them (more than 100 MHz).
- ** : Bands that between the two carrier bands but close to one of the two carrier bands (less than 100 MHz).
- *** : Bands that are inside one of the two carrier bands (or part of the band are inside it).

APPENDIX B

The passband output $y(t)$ is related to the bandpass inputs $x_1(t)$ and $x_2(t)$ by:

$$y(t) = \sum_{k=1}^N a_k (\alpha_1 x_1(t) + \alpha_2 x_2(t))^k \quad (1)$$

Therefore, $y(t)$ can be expressed as:

$$y(t) = \sum_{k=1}^N \sum_{r_1=0}^k C_{r_1}^k a_{kr_1} (x_1(t))^{k-r_1} (x_2(t))^{r_1} \quad (2)$$

where the set of coefficients a_{kr_1} is equal to $a_{kr_1} = a_k (a_1)^{k-r_1} (a_2)^{r_1}$ and $C_a^b = \frac{b!}{(b-a)!a!}$.

The complex representation of the passband signal $x(t)$ in terms of its complex envelope $\tilde{x}(t)$ is:

$$x(t) = \frac{\tilde{x}(t)e^{j\omega t} + \tilde{x}^*(t)e^{-j\omega t}}{2} \quad (3)$$

where the complex envelope $\tilde{x}(t)$ can be represented as $\tilde{x}(t) = X(t)e^{j\theta(t)}$, where $X(t)$ and $\theta(t)$ are the instantaneous amplitude and phase of $\tilde{x}(t)$, respectively.

For convenience, the notation (t) is dropped hereafter. Replacing the passband signals x_1 and x_2 in (2) with their complex representations results in [20]:

$$y(t) = \sum_{k=1}^N \sum_{r_1=0}^k \frac{1}{2^k} C_{r_1}^k a_{kr_1} (\tilde{x}_1(t)e^{j\omega_1 t} + \tilde{x}_1^*(t)e^{-j\omega_1 t})^{k-r_1} (\tilde{x}_2(t)e^{j\omega_2 t} + \tilde{x}_2^*(t)e^{-j\omega_2 t})^{r_1} \quad (4)$$

By applying the binomial theorem, the above relation ends up to as [16]:

$$y(t) = \sum_{k=1}^N \sum_{r_1=0}^k \frac{1}{2^k} C_{r_1}^k a_{kr_1} \sum_{r_2=0}^{k-r_1} C_{r_2}^{k-r_1} \tilde{x}_1(t)^k \tilde{x}_1^*(t)^{r_1} \tilde{x}_2(t)^{k-r_1-r_2} \tilde{x}_2^*(t)^{r_2} \times e^{j\omega_1 t(k-2r_1)t} e^{j\omega_2(k-r_1-2r_2)t} \quad (5)$$

Therefore, the general basis function series ϕ_{kr} for the dual-band model is given by:

$$\phi_{kr}(\tilde{x}_1, \tilde{x}_2) = (\tilde{x}_1)^k (\tilde{x}_1^*)^{r_1} (\tilde{x}_2)^{k-r_1-r_2} (\tilde{x}_2^*)^{r_2} e^{j\omega_1 t(k-2r_1)t} e^{j\omega_2(k-r_1-2r_2)t} \quad (6)$$

For the terms around ω_1 :

$$\begin{cases} k - 2r_1 = 1 \\ k - r_1 - 2r_2 = 0 \end{cases}$$

The basis function for the terms around ω_1 is then given as:

$$\left| \phi_{kr_1}(\tilde{x}_1, \tilde{x}_2) \right|_{\omega_1} = (\tilde{x}_1)^{1+r_1} (\tilde{x}_1^*)^{r_1} (\tilde{x}_2)^{r_2} (\tilde{x}_2^*)^{r_2} e^{j\omega_1 t} = \tilde{x}_1 |\tilde{x}_1|^{2r_1} |\tilde{x}_2|^{2r_2} e^{j\omega_1 t} \quad (7)$$

Similarly, the terms grouped around the different frequencies are calculated, and the general equation for the dual-band PA can be given by:

$$\begin{aligned} y = & \sum_{k=1}^N \sum_{r_1=0}^{k-1} \sum_{r_2=0}^{k-r_1-1} \frac{1}{2^k} a_{k,r_1,r_2} C_{r_1}^{k-1} C_{r_2}^{k-r_1-1} \\ & \times \left[\left(\tilde{x}_1 |\tilde{x}_1|^{2r_1} |\tilde{x}_2|^{2r_2} \right) e^{j\omega_1 t} \right. \\ & + \left(\tilde{x}_1 |\tilde{x}_1|^{2r_1} |\tilde{x}_2|^{2r_2} \right) e^{j\omega_2 t} \\ & + \left(\tilde{x}_1^* \tilde{x}_2^2 |\tilde{x}_1|^{2(r_1-1)} |\tilde{x}_2|^{2r_2} \right) e^{j(2\omega_2 - \omega_1)t} \\ & + \left(\tilde{x}_1^2 \tilde{x}_2^* |\tilde{x}_1|^{2r_1} |\tilde{x}_2|^{2(r_2-1)} \right) e^{j(2\omega_1 - \omega_2)t} \\ & \left. + \left(\tilde{x}_1^3 \tilde{x}_2^{*2} |\tilde{x}_1|^{2r_1} |\tilde{x}_2|^{2(r_2-2)} \right) e^{j(3\omega_1 - 2\omega_2)t} + \dots \right] \quad (8) \end{aligned}$$

In order to take out the products that can be easily filter from the equation (as the inter-band third-order inter-modulation products around $(2\omega_2 - \omega_1)$ and $(2\omega_1 - \omega_2)$ and higher

order inter-modulation products), y can also be expressed in terms of its complex envelope components around ω_1 and ω_2 , similar to (3):

$$y = \frac{\tilde{y}_1 e^{j\omega_1 t} + \tilde{y}_1^* e^{-j\omega_1 t}}{2} + \frac{\tilde{y}_2 e^{j\omega_2 t} + \tilde{y}_2^* e^{-j\omega_2 t}}{2} + \dots \quad (9)$$

By equating the coefficients in (8) and (9) around ω_1 , the complex envelope \tilde{y}_1 of the output signal around ω_1 can be given as:

$$\tilde{y}_1 = \sum_{k=1}^N \sum_{r_1=0}^k \sum_{r_2=0}^{k-r_1} \frac{1}{2^{k-1}} a_{k,r_1,r_2}^{(1)} C_{r_1}^k C_{r_2}^{k-r_1} \times \tilde{x}_1 |\tilde{x}_1|^{2r_1} |\tilde{x}_2|^{2r_2} \quad (10)$$

Similarly, the complex envelope \tilde{y}_2 of the output signal around ω_2 can be given as:

$$\tilde{y}_2 = \sum_{k=1}^N \sum_{r_1=0}^k \sum_{r_2=0}^{k-r_1} \frac{1}{2^{k-1}} a_{k,r_1,r_2}^{(2)} C_{r_1}^k C_{r_2}^{k-r_1} \times \tilde{x}_2 |\tilde{x}_1|^{2r_1} |\tilde{x}_2|^{2r_2} \quad (11)$$

where the set of coefficients for each band can be grouped in one term as follows:

$$\begin{aligned} A_{k,r_1,r_2}^{(1)} &= \frac{1}{2^{k-1}} a_{k,r_1,r_2}^{(1)} C_{r_1}^k C_{r_2}^{k-r_1} \\ A_{k,r_1,r_2}^{(2)} &= \frac{1}{2^{k-1}} a_{k,r_1,r_2}^{(2)} C_{r_1}^k C_{r_2}^{k-r_1} \end{aligned} \quad (12)$$

where $A_{k,r_1,r_2}^{(1)}$ and $A_{k,r_1,r_2}^{(2)}$ are the model baseband coefficients for the lower and upper bands, respectively.

REFERENCES

- [1] M. Valkama, A. Springer, G. Hueber, "Digital signal processing for reducing the effects of RF imperfections in radio devices-An overview," in Proceeding of 2010 IEEE International Symposium on Circuits and Systems (ISCAS), pp. 813-816, June 2010.
- [2] S. C. Cripps, "RF power amplifiers for wireless communications", 2nd ed. Boston, MA: Artech House Publishers, 2006.
- [3] Z. Zhu, H. Leung, X. Huang, "Challenges in Reconfigurable Radio Transceivers and Application of Nonlinear Signal Processing for RF Impairment Mitigation," IEEE Circuits and Systems Magazine, vol. 13, no. 1, pp. 44-65, Feb. 2013.
- [4] L. Anttila, M. Valkama, M. Renfors, "Frequency-Selective I/Q Mismatch Calibration of Wideband Direct-Conversion Transmitters," IEEE Trans. Circuits Syst. II: Exp. Briefs, vol. 55, no. 4, pp. 359-363, Apr. 2008.
- [5] F. H. Raab, P. Asbeck, S. Cripps, P. B. Kenington, Z. B. Popovic, N. Pothecary, J. F. Sevic, and N. O. Sokal, "Power amplifiers and transmitters for RF and microwave," IEEE Trans. Microwave Theory Tech., vol. 50, no. 3, pp. 814-826, Mar. 2002.
- [6] P. M. Lavrador, T. R. Cunha, P. M. Cabral, and J. C. Pedro, "The linearity-efficiency compromise," IEEE Microw. Mag., vol. 11, no. 5, pp. 54-58, Aug. 2010.
- [7] A. Katz, "Linearization: reducing distortion in power amplifiers," IEEE Microw. Mag., vol. 2, no. 4, pp. 37-49, Dec. 2001.
- [8] F. M. Ghannouchi, "Power amplifier and transmitter architectures for software defined radio systems," IEEE Circuits Syst. Mag., vol. 10, pp. 56-63, 4th Quart, 2010.

- [9] P. L. Gilabert, G. Montoro, P. Vizarreta, and J. Berenguer, “Digital processing compensation mechanisms for highly efficient transmitter architectures,” *IET Microwaves, Antennas & Propagation*, vol. 5, no. 8, pp. 963-974, 2011.
- [10] M. Iwamura, K. Etemad, M. H. Fong, R. Nory, and R. Love, “Carrier aggregation framework in 3GPP LTE-advanced,” *IEEE Commun. Mag.*, vol. 48, no. 8, pp. 60–67, 2010.
- [11] K. I. Pedersen, F. Frederiksen, C. Rosa, H. Nguyen, L. G. U. Garcia, and Y. Wang, “Carrier aggregation for LTE-advanced: Functionality and performance aspects,” *IEEE Commun. Mag.*, vol. 49, no. June, pp. 89–95, 2011.
- [12] "Carrier Aggregation explained", 3gpp.org, 2016. [Online]. Available: <http://www.3gpp.org/technologies/keywords-acronyms/101-carrier-aggregation-expla>.
- [13] T. Nakamura, “LTE-Advanced (3GPP Release 10 and beyond) - RF aspects,” *3GPP*, pp. 1–22, Dec 2009.
- [14] A. Z. Yonis, M. Faiz, and L. Abdullah, “Wider Bandwidth of non-Contiguous Component Carriers in LTE- Advanced,” *International Journal of Future Generation Communication and Networking*, vol. 6, no. 2, pp. 49–62, 2013.
- [15] S. A. Bassam, W. Chen, M. Helaoui, and F. M. Ghannouchi, “Transmitter architecture for ca: Carrier aggregation in LTE-advanced systems,” *IEEE Microw. Mag.*, vol. 14, no. August, pp. 78–86, 2013.
- [16] M. F. Younes “Advanced Digital Signal Processing Techniques for Linearization of Multi-band Transmitters”, Ph.D. Thesis. University of Calgary, 2014.
- [17] N. Boulejfen, A. Harguem, and F. M. Ghannouchi, “New closed-form expressions for the prediction of multitone intermodulation distortion in fifth-order nonlinear RF circuits/systems,” *IEEE Trans. Microw. Theory Tech.*, vol. 52, no. 1, pp. 121–132, 2004.

- [18] M. Rawat, P. Roblin, C. Quindroit, N. Naraharisetti, and R. Pond, "Characterization and modeling scheme for harmonics at power amplifier output," 83rd ARFTG Microwave Measurement Conference, pp. 5–8, Jun 2014.
- [19] S. A. Bassam, M. H. Heloui, and F. M. Ghannouchi, "2-D digital predistortion (2-D-DPD) architecture for concurrent dual-band transmitters," *IEEE Trans. Microw. Theory Tech.*, vol. 59, no. 10 PART 1, pp. 2547–2553, 2011.
- [20] H. Wang, C. Rosa, and K. Pedersen, "Performance Analysis of Downlink Inter-band Carrier Aggregation in LTE-Advanced," 2011 IEEE Vehicular Technology Conference (VTC Fall), pp. 1–5, Sep. 2011.
- [21] 3GPP, 3rd generation partnership project; LTE; Feasibility study for Further Advancements for E-UTRA (LTE-Advanced) (Release 12), 3GPP TR 136 912 Version 12.0.0, vol. 0, Sep. 2014.
- [22] P. I. Mak, S. P. U, and R. P. Martins, "Transceiver Architecture Selection: Review, State-of-the-Art Survey and Case Study," *IEEE Circuits Syst. Mag.*, vol. 7, no. 2, pp. 6–25, 2007.
- [23] M. Windisch and G. Fettweis, "Adaptive I/Q imbalance compensation in low-IF transmitter architectures," *IEEE 60th Veh. Technol. Conf. 2004. VTC2004-Fall. 2004*, vol. 3, no. C, pp. 2096–2100, 2004.
- [24] W. Chen, S. A. Bassam, X. Li, Y. Liu, K. Rawat, M. Heloui, F. M. Ghannouchi, and Z. Feng, "Design and linearization of concurrent dual-band Doherty power amplifier with frequency-dependent power ranges," *IEEE Trans. Microw. Theory Tech.*, vol. 59, no. 10, pp. 2537–2546, 2011.
- [25] S. Amin, S. Member, W. Van Moer, S. Member, P. Händel, S. Member, and D. Rönnow, "Characterization of Concurrent Dual-Band Power Amplifiers Using a Dual Two-Tone Excitation Signal," vol. 64, no. 10, pp. 2781–2791, 2015.

- [26] 3GPP, 3rd generation partnership project; Technical specification group radio access network; Multiplexing and Channel Coding (Release 12), 3GPP TS 36.211. Version 12.7.0, vol. 0, 2015.
- [27] 3GPP, 3rd generation partnership project; Technical specification group radio access network; Physical Channels and Modulation (Release 12), 3GPP TS 36.211. Version 12.6.0, vol. 0, 2015.
- [28] ITU-R, “Unwanted Emissions in the Spurious Domain, Recommendation ITU-R.” vol. SM.1541–5. 2013.
- [29] 3GPP, 3rd generation partnership project; Technical specification group radio access network; Physical layer Procedures (Release 12), 3GPP TS 36.211. Version 12.7.0, vol. 0, 2015.
- [30] 3GPP, 3rd generation partnership project; Technical specification group radio access network; Physical layer Measurements (Release 12), 3GPP TS 36.211. Version 12.2.0, vol. 0, 2015.
- [31] 3GPP, 3rd generation partnership project; “Proposed SID on LTE-Advanced,” RP-0801373 NTT DoCoMo, 2008.
- [32] S. Sesia, I. Toufik, M. Baker “LTE-The UMTS Long Term Evolution, from Theory to Practice” 2nd Ed., John Wiley, UK, pp. 623-650, 2011.
- [33] I. T. Union, “Requirements, Evaluation Criteria and Submission Templates for the Development of IMT-Advanced,” REPORT ITU-R M.2133, 2008.
- [34] I. T. Union, “Requirements related to technical performance for IMT-Advanced radio interface(s),” REPORT ITU-R M.2134, 2008.
- [35] 3-Gpp, “LTE Evolved Universal Terrestrial Radio Access (E-UTRA); Base Station (BS) radio transmission and reception (3GPP TS 36.104 version 10.11.0 Release 10),” vol. 0, 2013.

- [36] D. Astély, E. Dahlman, A. Furuskär, Y. Jading, M. Lindström, and S. Parkvall, “LTE: The evolution of mobile broadband,” *IEEE Commun. Mag.*, vol. 47, no. 4, pp. 44–51, 2009.
- [37] G. Yuan, X. Zhang, W. Wang, and Y. Yang, “Carrier aggregation for LTE-advanced mobile communication systems,” *IEEE Commun. Mag.*, vol. 48, no. 2, pp. 88–93, 2010.
- [38] 3-Gpp, 3rd Generation Partnership Project; Technical Specification Group Radio Access Network; Further advancements for E-UTRA; LTE-Advanced feasibility studies in RAN WG4 (Release 9),” TR 36.815, V9.1.0, section 5.3, Jun 2010.
- [39] 3-Gpp, “LTE Evolved Universal Terrestrial Radio Access (E-UTRA); Base Station (BS) radio transmission and reception (3GPP TS 36.104 version 12.9.0 Release 12),” vol. 0, 2015.
- [40] 3-Gpp, “LTE Evolved Universal Terrestrial Radio Access (E-UTRA); Base Station (BS) radio transmission and reception (3GPP TS 36.104 version 8.13.0 Release 8),” vol. 0, 2012.
- [41] 3-Gpp, “LTE Evolved Universal Terrestrial Radio Access (E-UTRA); Base Station (BS) radio transmission and reception (3GPP TS 36.104 version 9.13.0 Release 9),” vol. 0, 2012.
- [42] 3-Gpp, “LTE Evolved Universal Terrestrial Radio Access (E-UTRA); Base Station (BS) radio transmission and reception (3GPP TS 36.104 version 11.13.0 Release 11),” vol. 0, 2015.
- [43] 4G Americas, “Executive Summary: Inside 3GPP Release 13: Understanding the standards for HSPA+ and LTE-Advanced Enhancements”, September 2015.
- [44] J. Nyström, P. Ojanen, H. Schöneich, J. P. Desbat, M. Mustonen, E. Mohyeldin, M. Siebert,” *IMT-Advanced: requirements and evaluation criteria*”, *Wireless World Initiative New Radio – WINNER+*, May 2009.

- [45] P. Colantonio, F. Giannini, R. Giofre, and L. Piazzon, "A Design Technique for Concurrent Dual-Band Harmonic Tuned Power Amplifier," *IEEE Trans. Microw. Theory Tech.*, vol. 56, no. 11, pp. 2545–2555, Nov. 2008.
- [46] Z. Wang and C.-W. Park, "Concurrent tri-band GaN HEMT power amplifier using resonators in both input and output matching networks," *WAMICON 2012 IEEE Wireless & Microwave Technology Conference*, , pp. 1–4, Apr. 2012.
- [47] S. A. Bassam, M. Helaoui, and F. M. Ghannouchi, "Channel-Selective Multi-Cell Digital Predistorter for Multi-Carrier Transmitters," *IEEE Trans. Commun.*, vol. 60, no. 8, pp. 2344–2352, Aug. 2012.
- [48] L. Ding, G. T. Zhou, D. R. Morgan, Z. Ma, J. S. Kenney, J. Kim, and C. R. Giardina, "A Robust Digital Baseband Predistorter Constructed Using Memory Polynomials," *IEEE Trans. Commun.*, vol. 52, no. 1, pp. 159–165, Jan. 2004.
- [49] M. O’Droma, S. Meza, and Y. Lei, "New modified Saleh models for memoryless nonlinear power amplifier behavioural modelling," *IEEE Commun. Lett.*, vol. 13, no. 6, pp. 399–401, Jun. 2009.
- [50] A. Toledano, Y. Zhang, "Multiband, Multistandard Transmitter Design Using the RF DAC," *Analog Devices Technical Article*, pp. 3–6. 2015.
- [51] C. F. Lanzani, G. Karadars, and D. Boppana, "Remote radio heads and the evolution towards 4G networks", *MTI Radio comp & Altera*, March. 2009.
- [52] Nokia, "Study of UE architectures for LTE-A deployment scenarios," R4-091204 Tech. Rep., March 2009 [Online]. Available: http://ftp.3gpp.org/tsg_ran/WG4_Radio/TSGR4_50bis/Documents/R4091204.zip.
- [53] S. Jatmiko, a B. Mutiara, and M. Indriati, "Prototype of Water Level Detection System," *Theor. Appl. Inf. Technol.*, vol. 37, no. 1, 2012.

- [54] A. Abdelhafiz, A. Kwan, O. Hammi, and F. M. Ghannouchi, "Digital Predistortion of LTE-A Power Amplifiers Using Compressed-Sampling-Based Unstructured Pruning of Volterra Series," *IEEE Trans. Microw. Theory Tech.*, vol. 62, no. 11, pp. 2583–2593, 2014.
- [55] D. Schreurs, M. O'Droma, and A. A. Goacher, Eds., "RF power amplifier behavioral modeling", (Hardback). Cambridge, UK: CAMBRIDGE UNIVERSITY PRESS, United Kingdom, 2008.
- [56] H. Ku and J. S. Kenney, "Behavioral modeling of nonlinear RF power amplifiers considering memory effects," *IEEE Trans. Microw. Theory Tech.*, vol. 51, no. 12, pp. 2495–2504, 2003.
- [57] M. Isaksson, D. Wisell, and D. Ronnow, "A comparative analysis of behavioral models for RF power amplifiers," *Microw. Theory Tech. IEEE Trans.*, vol. 54, no. 1, pp. 348–359, 2006.
- [58] J. C. Pedro and S. a. Maas, "A comparative overview of microwave and wireless power-amplifier behavioral modeling approaches," *IEEE Trans. Microw. Theory Tech.*, vol. 53, no. 4 I, pp. 1150–1163, 2005.
- [59] O. Hammi, S. Bensmida, and K. Morris, "Behavioral modeling of class-j amplifier driven by 100MHz LTE-advanced signal using dynamic nonlinearity reduction," 2014 IEEE Topical Conference on Power Amplifiers for Wireless and Radio Applications (PAWR), no. 1, pp. 67–69, Jan. 2014.
- [60] H. Zhou, G. Wan, and L. Chen, "A Nonlinear memory power amplifier behavior modeling and identification based on memory polynomial model in soft-defined Shortwave transmitter," 2010 International Conference on Computational Intelligence and Software Engineering, pp. 1–4, Sep. 2010.
- [61] A. Zhu, J. C. Pedro, and T. J. Brazil, "Dynamic Deviation Reduction-Based Volterra Behavioral Modeling of RF Power Amplifiers," *IEEE Trans. Microw. Theory Tech.*, vol. 54, no. 12, pp. 4323–4332, Dec. 2006

- [62] L. Ding. PhD. Thesis: "Digital Predistortion of Power Amplifiers for Wireless Applications," School of Electrical and Computer Engineering, Georgia Institute of Technology, March 2004.
- [63] Bosch, W.; Gatti, G., "Measurement and simulation of memory effects in predistortion linearizers," *IEEE Transactions on MTT*, vol. 37, no. 2, pp. 1885-1890, 2003.
- [64] Vuolevi, J.H.K.; Rahkonen, T.; Manninen, J.P.A., "Measurement technique for characterizing memory effects in RF power amplifiers," *IEEE Transactions on Microwave Theory and Techniques*, vol. 29, no. 8, pp. 1383-1389, Aug. 2001.
- [65] Z. Fu, L. Anttila, M. Abdelaziz, M. Valkama, and A. Wyglinski, "Frequency-Selective Digital Predistortion for Unwanted Emission Reduction," *IEEE Trans. Commun.*, vol. PP, no. 99, pp. 254 - 267, 2014.
- [66] Y. Zhao, Z. Qin, X. I. a Gaofeng, and L. I. U. Jiong, "PA Linearization Using Multi-stage Look-Up-Table Predistorter with Optimal Linear Weighted Delay," *IEEE 11th Int. Conf. Signal Process. (ICSP)*, 2012.
- [67] J. T. Valliarampath and S. Sinha, "Designing linear pAs at millimeter-wave frequencies using Volterra series analysis," *Canadian Journal of Electrical and Computer Engineering*, vol. 38, no. 3, pp. 232–237, 2015.
- [68] J. Reina-Tosina, M. Allegue-Martinez, C. Crespo-Cadenas, C. Yu, and S. Cruces, "Behavioral modeling and Predistortion of power amplifiers under Sparsity hypothesis," *IEEE Transactions on Microwave Theory and Techniques*, vol. 63, no. 2, pp. 745–753, Feb. 2015.
- [69] M. V. Deepak Nair, R. Giofre, L. Piazzon, and P. Colantonio, "A comparative study on digital predistortion techniques for Doherty amplifier for LTE applications," *2014 Int. Work. Integr. Nonlinear Microw. Millimetre-wave Circuits*, pp. 1–3, 2014.

- [70] O. Hammi, A. Kwan, S. Bensmida, K. A. Morris, and F. M. Ghannouchi, "A digital Predistortion system with extended correction bandwidth with application to LTE-A Nonlinear power amplifiers," *IEEE Transactions on Circuits and Systems I: Regular Papers*, vol. 61, no. 12, pp. 3487–3495, Dec. 2014
- [71] C. Sanchez, J. de Mingo, P. Garcia, P. L. Carro, and A. Valdovinos, "Memory behavioral modeling of RF power amplifiers," *VTC Spring 2008 - IEEE Vehicular Technology Conference*, May 2008.
- [72] S. Glock, J. Rascher, B. Sogl, T. Ussmueller, J.-E. Mueller, and R. Weigel, "A Memoryless Semi-Physical power amplifier behavioral model based on the correlation between AM–AM and AM–PM distortions," *IEEE Transactions on Microwave Theory and Techniques*, vol. 63, no. 6, pp. 1826–1835, Jun. 2015.
- [73] J. Moon and B. Kim, "Enhanced Hammerstein Behavioral Model for Broadband Wireless Transmitters," *IEEE Trans. Microw. Theory Tech.*, vol. 59, no. 4, pp. 924–933, 2011.
- [74] C. Mateo, P. L. Carro, P. Garcia, and J. D. Mingo, "RF power amplifier behavioral modeling using wavelet multiresolution," *2015 IEEE Topical Conference on Power Amplifiers for Wireless and Radio Applications (PAWR)*, Jan. 2015.
- [75] M. O. H. Khalifa, A. Abdelhafiz, A. Kwan, F. M. Ghannouchi, and O. Hammi, "Behavioral modeling of envelope tracking power amplifier using Volterra series model and compressed sampling," *2015 IEEE International Wireless Symposium (IWS 2015)*, Mar. 2015.
- [76] S. Zhang, G. Su, X. Chen, and W. Chen, "Extraction of wideband behavioral model of power amplifier with multi groups of narrow band signals," *2014 IEEE International Wireless Symposium (IWS 2014)*, Mar. 2014.
- [77] W. Chen, S. Zhang, Y.-J. Liu, F. M. Ghannouchi, Z. Feng, and Y. Liu, "Efficient Pruning Technique of Memory Polynomial Models Suitable for PA Behavioral Modeling and Digital Predistortion," *IEEE Trans. Microw. Theory Tech.*, vol. 62, no. 10, pp. 2290–2299, Oct. 2014.

- [78] O. Hammi, A. M. Kedir, and F. M. Ghannouchi, "Nonuniform memory polynomial behavioral model for wireless transmitters and power amplifiers," 2012 Asia Pacific Microwave Conference Proceedings, pp. 836–838, Dec. 2012.
- [79] Q. Zhang, Y. Liu, J. Zhou, and W. Chen, "A complexity-reduced band-limited memory polynomial behavioral model for wideband power amplifier," 2015 IEEE International Wireless Symposium (IWS 2015), pp. 1-4, Mar. 2015.
- [80] Y.-J. Liu, J. Zhou, W. Chen, and B.-H. Zhou, "A Robust Augmented Complexity-Reduced Generalized Memory Polynomial for Wideband RF Power Amplifiers," IEEE Trans. Ind. Electron., vol. 61, no. 5, pp. 2389–2401, May 2014.
- [81] M. Rawat, K. Rawat, F. M. Ghannouchi, S. Bhattacharjee, and H. Leung, "Generalized Rational Functions for Reduced-Complexity Behavioral Modeling and Digital Predistortion of Broadband Wireless Transmitters," IEEE Trans. Instrum. Meas., vol. 63, no. 2, pp. 485–498, Feb. 2014.
- [82] W. Chen, X. Chen, G. Su, S. Zhang, and F. M. Ghannouchi, "Advanced power amplifier technologies for multistandard and broadband wireless communications," 2014 International Workshop on Integrated Nonlinear Microwave and Millimetre-wave Circuits (INMMiC), pp. 1-3, Apr. 2014.
- [83] G. Xu, T. Liu, Y. Ye, T. Xu, H. Wen, and X. Zhang, "Generalized Two-Box Cascaded Nonlinear Behavioral Model for Radio Frequency Power Amplifiers With Strong Memory Effects," IEEE Trans. Microw. Theory Tech., vol. 62, no. 12, pp. 2888–2899, Dec. 2014.
- [84] S. A. Bassam, M. Helaoui, and F. M. Ghannouchi, "2-D digital architecture for concurrent dual-band transmitters," IEEE Trans. on Micro. Theory and Techs, vol. 59, no. 10, pp. 2547–2553, Oct. 2011.
- [85] A. Kwan, S. Bassam, M. Helaoui, and F. Ghannouchi, "Concurrent dual band digital predistortion using look up tables with variable depths," in IEEE Power Amplifiers Wireless Radio Appl. Top. Conf., pp. 25–27, 2013.

- [86] X. Wu, J. Shi, and H. Chen, "On the numerical stability of RF power amplifier's digital predistortion," 2009 15th Asia-Pacific Conference on Communications, pp. 430–433, Oct. 2009.
- [87] M. Younes, O. Hammi, A. Kwan, and F. M. Ghannouchi, "An Accurate Complexity-Reduced "PLUME" Model for Behavioral Modeling and Digital Predistortion of RF Power Amplifiers," IEEE Trans. Ind. Electron., vol. 58, no. 4, pp. 1397–1405, Apr. 2011. |
- [88] E. W. Cheney and D. Kincaid, Numerical Mathematics and Computing, 7th ed. Pacific Grove, CA, USA: Brooks/Cole, chapter. 8, p. 321, 2008.

Vitae

Name :Mohammed Abdalla Abdelrahim Ali |

Nationality :Sudan |

Date of Birth :12/1/1990|

Email :Eng.m.a4@hotmail.com|

Address :Bahri, Khartoum, Sudan|

Academic Background :August 2015: Master Degree of Electrical and Electronics Engineering (Major in Network and Computer Architecture),first class.
October 2012: B.Sc. in Electronics engineering (1st Class Division Honor)
University of Khartoum Electrical & Electronics Engineering Department.|

Publication

1. Mohammed A. A. Ali, “Proposed Memory Polynomial Model for Concurrent Dual-Band Power Amplifiers Behavioural Models, “under preparation, IEEE Trans. Microw. Theory Tech, Oct 2016.